Global Biogeochemical Cycles®

Key Points:
- We synthesize air-sea fluxes of CO_2, nitrous oxide and methane in the global coastal ocean using observation-based products and ocean models
- The coastal ocean CO_2 sink is 60% larger in ocean models than in observation-based products due to systematic differences in seasonality
- Coastal nitrous oxide and methane emissions offset 30%–60% of the CO_2 coastal uptake in the net radiative balance

Supporting Information:
Supporting Information may be found in the online version of this article.

Correspondence to:
L. Resplandy,
laurer@princeton.edu

Author Contributions:
Conceptualization: L. Resplandy, P. Regnier

A Synthesis of Global Coastal Ocean Greenhouse Gas Fluxes

L. Resplandy[1], A. Hogikyan[2], J. D. Müller[3], R. G. Najjar[4], H. W. Bange[5], D. Bianchi[6], T. Weber[7], W.-J. Cai[8], S. C. Doney[9], K. Fennel[10], M. Gehlen[11], J. Hauck[12], F. Lacroix[13], P. Landschützer[14], C. Le Quéré[15], A. Roobaert[14,16], J. Schwinger[17], S. Berthet[18], L. Bopp[19], T. T. T. Chau[11], M. Dai[20], N. Gruber[3], T. Ilyina[21], A. Kock[5,22], M. Manizza[23], Z. Lachkar[24], G. G. Laruelle[16], E. Liao[1,25], I. D. Lima[26], C. Nissen[12,27], C. Rödenbeck[28], R. Séférian[18], K. Toyama[29], H. Tsujino[29], and P. Regnier[16]

[1]Department of Geosciences and High Meadows Environmental Institute, Princeton University, Princeton, NJ, USA, [2]Atmospheric and Oceanic Sciences Program, Princeton University, Princeton, NJ, USA, [3]Environmental Physics, Institute of Biogeochemistry and Pollutant Dynamics, ETH Zurich, Zürich, Switzerland, [4]Department of Meteorology and Atmospheric Science, The Pennsylvania State University, University Park, PA, USA, [5]GEOMAR Helmholtz Centre for Ocean Research Kiel, Kiel, Germany, [6]Department of Atmospheric and Oceanic Sciences, University of California Los Angeles, Los Angeles, CA, USA, [7]Department of Earth and Environmental Science, University of Rochester, Rochester, NY, USA, [8]School of Marine Science and Policy, University of Delaware, Newark, DE, USA, [9]Department of Environmental Sciences, University of Virginia, Charlottesville, VA, USA, [10]Department of Oceanography, Dalhousie University, Halifax, NS, Canada, [11]Laboratoire des Sciences du Climat et de l'Environnement, LSCE/IPSL, CEA-CNRS-UVSQ, Université Paris-Saclay, Gif-sur-Yvette, France, [12]Alfred-Wegener-Institut, Helmholtz-Zentrum für Polar- und Meeresforschung, Bremerhaven, Germany, [13]Climate and Environmental Physics, Oeschger Centre for Climate Change Research (OCCR), University of Bern, Bern, Switzerland, [14]Flanders Marine Institute (VLIZ), Ostend, Belgium, [15]School of Environmental Sciences, University of East Anglia, Norwich Research Park, Norwich, UK, [16]Department Geoscience, Environment and Society—BGEOSYS, Université Libre de Bruxelles, Brussels, Belgium, [17]NORCE Climate & Environment, Bjerknes Centre for Climate Research, Bergen, Norway, [18]CNRM, Université de Toulouse, Météo France, CNRS, Toulouse, France, [19]LMD/IPSL, ENS, Université PSL, École Polytechnique, Institut Polytechnique de Paris, Sorbonne Université, CNRS, Paris, France, [20]State Key Lab of Marine Environmental Science, College of Ocean and Earth Sciences, Xiamen University, Xiamen, China, [21]Max Planck Institute for Meteorology, Hamburg, Germany, [22]Now at State Office for the Environment of the State of Schleswig-Holstein, Flintbek, Germany, [23]Geosciences Research Division, Scripps Institution of Oceanography, University of California—San Diego, La Jolla, CA, USA, [24]Arabian Center for Climate and Environmental Sciences, New York University Abu Dhabi, Abu Dhabi, United Arab Emirates, [25]Now at School of Oceanography, Shang Jiao Tong University, Shanghai, China, [26]Department of Marine Chemistry and Geochemistry, Woods Hole Oceanographic Institution, Woods Hole, MA, USA, [27]Department of Atmospheric and Oceanic Sciences, Institute of Arctic and Alpine Research, University of Colorado, Boulder, CO, USA, [28]MPI Biogeochemistry, Jena, Germany, [29]JMA Meteorological Research Institute, Tsukuba, Japan

Abstract The coastal ocean contributes to regulating atmospheric greenhouse gas concentrations by taking up carbon dioxide (CO_2) and releasing nitrous oxide (N_2O) and methane (CH_4). In this second phase of the Regional Carbon Cycle Assessment and Processes (RECCAP2), we quantify global coastal ocean fluxes of CO_2, N_2O and CH_4 using an ensemble of global gap-filled observation-based products and ocean biogeochemical models. The global coastal ocean is a net sink of CO_2 in both observational products and models, but the magnitude of the median net global coastal uptake is ~60% larger in models (−0.72 vs. −0.44 PgC year^{-1}, 1998–2018, coastal ocean extending to 300 km offshore or 1,000 m isobath with area of 77 million km^2). We attribute most of this model-product difference to the seasonality in sea surface CO_2 partial pressure at mid- and high-latitudes, where models simulate stronger winter CO_2 uptake. The coastal ocean CO_2 sink has increased in the past decades but the available time-resolving observation-based products and models show large discrepancies in the magnitude of this increase. The global coastal ocean is a major source of N_2O (+0.70 PgCO$_2$-e year^{-1} in observational product and +0.54 PgCO$_2$-e year^{-1} in model median) and CH_4 (+0.21 PgCO$_2$-e year^{-1} in observational product), which offsets a substantial proportion of the coastal CO_2 uptake in the net radiative balance (30%–60% in CO_2-equivalents), highlighting the importance of considering the three greenhouse gases when examining the influence of the coastal ocean on climate.

Plain Language Summary The coastal ocean regulates greenhouse gases. It acts as a sink of carbon dioxide (CO_2) but also releases nitrous oxide (N_2O) and methane (CH_4) into the atmosphere. This synthesis contributes to the second phase of the Regional Carbon Cycle Assessment and Processes (RECCAP2) and provides a comprehensive view of the coastal air-sea fluxes of these three greenhouse gases at the global scale. We use a multi-faceted approach combining gap-filled observation-based products and ocean biogeochemical

Data curation: L. Resplandy, A. Hogikyan, J. D. Müller, D. Bianchi, T. Weber, S. C. Doney, K. Fennel, M. Gehlen, J. Hauck, P. Landschützer, C. Le Quéré, A. Roobaert, J. Schwinger, S. Berthet, L. Bopp, T. T. T. Chau, N. Gruber, A. Kock, G. G. Laruelle, E. Liao, I. D. Lima, C. Nissen, C. Rödenbeck, R. Séférian, K. Toyama, H. Tsujino
Formal analysis: L. Resplandy, A. Hogikyan, J. D. Müller
Funding acquisition: L. Resplandy
Investigation: L. Resplandy, J. D. Müller, D. Bianchi, T. Weber, S. C. Doney, K. Fennel, M. Gehlen, J. Hauck, P. Landschützer, C. Le Quéré, A. Roobaert, J. Schwinger, S. Berthet, L. Bopp, T. T. T. Chau, N. Gruber, A. Kock, G. G. Laruelle, E. Liao, I. D. Lima, C. Nissen, C. Rödenbeck, R. Séférian, K. Toyama, H. Tsujino
Methodology: L. Resplandy, A. Hogikyan, P. Regnier
Project Administration: L. Resplandy, J. D. Müller, J. Hauck, N. Gruber, P. Regnier
Software: L. Resplandy, A. Hogikyan
Supervision: L. Resplandy, J. D. Müller, J. Hauck, N. Gruber, P. Regnier
Visualization: L. Resplandy, A. Hogikyan, J. D. Müller
Writing – original draft: L. Resplandy, H. W. Bange, D. Bianchi, T. Weber, P. Regnier
Writing – review & editing: L. Resplandy, A. Hogikyan, J. D. Müller, R. G. Najjar, H. W. Bange, D. Bianchi, T. Weber, W.-J. Cai, S. C. Doney, K. Fennel, M. Gehlen, J. Hauck, F. Lacroix, P. Landschützer, C. Le Quéré, A. Roobaert, J. Schwinger, S. Berthet, L. Bopp, T. T. T. Chau, M. Dai, N. Gruber, T. Ilyina, A. Kock, M. Manizza, Z. Lachkar, G. G. Laruelle, E. Liao, I. D. Lima, C. Nissen, C. Rödenbeck, R. Séférian, K. Toyama, H. Tsujino, P. Regnier

models. We show that the global coastal ocean is a net sink of CO_2 in both observational products and models, but the coastal uptake of CO_2 is ~60% larger in models than in observation-based products due to model-product differences in seasonality. The coastal CO_2 sink is strengthening but the magnitude of this strengthening is poorly constrained. We also find that the coastal emissions of N_2O and CH_4 counteract a substantial part of the effect of coastal CO_2 uptake in the atmospheric radiative balance (by 30%–60% in CO_2-equivalents), highlighting the need to consider these three gases together to understand the influence of the coastal ocean on climate.

1. Introduction

Coastal oceans play an important role in the global carbon cycle by serving as a hub of exchange between the land, tidal wetlands, estuaries, sediments, the atmosphere, and the open ocean (Bauer et al., 2013; Chen & Borges, 2009; Mackenzie et al., 1998; Ward et al., 2020). They contribute to the global oceanic uptake of anthropogenic carbon by absorbing carbon dioxide (CO_2) directly from the atmosphere and by burying, transforming, or outgassing the carbon delivered by terrestrial ecosystems to the coastal ocean (e.g., Regnier et al., 2022). A notable milestone in the efforts to quantify the CO_2 exchange between the atmosphere and coastal oceans was reached by Chen et al. (2013) during the first phase of the Regional Carbon Cycle Assessment and Processes (RECCAP), an international effort to establish the mean carbon balance and change over the period 1990–2009 for all subcontinents and ocean basins. These authors expanded on prior work at the scale of continental shelves (Borges et al., 2005; Cai et al., 2006; Chen & Borges, 2009; Laruelle et al., 2010) and examined the global atmospheric CO_2 uptake by coastal oceans using a compilation of surface ocean partial pressure of CO_2 (pCO_2) data available for 87 shelves. They concluded that most coastal ocean waters act as a sink for atmospheric CO_2, except for tropical coastal ocean systems that were identified as weak CO_2 sources and found the global coastal ocean CO_2 uptake to be 0.4 PgC year^{-1} (for a surface area of coastal ocean of 30.3 million km^2).

Since the completion of RECCAP, the amount of available pCO_2 measurements in the coastal ocean has increased tremendously, reaching millions shortly after the RECCAP assessment was released (e.g., Surface Ocean CO_2 Atlas database SOCAT; Bakker et al., 2014) and ~19 million in the most recent publication (Bakker et al., 2022). In parallel, statistical gap-filling methods, initially developed for the open ocean, have been applied to these fast expanding data sets to resolve the spatio-temporal variability of the air-sea CO_2 flux in the coastal ocean (Chau et al., 2022; Landschützer et al., 2020; Laruelle et al., 2014; Roobaert et al., 2019). These global gap-filled observation-based coastal products led to a downward revision of the global coastal ocean CO_2 uptake to about half of the RECCAP value (0.15–0.20 PgC year^{-1}; Chau et al., 2022; Roobaert et al., 2019). This downward revision was corroborated by a recent synthesis of 214 regionally aggregated CO_2 flux estimates, leading to a net uptake of 0.25 PgC year^{-1} (Dai et al., 2022), although these assessments covered slightly different periods and coastal areas (1985–2019 and ~22 million km^2 in Chau et al. (2022); 1998–2015 and 28 million km^2 in Roobaert et al. (2019); 1998-present and ~30 million km^2 in Dai et al. (2022)).

While coastal ocean waters are a sink of CO_2, they are also the main oceanic source of two other important greenhouse gases: nitrous oxide (N_2O) and methane (CH_4) (e.g., Saunois et al., 2020; Wan et al., 2022; Weber et al., 2019; Yang et al., 2020). RECCAP did not consider N_2O and CH_4, but recent studies have compiled oceanic N_2O and CH_4 measurements (Kock & Bange, 2015) and applied statistical gap-filling techniques similar to those employed for CO_2 to assess the global ocean air-sea N_2O and CH_4 fluxes (Weber et al., 2019; Yang et al., 2020). These studies have greatly improved the quantification of N_2O and CH_4 air-sea fluxes at the global scale, but coastal ocean N_2O and CH_4 emissions remain highly uncertain and the extent to which these emissions offset the present-day coastal CO_2 uptake is unknown.

Coastal air-sea fluxes of CO_2, N_2O and CH_4 have strong spatial and seasonal variability. Regional-scale observational and modeling studies have greatly improved the quantification of the mean and temporal variability of air-sea fluxes of greenhouse gases in individual regions across the globe (e.g., Anderson et al., 2009; Arévalo-Martínez et al., 2015; Fennel et al., 2019; Gomez et al., 2020; Gülzow et al., 2013; Hauri et al., 2021; Louchard et al., 2021; Mayer et al., 2018; Pipko et al., 2017; Turi et al., 2014). However, the limited spatial coverage of these studies largely inhibits a global-scale perspective. Global gap-filled observational products and global ocean biogeochemical models now have horizontal resolutions of ~25–50 km to estimate coastal CO_2 (Bourgeois et al., 2016; Lacroix et al., 2020, 2021; Roobaert et al., 2022) and N_2O (Berthet et al., 2023; Ganesan

et al., 2020; Stell et al., 2022) fluxes, recently complemented these regional-scale studies in global-scale studies (e.g., Friedlingstein et al., 2022).

As a result of observational and modeling advances since RECCAP, a global view of the coastal ocean's spatial and seasonal patterns in air-sea greenhouse gas fluxes has started to emerge, at least for CO_2 fluxes. Polar and subpolar coastal oceans, such as the northwest North Atlantic along the Canadian and US coast (Cahill et al., 2016; Fennel & Wilkin, 2009; Gustafsson et al., 2019; Lachkar & Gruber, 2013; Laruelle et al., 2015; Previdi et al., 2009; Signorini et al., 2013; Thomas et al., 2004), the European shelves (Cossarini et al., 2015; Gustafsson et al., 2019; Neumann et al., 2022; Thomas et al., 2004) and Arctic and Antarctic shelf (Arrigo et al., 2008; Ouyang et al., 2022; Pipko et al., 2017, 2021) generally are strong sinks of CO_2 characterized by large seasonal variations, and likely account for about 90% of the annual global coastal CO_2 uptake (while representing ~45% of the global coastal surface area, see Dai et al., 2022; Laruelle et al., 2014; Roobaert et al., 2019). There are exceptions to subpolar and polar shelves where outgassing has been identified, such as the Scotian Shelf (Rutherford et al., 2021; Rutherford & Fennel, 2022) or the Laptev Sea in the Arctic (Anderson et al., 2009). Coastal upwelling regions, such as the nearshore California Current, are sources of CO_2 to the atmosphere with a marked seasonality that follows the upwelling dynamics (Dai et al., 2013; Damien et al., 2023; Fiechter et al., 2014; Lachkar & Gruber, 2013; Turi et al., 2014). Tropical systems, such as the Gulf of Mexico (Laurent et al., 2017; Xue et al., 2016) and the South China Sea (Wan et al., 2022), are mostly identified as weak CO_2 sources with weak seasonal variability (Dai et al., 2022; Laruelle et al., 2014, 2015; Roobaert et al., 2019). Our knowledge of N_2O and CH_4 variability in the global coastal ocean is more limited, but gap-filled products and global models suggest that N_2O and CH_4 annual emissions strongly vary between coastal regions (e.g., Ganesan et al., 2020; Stell et al., 2022; Weber et al., 2019; Yang et al., 2020). These products and models offer a remarkable opportunity to establish a greenhouse gas budget for the global coastal ocean and improve our understanding of its spatial and seasonal variability.

Rising atmospheric CO_2 levels influence coastal CO_2 uptake on multi-decadal time-scales. Prior syntheses at the global scale including RECCAP (Bauer et al., 2013; Cai et al., 2006; Chen et al., 2013; Laruelle et al., 2010; Regnier et al., 2013) and at the regional scale (Fennel & Testa, 2019; Legge et al., 2020; Liu et al., 2018) clearly support the view that the coastal ocean is currently a sink of atmospheric CO_2, but the extent to which it has changed on longer time-scales remains controversial (see Dai et al., 2022, for a review). Mackenzie et al. (2005) from a modeling perspective and later Cai (2011) from observations first hypothesized that the potential of the coastal ocean to act as a sink for CO_2 might be increasing with time. This view is increasingly supported by time series analyses that suggest that trends in sea surface pCO_2 are overall weaker than the atmospheric pCO_2 trend in most coastal regions. This finding further implies an intensified CO_2 uptake or decreased outgassing, although potential trends in winds and sea ice may also play a role (Bauer et al., 2013; Dai et al., 2022; Laruelle et al., 2018; Wang et al., 2017). However, exceptions have been identified in regions where coastal ocean pCO_2 increases at a similar rate (i.e., near-zero changes in the flux) or even at higher rates (i.e., reduced CO_2 uptake or intensified outgassing) than atmospheric pCO_2 (e.g., California Current, South and Mid Atlantic Bight, Baltic Sea; Dai et al., 2022; Laruelle et al., 2018; Reimer et al., 2017; Schneider & Müller, 2018). The quantification of coastal CO_2 flux trends from observations is, however, still strongly restricted by the limited spatial coverage and/or the relatively short duration of time series.

Global ocean biogeochemical models offer an attractive means of assessing long-term trends in air-sea CO_2 flux densities in the coastal ocean and how they differ from those of the open ocean (Regnier et al., 2022). Two such models, with reasonable agreement in regions where time series are available (0.2–0.5° resolution in Bourgeois et al. (2016); 0.4° resolution in Lacroix et al. (2021)), suggest that the global coastal CO_2 sink density has increased at a slightly slower rate than the open ocean CO_2 sink since the preindustrial era, even when accounting for increasing global nutrient sources via river and atmospheric transport (Lacroix et al., 2020). However, both models have important limitations and potential biases related to their representation of fine-scale hydrodynamics of shelf circulation and biophysical processes that impact biogeochemical cycling in the shallow ocean (Mathis et al., 2022; Rutherford & Fennel, 2018).

In this second phase of the Regional Carbon Cycle Assessment and Processes (RECCAP2), we aim to address gaps in our understanding of air-sea greenhouse gas fluxes for the global coastal ocean. Our objectives are threefold. First, we revisit the estimate of the net coastal ocean CO_2 flux and combine it with CH_4 and N_2O emissions to derive a global climatological coastal ocean budget of greenhouse gas fluxes (Section 3.1). Second, we
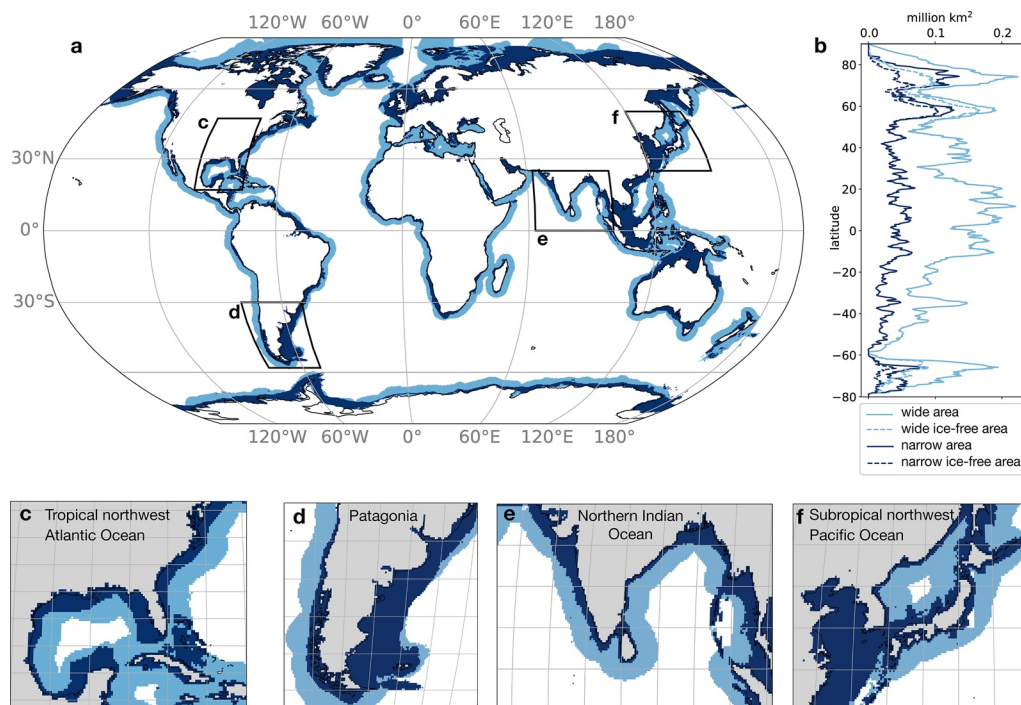
Figure 1. (a) Coastal masks used in this study for the wide (dark + light blue) and narrow (dark blue) coastal oceans, (b) Surface area (in km^2) at each latitude in the wide (light blue) and narrow (dark blue) coastal ocean masks (solid lines) and the 1998–2018 averaged sea-ice free surface area (dashed lines). (c–f) Insets showing the extent of the narrow and wide coastal oceans in four coastal regions. Sea ice coverage used in b is from NOAA OISST. See Methods for details.

analyze the spatial and seasonal variability in the CO_2 flux density and how it might differ from that of the open ocean and examine spatial patterns in coastal CH_4 and N_2O fluxes (Sections 3.2 and 3.3). Third, we investigate trends in the coastal CO_2 flux over the last four decades (Section 3.3). This synthesis complements the global ocean RECCAP2 chapter (DeVries et al., 2023), which includes the coastal ocean area, but does not specifically address the spatio-temporal dynamics of coastal CO_2 fluxes or present an integrated budget of CO_2, N_2O and CH_4 fluxes. We consider the net contemporary air-sea fluxes (natural + anthropogenic) of CO_2, N_2O and CH_4 using the 1998–2018 period (except if specified otherwise) over the coastal ocean but exclude estuaries and coastal vegetation, which are examined in the RECCAP2 synthesis of Rosentreter et al. (2023). Our approach combines observation-based and model-based estimates with different strengths and limitations discussed in the method and discussion sections.

2. Methods

2.1. Coastal Ocean Definition and Analysis Period

Different definitions of coastal oceans are used in the literature (Chen et al., 2013; Laruelle et al., 2017). We use two definitions of the coastal ocean. We primarily use a "wide" coastal ocean definition following Laruelle et al. (2017), where the seaward boundary is 300 km from shore or the 1,000-m isobath, whichever is further from shore, amounting to a total coastal ocean area of 77.2 million km^2 (Figure 1). This wide delineation of the shelf allows us to include the effect of upwelling systems and deep arctic shelves on the shelf greenhouse gas budget, which are only partly included in the narrow definition (Laruelle et al., 2017). We also use a "narrow" coastal ocean definition, which is delimited by the shelf break (defined as the isobath with maximum slope increase in the 0–1,000 m interval) and amounts to a total area of 28 million km^2 (see details in Laruelle et al., 2013, 2014). The landward boundary in the masks used to define the narrow and wide coastal oceans excludes estuaries and coastal vegetation, which are described in the RECCAP2 chapter of Rosentreter et al. (2023), but includes greenhouse gas uptake and emissions from large river plumes. The partitioning of coastal vegetation between estuarine systems and very nearshore shelf environments is poorly known, especially for submerged vegetation

Table 1
Description of Observation-Based Products Used in This Study, Including the Wind Speed Product and Gas Exchange Coefficient (k_w) Formulation Used to Compute the Fluxes

Product	Gases	Land-sea inputs	Domain	Frequency/period in this study	Horizontal resolution	Wide area (million km^2)	Wind speed and k_w	Reference
Carboscope-1	CO_2	N/A	Global	Mon[a] 1998–2018	1°	73.9	JRA55-do v1.5.0 W92[b]	Rödenbeck et al. (2022)
CMEMS*	CO_2	N/A	Global[c]	Mon 1998–2018	1°	55.8	ERA5 W14[b]	Chau et al. (2022)
Coastal-SOM-FFN	CO_2	N/A	Global	Mon 1998–2015	0.25°	77.2	ERA-interim H11	Roobaert et al. (2019)
Coastal-SOM-FFN-k_w	CO_2	N/A	Global	Mon 1998–2015	0.25°	77.2	JRAv1.3 W92	
Merged-SOM-FFN	CO_2	N/A	Global	Mon 1998–2015	0.25°	77.2	ERA-interim H11	Landschützer et al. (2020)
Yang-N2O	N_2O	N/A	Global	Mon 1998–2015	0.25°	73.4	ERA-5 W14[b], L13[b]	Yang et al. (2020)
Weber-CH4	CH_4	N/A	Global	Ann 1999–2016	0.25°	73.7	ERA-5 W14[b], L13[b]	Weber et al. (2019)
MARCATS-N2O & MARCATS-CH4	N_2O, CH_4	N/A	Global	Ann 1980–2016	Regional[d]	77.2	NCEP II N00	Kock and Bange (2015)

Note. W92, H11, W14, L13, N00 stands for k_w-formulations from Ho et al. (2011), Liang et al. (2013), Nightingale et al. (2000), and Wanninkhof (1992, 2014) respectively. Mon and Ann stands for monthly and annual mean frequencies. Wide coastal areas are calculated after the products and models have been regridded on the 0.25° × 0.25° grid. Further details and references on observation-based products and models are provided in Supporting Information S1.
[a]From originally daily. [b]Scaled to global ocean mean value of 16.5 cm/hr. [c]Missing Arctic filled with Coastal-SOM-FFN climatology north of 75°N. [d]No gap filling, one value per MARgins and CATchments Segmentation (MARCATS).

such as seagrasses. In RECCAP2, their contribution to the greenhouse gas balance was estimated in the study by Rosentreter et al. (2023) and explicitly excluded from the present study to avoid double counting issues. The seagrass greenhouse gas flux, however, might slightly overlap with the present shelf estimate, as some of the greenhouse gas data used here might record the effect of the submerged vegetation on the air-water exchange. Note that the RECCAP2 global ocean chapter of DeVries et al. (2023) includes the surface area of the coastal ocean, that is, the CO_2 fluxes reported here should not be added to the global ocean CO_2 flux (global ocean chapter does not report CH_4 and N_2O fluxes). See Figure 1 for maps area latitudinal distribution of the narrow and wide coastal ocean waters.

The analysis is done over the 1998–2018 period to maximize the number of models and observation-based products available (see Tables 1–3 for periods covered by models and observation-based products). Note that this period differs from the one used in the open-ocean RECCAP2 studies that analyze oceanic CO_2 fluxes since 1985. All trends are calculated as linear trends over the 1998–2018 period.

2.2. Data Sets

We use observation-based and process model-based estimates because they have different strengths and limitations. Notably, gap-filled global observational-based products rely on machine learning algorithms or a mixed-layer model to fill the gaps of observations that are often too sparse to capture the full range of spatio-temporal variability in coastal regions (except in densely sampled regions such as major parts of the North American and European ocean margins), and are highly sensitive to the wind product and the choice of the gas exchange coefficient formulation (e.g., Roobaert et al., 2018). In contrast, ocean biogeochemical models can be associated with systematic biases. For instance, only some of the models used here include land-sea riverine

carbon inputs which sustain an oceanic CO_2 outgassing flux, and land-sea nutrient inputs which would yield an opposing biologically-driven oceanic CO_2 uptake in coastal ocean waters (Gao et al., 2023; Hauck et al., 2020; Regnier et al., 2022; Resplandy et al., 2018, see Tables 1–3).

2.2.1. Observation-Based pCO₂-Products

We use 4 global pCO_2-products that provide global monthly gridded surface ocean pCO_2 (noted pCO_2 here) and air-sea CO_2 flux fields based on observations from the SOCAT database, which compiles surface ocean pCO_2 observations and provides a subset after quality control (Bakker et al., 2016, 2022). Three of them use neural network-based interpolation methods: Coastal-SOM-FFN (Laruelle et al., 2017; Roobaert et al., 2019, 2022), merged-SOM-FFN (Landschützer et al., 2020) and CMEMS-LSCE-FFNN (which we refer as CMEMS, Chau et al., 2022), while the fourth product, Carboscope-1, uses a simple statistical representation of mixed-layer biogeochemistry fitted to the pCO_2 data (Rödenbeck et al., 2022). All these products are using SOCAT pCO_2 observations and are therefore not independent (see Supporting Information S1 for details on SOCAT versions and Figure S1 in Supporting Information S1 for SOCAT data coverage). In particular, the Merged-SOM-FFN product merged the Coastal-SOM-FFN (Laruelle et al., 2017) with an open ocean SOM-FFN product (Landschützer et al., 2014) to produce a global ocean product; the Coastal-SOM-FFN and Merged-SOM-FFN are therefore identical in the nearshore coastal region and only differ in the more offshore band of the wide coastal domain (see details in Landschützer et al., 2020). Coastal-SOM-FFN (and therefore also the near-shore product in Merged-SOM-FFN) was designed for the coastal ocean and uses coastal SOCAT data for their neural network training. In the three other products that use both open ocean and coastal ocean data (i.e., CMEMS, Carboscope-1 and offshore portion of Merged-SOM-FFN), the coastal estimate may be strongly influenced by open-ocean information extrapolated toward the coast. See Tables 1–3 and Supporting Information S1 for details on pCO_2-products (e.g., period, wind speed product, gas exchange formulation).

Carboscope-1 and CMEMS products resolve interannual variability over the whole 1998–2018 period and may be used to estimate decadal trends, while Coastal-SOM-FFN and Merged-SOM-FFN provide a 1998–2015 monthly climatology and do not resolve interannual variability. pCO_2-products often have unrealistic pCO_2 values under sea-ice (Laruelle et al., 2017). We therefore used the sea-ice fraction from the NOAA-OISST product (Reynolds et al., 2007) to mask pCO_2 and CO_2 flux values under sea-ice in the four products. We mask both to maintain consistency, but this method should not impact the flux dramatically since it is often inhibited by sea-ice in flux formulations. In this study, we also filled in the missing values north of 75N in CMEMS using the Coastal-SOM-FFN climatology. This approach only marginally impacts the results (adds -0.03 PgC year^{-1} to the wide coastal ocean net CO_2 flux) because the surface area north of 75N contributes 5 million km^2 to the wide coastal ocean (6% of the total wide area) but only 1.4 million km^2 is ice-free on average for the entire study period. This filled-in version of CMEMS is referred to as CMEMS* and we report no long-term trend in the Arctic for this product.

We also illustrate the sensitivity of the flux in pCO_2-products to the choice of the wind speed product and gas transfer coefficient (k_w) formulation (e.g., Roobaert et al., 2018) by presenting a second version of the Coastal-SOM-FFN flux product but with a different wind product and k_w (labeled Coastal-SOM-FFN-k_w) in which the CO_2 flux is calculated as $F = k_w \, Ko \, (pCO_{2a} - pCO_2)$ where Ko is the gas solubility and pCO_{2a} the atmospheric pCO_2. The default version of Coastal-SOM-FFN uses the ERA5 wind speeds and the k_w formulation from Ho et al. (2011), whereas Coastal-SOM-FFN-k_w uses JRA55v1.3 winds and the Wanninkhof (1992) k_w formulation (i.e., wind and formulation used in some ocean biogeochemical models, see Tables 1–3 for details on k_w parametrization and wind products used in models and products). The four pCO_2-products are used for the analysis of the wide and narrow coastal oceans, and the three pCO_2-products that extend outside the coastal domain are used for the open ocean (CMEMS*, Merged-SOM-FFN, and Carboscope-1). Coastal-SOM-FFN-k_w is shown only in the wide coastal ocean for discussion and is not used to compute the pCO_2-product median.

2.2.2. Observation-Based N₂O and CH₄ Flux Products

We used two observation-based estimates of the N_2O and CH_4 fluxes. In each case, we use an estimate based on simple extrapolation of the MEMENTO (MarinE MethanE and NiTrous Oxide) database to the 45 MARgins and CATchments Segmentation (MARCATS, Figure S2 in Supporting Information S1) coastal regions (referred to as MARCATS-N2O and MARCATS-CH4 Kock & Bange, 2015), and an estimate that extrapolates MEMENTO and supplementary observations to global 0.25° climatology using supervised machine learning

models (Weber et al., 2019; Yang et al., 2020, referred to as Weber-CH4 and Yang-N2O). The MARCATS-N2O and MARCATS-CH4 products provide an annual mean value based on data from 1980 to 2016, Yang-N2O provides monthly climatology for 1988–2017 and Weber-CH4 an annual mean value for 1999–2016 (Table 1). In Yang-N2O surface N_2O disequilibrium was extrapolated globally using an ensemble of 100 Random Regression Forest (RRF) models, and in Weber-CH4 surface CH_4 disequilibrium was extrapolated using 1,000 RRF models and 1,000 Artificial Neural Network models. In both cases, diffusive fluxes were calculated and uncertainty propagated by coupling the mapped disequilibrium to multiple high-resolution wind reanalysis products (two in Yang-N2O, four in Weber-CH4), and multiple piston velocity parameterizations (two in Yang-N2O and four in Weber-CH4). These estimates for each gas are not independent as they use the same MEMENTO database. The Yang-N2O and Weber-CH4 products use interpolation techniques to fill observational gaps, but the lack of observations likely leads to large uncertainties in coastal regions.

For CH_4 emissions, the contribution from gas bubble plumes must be taken into account in addition to the diffusive flux (arising from the air-sea difference in partial pressure and a gas exchange coefficient). The MEMENTO database allows the calculation of the diffusive CH_4 flux only because CH_4 from bubble plumes is usually not captured by the conventional CH_4 measurements based on discrete samples or continuous underway measurement systems. However, an estimate of the ebullitive (i.e., bubbling) CH_4 fluxes is, however, included in Weber-CH4 (but not in MARCATS-CH4), by combining previous seafloor emissions estimates with models of bubble transfer to the surface (Weber et al., 2019). We evaluated the uncertainty on the net Weber-CH4 flux in the narrow and wide coastal oceans from the quadrature of uncertainties on diffusive and ebullitive fluxes, using a 50% uncertainty on diffusive flux and a 60% uncertainty on ebullitive flux (Weber et al., 2019). More details on these products can be found in Supporting Information S1.

2.2.3. Ocean Models for CO_2 and N_2O Fluxes

For CO_2, we used 15 ocean general circulation models coupled with biogeochemical modules: 11 are global and 4 are regional models, all covering the study period of 1998–2018 except CCSM-WHOI, which ends in 2017 (see details in Tables 2 and 3). Most global models have native horizontal grid resolutions varying between 0.25° and 1° in the coastal domain, except FESOM-HR which has an unstructured mesh that reaches a higher resolution (see Figure S3 in Supporting Information S1) and MPIOM-HAMMOC, NEMO-PlankTOM12 and CCSM-WHOI which have a coarser resolution of ∼1.5°, ∼2° and ∼3° respectively (Table 2). The regional models covering the Indian Ocean (NYUAD-ROMS-Indian) and Northwest Atlantic Ocean (NW-Atl) have horizontal resolutions of approximately 10 km. The regional models covering the Atlantic (ETHZ-ROMS-Atl) and the Pacific Ocean (ETHZ-ROMS-Pac) have resolution varying in space between 4 and 120 km: the ETHZ-ROMS-Atl telescopes focus on the Amazon outflow region where the resolution is higher and the ROMS-ETHZ-Pac grid focuses on the California Current region (Table 3). We note that some of these models include land-sea nutrient and carbon inputs by rivers, while others do not. Details on these models can be found in Tables 2 and 3 and Supporting Information S1.

For N_2O, we use five models: three of them are also used for CO_2 (CNRM-HR, CNRM-LR, and NEMO-PlankTOM5) and cover the full study period (1998–2018), while the two other models are from the ECCO family (ECCO-Darwin and ECCO2-Darwin) in which the circulation is optimized to capture the distribution of tracers such as temperature and salinity in the ocean but cover shorter periods (ECCO-Darwin for 1997–2013 and ECCO2-Darwin for 2006–2013). See Table 2 and Supporting Information S1 for further details and references of each model.

Model-based analyses in this study use all global models available for the wide coastal ocean (i.e., 11 models for CO_2 and 5 for N_2O), but subsets of models that are eddy-permitting due to their higher native horizontal resolution are used for the narrow coastal ocean (4 models for CO_2: CNRM-HR, FESOM-HR, MOM6, MRI-ESM2.1, and 3 models for N_2O: CNRM-HR, ECCO-Darwin and ECCO2-Darwin, see Table 2). Global averages and integrated fluxes are based on the global models, while regional models were used in addition to the global models for the analysis at the grid-point scale (e.g., maps). Note that we did not examine the seasonal and interannual variability in N_2O and CH_4 fluxes, as these temporal scales are either unresolved (CH_4) or have not yet been analyzed (N_2O) in the coastal ocean.

2.3. Grid Harmonization and Coastal Ocean Waters Area Rescaling

All models and data products were re-gridded from their native grid onto the same 1/4° grid for analysis. However, due to differences in horizontal resolution and ocean-land mask definition, observational products and

Table 2
Description of Global Ocean Biogeochemical Models Used in This Study, Including the Wind Speed Product and Gas Exchange Coefficient (k_w) Formulation Used to Compute the Fluxes

Model	Gases	Land-sea inputs	Domain	Frequency/period in this study	Horizontal resolution	Wide area (million km^2)	Wind speed and k_w	Reference
CCSM-WHOI	CO_2	No	Global	Mon 1998–2017	3.6°lon 0.8–1.8°lat	34.5	NCEP W92	Doney et al. (2009)
CNRM-LR	CO_2,N_2O	Yes	Global	Mon 1998–2018	1°lon 0.3–1°lat	64.8	JRA55-do W14	Séférian et al. (2019)
CNRM-HR	CO_2,N_2O	Yes	Global	Mon 1998–2018	0.25°	71.3	JRA55-do W14	Berthet et al. (2019)
FESOM-LR	CO_2	No	Global	Mon 1998–2018	Unstructured ~1°	75.5	JRA55-do W14	Hauck et al. (2020)
FESOM-HR	CO_2	No	Global	Mon 1998–2018	Unstructured ~0.25°	76.4	JRA55-do W14	Hauck et al. (2020)
IPSL	CO_2	Yes	Global	Mon 1998–2018	1°lon 0.3–1°lat	65	JRA55-do W14	Bopp et al. (2015)
MOM6-Princeton	CO_2	Yes[a]	Global	Mon 1998–2018	0.5°lon 0.25–0.5°lat	63.8	JRA55-do v1.3 W92	Liao et al. (2020)
MPIOM-HAMMOC	CO_2	Yes	Global	Mon 1998–2018	1.5°	44.5	NCEP W14	Ilyina et al. (2013)
MRI-ESM2.1	CO_2	No	Global	Mon 1998–2018	1°lon 0.3–0.5°lat	66.3	JRA55-do W14	Yukimoto et al. (2019)
NEMO-PlankTOM12	CO_2	Yes	Global	Mon 1998–2018	2°lon 0.3–1.5°lat	62.8	NCEP W92	Wright et al. (2021)
NEMO-PlankTOM5	N_2O	Yes	Global	Mon 1998–2018	2°lon 0.3–1.5°lat	62.8	NCEP W92	Buitenhuis et al. (2018)
NorESM-OC2.0	CO_2	Yes	Global	Mon 1998–2018	Nominal 1°	63.9	JRAv1.3 W14	Tjiputra et al. (2020)
ECCO-Darwin	N_2O	No	Global	Mon 1997–2014	1/3°lon	66.5	ERA-Interim W92	Carroll et al. (2020)
ECCO2-Darwin	N_2O	No	Global	Mon 2006–2013	1/6°lon	90.5	ECMWF & JRA-55 W92	Manizza et al. (2019)

Note. W92 and W14 stand for k_w-formulations from Wanninkhof (1992, 2014) respectively. Mon stands for monthly frequency. Wide coastal areas are calculated after the products and models have been regridded on the 0.25° × 0.25° grid. Further details and references on observation-based products and models are provided in Supporting Information S1.

[a]Carbon inputs are only partial and calculated to roughly balance burial.

ocean biogeochemical models can have different coastal ocean areas even after they have been re-gridded to the same 1/4° grid (e.g., wide coastal ocean areas resolved by the models range from 34 to 76 million km^2 vs. 77.2 million km^2 in the mask of Laruelle et al. (2017), see Tables 1–3 and Figure 1). To minimize the effect of this common issue, most results are presented as area-weighted averages of CO_2, N_2O and CH_4 flux densities (per m^2) and surface ocean pCO_2 masked using time varying ice-free surface to account for fractional sea ice coverage (in µatm). We used the ice fraction from the NOAA-OISST product for pCO_2-products and the ice fraction of each individual model for models. For the globally integrated CO_2 flux (in PgC year^{-1}), we used the globally averaged CO_2 flux densities found in each pCO_2-product and model for the narrow and wide coastal oceans and multiplied them by the corresponding coastal area of Laruelle et al. (2017, narrow area = 28 million km^2; wide area = 77

Table 3
Description of Regional Ocean Biogeochemical Models Used in This Study, Including the Wind Speed Product and Gas Exchange Coefficient (k_w) Formulation Used to Compute the Fluxes

Model	Gases	Land-sea inputs	Domain	Frequency/period in this study	Horizontal resolution	Wind speed and k_w	Reference
ETHZ-ROMS-Atl	CO_2	Yes	Regional Atlantic Ocean	Mon 1998–2018	~4–120 km[a]	ERA5 W14	Louchard et al. (2021)
ETHZ-ROMS-Pac	CO_2	Yes	Regional Pacific Ocean	Mon 1998–2018	~4–60 km[b]	ERA5 W14	Desmet et al. (2022)
ACM-NWAtl	CO_2	Yes	Regional Northwest Atlantic (36.3–53.8N; −74.6 to −45.2 E)	Mon 1998–2018	~9.5 km	ERA-interim H06, W14	Rutherford et al. (2021)
NYUAD-ROMS-Indian	CO_2	Nutrients No carbon	Regional Indian Ocean (31.5°S to 31°N; 30°E to 120°E)	Mon 1998–2018	1/10°	ERA-interim W14	Lachkar et al. (2021)

Note. W92, H06 and W14 stand for k_w-formulations from Ho et al. (2006) and Wanninkhof (1992, 2014) respectively. Mon stands for monthly frequency. Further details and references on observation-based products and models are provided in Supporting Information S1.
[a]Highest resolution in Amazon plume and western Africa (2 poles). [b]Highest resolution in California Current (1 pole).

million km^2). We did not apply this area rescaling to the globally integrated fluxes of N_2O and CH_4 given the smaller number of products/models available.

2.4. Calculation of the Global Coastal Radiative Balance

We computed the coastal contribution to the radiative balance by converting global N_2O and CH_4 fluxes (i.e., spatially integrated annual net air-sea flux of greenhouse gases) to a mass of CO_2 equivalent (PgCO$_2$-e). Our analysis is based on contemporary greenhouse gas sinks and sources (not on the historical changes in those sinks/sources from a pre-industrial baseline), and therefore informs on the contribution of coastal oceans to the radiative balance but does not provide any information on the radiative forcing (e.g., perturbations of the pre-industrial radiative balance, Neubauer, 2021).

We used the Intergovernmental Panel on Climate Change (IPCC) Assessment Report 6 (Arias et al., 2021) updated 100-year global warming potential for N_2O (GWP$_{N2O}$ = 273, i.e., the 100-year time integrated radiative forcing from the instantaneous release of 1 kg of N_2O is 273 times larger than the forcing of 1 kg of CO_2) and for CH_4 of non-fossil fuel origin (GWP$_{CH4}$ = 27.2). We calculated two versions of this radiative balance for the wide coastal ocean: one using observation-based flux products only and one using mostly models. The observation-based budget uses the global gap-filled observational products, that is, the 4 pCO$_2$-product median flux for CO_2 (CMEMS*, Carboscope-1, Coastal-SOM-FFN and Merged-SOM-FFN), the Yang-N2O flux for N_2O and the Weber-CH4 flux for CH_4. Uncertainty bars presented for this observation-based balance give the ranges of all products presented in this study, that is, the 4 pCO$_2$-product range for CO_2, the 2 observational-product range for N_2O (Yang-N2O and MARCATS-N2O) and the 2 observational-product range for CH_4 (i.e., the low bound corresponds to the low uncertainty bound of Weber-CH4 and the high bound to the value of MARCATS-CH4). The model-based balance uses the 11 global model median flux for CO_2, the 4 global model median flux for N_2O, and the product-based Weber-CH4 flux for CH_4 as no model is available. Uncertainty bars presented for this model-based balance are the 11-model range for CO_2, the 4-model range for N_2O, and the 2-observational product range for CH_4 (same as the product-based balance described above).

3. Results

3.1. Global Coastal Ocean Greenhouse Gas Fluxes

In this section, we present a compilation of gap-filled observation-based and modeled net air-sea fluxes of CO_2 (4 pCO$_2$-products and 11 global ocean models), N_2O (2 observation-based products and 4 global ocean models) and CH_4 (2 observation-based products) in the global coastal ocean (Figure 2), and assess the contribution of the coastal ocean to the atmospheric greenhouse gas budget by combining the three gases using a single CO_2-equivalent flux (Figure 3).
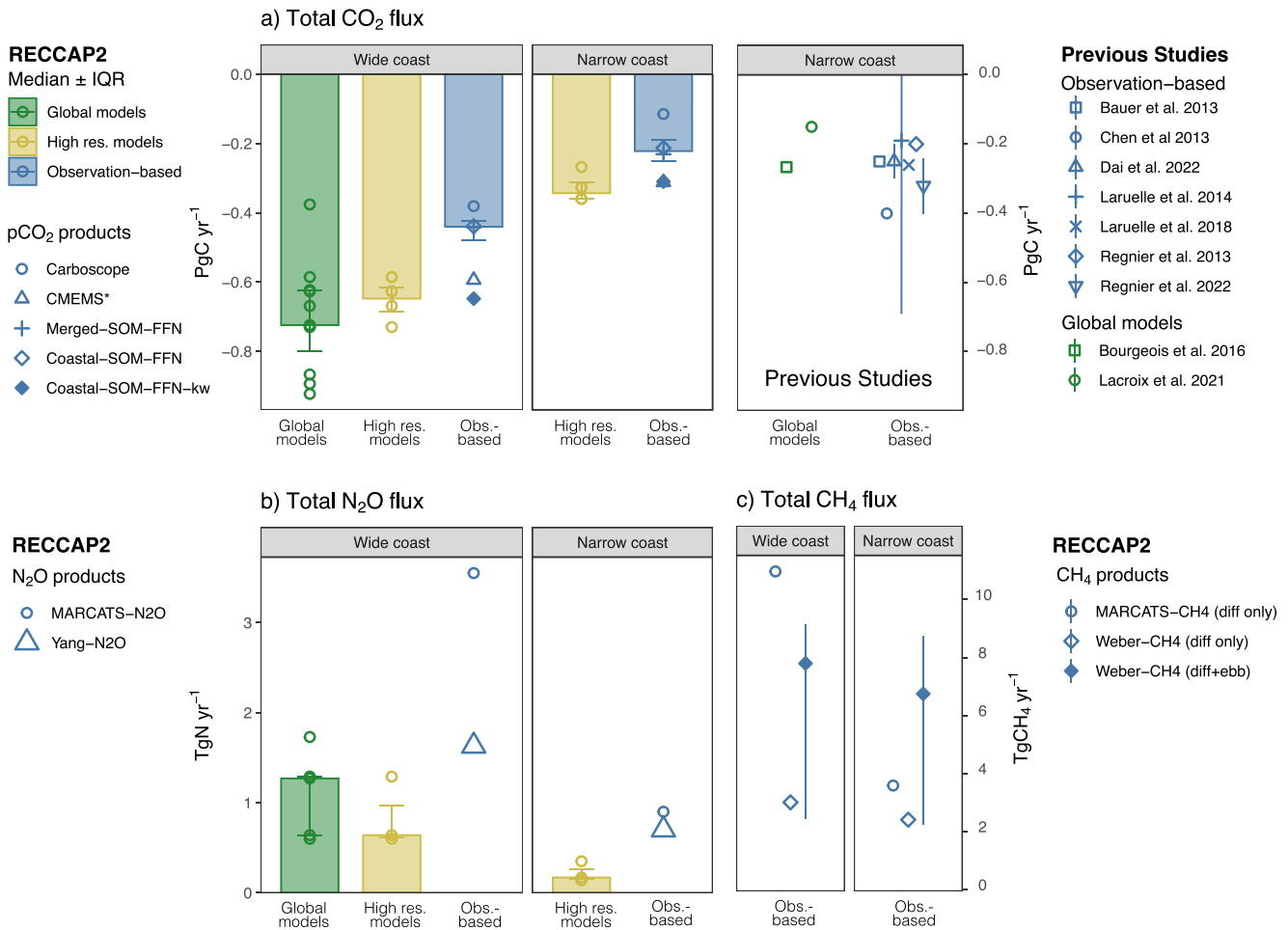
Figure 2. Net globally-integrated coastal fluxes of (a) CO_2 [PgC year^{-1}], (b) N_2O [Tg N year^{-1}] and (c) CH_4 [Tg CH_4 year^{-1}] over the wide and narrow coastal oceans. Figure shows individual products and models (symbols) and their median and interquartile ranges. Models are shown for the full ensemble available (11 models for CO_2 and 4 for N_2O) and a subset of higher resolution models (4 models for CO_2 and 2 for N_2O, see Methods and Table 2 for details). Previous estimates available for the narrow coastal ocean are shown on the right of panel a (see list in Table S2 in Supporting Information S1). Coastal-SOM-FFN-k_w, which is a second version of Coastal-SOM-FFN computed using different wind speed and k_w formulation (filled diamond, see Methods), is not used in the calculation of the pCO$_2$-product median. Weber-CH4 total flux (diffusive + ebullitive) and diffusive contribution (comparable to MARCATS-CH4 flux) are shown in panel (c).

3.1.1. Net Coastal Ocean CO_2 Uptake

The gap-filled pCO$_2$-products yield a weaker net CO_2 uptake than the global ocean biogeochemical models in the wide coastal ocean during the 1998–2018 period (Figure 2a). The pCO$_2$-product estimates (−0.59 to −0.37 PgC year^{-1}) fall at the upper (less negative) end of the model range (−0.92 to −0.38 PgC year^{-1}), and the pCO$_2$-product flux median (−0.44 PgC year^{-1}) is about two thirds of the model median (−0.72 PgC year^{-1}). Most of this model-product mismatch can be attributed to differences in ocean pCO$_2$ seasonality at mid- and high-latitudes (poleward of 25°N and 25°S), which tend to reinforce the northern hemisphere winter uptake in models compared to pCO$_2$-products (see details in Section 3.2.3). These differences in pCO$_2$ seasonality are likely amplified by differences in wind speed and gas exchange coefficient formulation (see Methods and Tables 1–3). For instance, the net CO_2 uptake in the Coastal-SOM-FFN product increases by about 50% and falls closer to the model median when changing the wind speed product (from ERA5 to JRA55) and gas exchange coefficient formulation (from Ho et al., 2011 to Wanninkhof, 1992) used to compute the flux (from −0.44 PgC year^{-1} in Coastal-SOM-FFN to −0.65 PgC year^{-1} in Coastal-SOM-FFN-k_w, blue dot vs. blue circle in Figure 2a, see further details in Section 3.2.3). We also note that using the subset of four global eddy-permitting models (CNRM-HR, FESOM-HR, MOM6, MRI-ESM2.1 with nominal horizontal resolution of 0.5° or higher) yields a weaker net CO_2 uptake (median of −0.65 PgC year^{-1} for only four models vs. −0.72 PgC year^{-1} for all global models), slightly closer to the pCO$_2$-products median (−0.44 PgC year^{-1}) and in relatively good agreement with
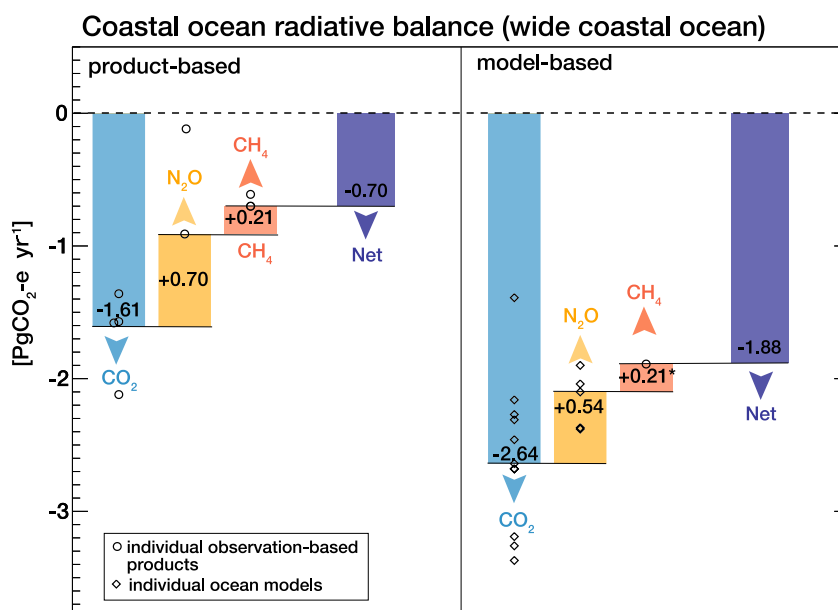
Figure 3. Wide coastal ocean atmospheric radiative balance (using $PgCO_2$-e year^{-1}) based on observational products and models of contemporary CO_2, N_2O and CH_4 fluxes. Observation-based central values are from 4 pCO_2-products, Yang-N2O and Weber-CH4. Model-based central values are from the 11 global models for CO_2 and 4 global models for N_2O, but the Weber-CH4 product is used for CH_4 as indicated by the asterisk (no model available for CH_4, hence minimizing the difference between the two assessments). Individual models and observation-based product estimates are shown by symbols. The net greenhouse gas flux in $PgCO_2$-e year^{-1} corresponds to the sum of the three gases' contributions.

one of the pCO_2-products (-0.59 PgC year^{-1} in CMEMS*, Figure 2a). Other factors that could contribute to the differences between ocean biogeochemical models and pCO_2-products (e.g., land-sea carbon and nutrient inputs) are discussed in Section 4.1.3.

We can compare the net CO_2 flux estimates presented here to prior work using the narrower definition of the coastal ocean ending at the shelf break (28 million km^2), a domain more aligned with the definition used in past studies (Table S2 in Supporting Information S1). For this comparison, we include all pCO_2-products but use only the subset of four global eddy-permitting models with higher horizontal resolution. We find that the narrow coastal ocean accounts for about half of the wide coastal ocean CO_2 uptake (-0.22 out of -0.44 PgC year^{-1} for the 4-pCO_2-product median and -0.34 PgC year^{-1} out of the -0.65 PgC year^{-1} for the 4-model median), while only accounting for about a third of the surface area. The pCO_2-product median in the narrow coastal ocean (-0.22 PgC year^{-1}) is consistent with the most recent observation-based estimates (Dai et al., 2022; Regnier et al., 2022; Roobaert et al., 2019), but the four pCO_2-products span a relatively large range with differences in the order of a factor 2 (-0.12 PgC year^{-1} in Carboscope-1 and -0.31 PgC year^{-1} in CMEMS*, see Table S2 in Supporting Information S1 for estimates). The 4-model median simulates a slightly stronger sink (-0.34 PgC year^{-1}) than these most recent estimates (although it is similar to the estimate of Regnier et al., 2022) but again differences in pCO_2 seasonality, and potentially in wind speed and gas exchange formulation could explain part of this discrepancy. Similar to the wide coastal ocean, the net CO_2 sink increases by nearly 50% in the narrow coastal ocean from Coastal-SOM-FFN to Coastal-SOM-FFN-k$_w$ (from -0.21 to -0.31 PgC year^{-1}, blue dot vs. circle, Figure 2a).

3.1.2. Net N_2O and CH_4 Coastal Ocean Emissions

Estimates of the global coastal emissions of N_2O range from 0.14 to 0.90 Tg N year^{-1} in the narrow coastal ocean and from 0.60 to 3.56 Tg N year^{-1} in the wide coastal ocean (Figure 2b). Part of this considerable variability comes from differences between model-based and observation-based estimates, but also from systematic differences between the two observation-based products (MARCATS-N2O and Yang-N2O). In the wide coastal ocean, the Yang-N2O estimate (1.63 Tg N year^{-1}) falls at the high end of the model estimates (0.60–1.73 Tg N year^{-1}), while MARCATS-N2O yields N_2O emissions that are more than twice the emissions of Yang-N2O (3.56 Tg N year^{-1}, Figure 2b). This finding implies that global ocean biogeochemical model emission estimates are overall lower

than those of the observation-based products. Furthermore, the subset of 3 high-resolution models generally simulates N_2O emissions that are lower than the full set of 5 models and therefore lower than both observation-based estimates (3-model median of 0.64 Tg N year^{-1} vs. 5-model median of 1.27 Tg N year^{-1} for the wide coastal ocean, Figure 2b). In the narrow coastal ocean, the two observation-based estimates are in relatively good agreement (0.90 Tg N year^{-1} in MARCATS-N2O and 0.70 Tg N year^{-1} in Yang-N2O), while the subset of 3 eddy-permitting high resolution global ocean models simulate emissions that are again about 2–4 times lower (0.14–0.35 Tg N year^{-1}). The Yang-N2O product suggests that the narrow coastal ocean accounts for about 50% of the emissions of the wide coastal ocean, while in the subset of 3 global ocean models and MARCATS-N2O it only accounts for about 25% (Figure 2b). We note, however, that the particularly low model values in both the 5-model ensemble and the 3-model high resolution subset are from ECCO-Darwin and ECCO2-Darwin (0.60–0.64 Tg N year^{-1} in the wide and 0.14–0.17 Tg N year^{-1} in the narrow coastal ocean) which are based on the same model and are therefore not independent.

Global CH_4 emissions in Weber-CH4 include both the diffusive and ebullitive (bubbling) components, and are estimated to be 6.80 [2.30–8.8] Tg CH_4 year^{-1} for the narrow coastal ocean and 7.85 [2.50–9.20] Tg CH_4 year^{-1} for the wide coastal ocean (Figure 2c). Note that the flux estimates presented here are observation-based only because no model-based estimates are available. The CH_4 flux from Weber-CH4 is dominated by the ebullitive flux, which occurs mostly in shallow waters of the narrow coastal ocean (accounting for 4.33 Tg CH_4 year^{-1} in the narrow and 4.79 Tg CH_4 year^{-1} in the wide coastal ocean). Subtracting the ebullitive flux from the total Weber-CH4 fluxes results in a CH_4 diffusive flux of 2.46 [1.23–3.69] Tg CH_4 year^{-1} in the narrow coastal ocean, which is in relatively good agreement with the diffusive flux estimated from MARCATS-CH4 (3.64 Tg CH_4 year^{-1}). In contrast, the diffusive flux of 3.06 [1.53, 4.59] Tg CH_4 year^{-1} obtained in the wide coastal ocean in Weber-CH4 has a central value ~3.5 times smaller than the diffusive flux of MARCATS-CH4 (11.02 Tg CH_4 year^{-1}).

3.1.3. Coastal Ocean Radiative Balance

We combined coastal greenhouse gas emissions of CO_2, N_2O and CH_4 to evaluate the coastal contribution to the radiative balance (in CO_2-equivalent, Figure 3). We find that from a net radiative perspective, N_2O and CH_4 coastal emissions offset much of the coastal CO_2 sink, by ~60% in the product-based balance and ~30% in the model-based balance. As a result, the net greenhouse gas flux into the coastal ocean is −0.66 PgCO$_2$-e year^{-1} in the product-based balance (−1.58 PgCO$_2$-e year^{-1} CO_2 flux offset by +0.70 and +0.21 PgCO$_2$-e year^{-1} of N_2O and CH_4) and −1.81 PgCO$_2$-e year^{-1} in the model-based balance (−2.57 PgCO$_2$-e year^{-1} CO_2 flux offset by +0.54 and +0.21 PgCO$_2$-e year^{-1} of N_2O and CH_4, Figure 3). Most of the difference between the product- and model-based radiative balances presented here comes from the stronger CO_2 uptake in the models mentioned above. However, there are very few global coastal N_2O and CH_4 estimates and the spread amongst the products and models are large (1–2 PgCO$_2$-e year^{-1}), indicating that the compensation of the coastal carbon sink could be substantially different from 30%–60% found here.

3.2. Coastal Ocean CO_2 Dynamics

3.2.1. Contrast Between Coastal Ocean and Open Ocean

When averaged globally, models and pCO$_2$-products show lower mean surface ocean pCO$_2$ and more negative CO_2 flux densities (i.e., more uptake) in narrow and wide coastal oceans than in the open ocean (Figure 4). This coastal to open ocean difference is found in the median of the four pCO$_2$ products, which shows an increase in global mean sea surface pCO$_2$ from the narrow coastal ocean to the wide coastal ocean (+15 µatm from 350 to 365 µatm) and from the wide coastal ocean to the open ocean (+7 µatm from 365 to 372 µatm for the 1998–2018 period, Figure 4a). The only pCO$_2$-product among the four without this apparent gradient is Carboscope-1, likely because of potential biases in the coastal Arctic Ocean (pCO$_2$ values generally higher in Carboscope-1 than in other pCO$_2$-products and models).

The 11-model median simulates slightly higher ocean pCO$_2$ than the product median but it also captures an increase in global mean pCO$_2$ from a wide coastal ocean to open ocean (+6 µatm from 369 to 375 µatm) similar to the pCO$_2$-products. The 4-model median (subset of eddy-permitting higher resolution models) also shows a consistently lower mean pCO$_2$ in the narrow coastal ocean (363 µatm), compared to the wide coastal ocean (370 µatm) and the open ocean (373 µatm). Thus, although observation-based and modeled pCO$_2$ values show

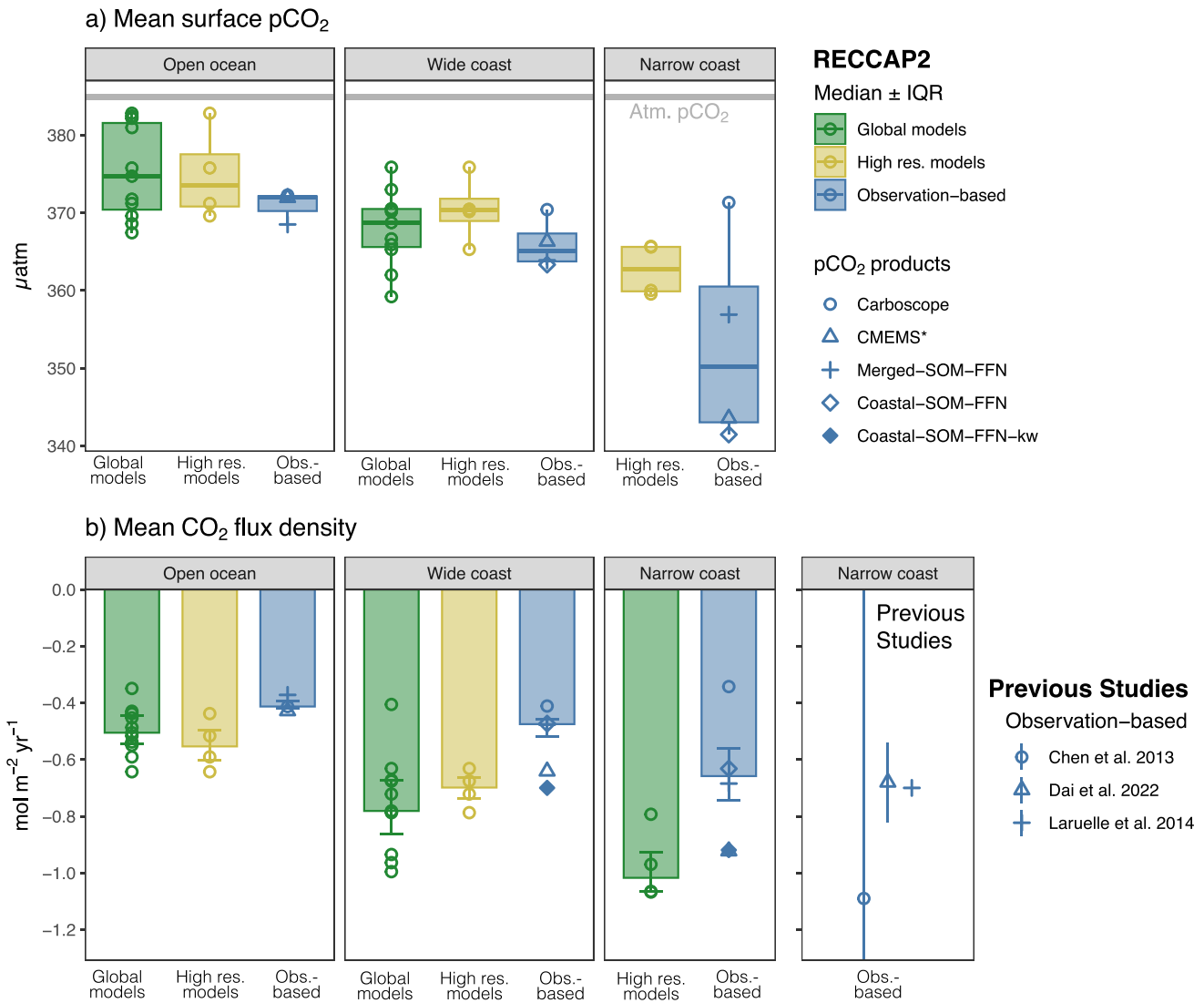**Figure 4.** Comparison of globally-averaged (a) sea surface pCO_2 [μatm] and (b) flux density [mol C m^2 year^{-1}] averaged over open ocean, wide coastal and narrow coastal ocean waters in pCO_2-products and ocean models. Figure shows individual products and models (symbols) and their median and interquartile ranges. Models are shown for the full ensemble available (11 models) and a subset of higher resolution models (4 models, see Methods and Table 2 for details). Previous estimates available for the narrow coastal ocean are shown on the right of panel (b). Coastal-SOM-FFN-k$_w$, which is a second version of Coastal-SOM-FFN computed using different wind speeds and k$_w$ formulation (filled diamond, see Methods), is not used in the calculation of the pCO_2-product median.

discrepancies in the mean within each domain, the narrow coastal to open ocean differences derived from observations and models are in remarkable agreement, and amount to about 10–15 μatm. This apparent coastal to open ocean gradient could be interpreted as decreasing pCO_2 landward, but should be interpreted carefully. As shown previously for the coastal-SOM-FFN product (Roobaert et al., 2019), this coastal to open ocean difference is attributable to the increasing contribution of polar waters, characterized by lower flux densities and stronger sinks, to the total surface area from open ocean to narrow coastal domains (polar coastal ocean waters account for 29% of the narrow coastal ocean, 17% of the wide coastal ocean and 2% of open ocean waters, contributions calculated as the percentage of ice-free surface area located poleward of 50° based on NOAA's OISST ice product, Figure 1).

A consequence of these coastal-to-open ocean differences in sea surface pCO_2 is that the mean partial pressure difference with the atmosphere (mean pCO_{2a} of 385 μatm for 1998–2018) is higher in the coastal ocean than in the open ocean. As a result, air-sea CO_2 flux densities are lower (stronger uptake) in the narrow coastal ocean (−1.02 and −0.66 mol m^2 year^{-1} for 4-model and 4-product medians) than in open ocean waters (−0.55 and

-0.41 mol m^2 year^{-1} for 4-model and 4-product medians, Figure 4b). In between, the wide coastal ocean shares characteristics of narrow coastal ocean and open ocean waters and is characterized by intermediate CO_2 flux densities (-0.70 and -0.48 mol m^2 year^{-1} for 4-model and 4-product medians, Figure 4b).

3.2.2. Spatial Variability in Coastal Ocean CO_2 Sources and Sinks

Coastal air-sea CO_2 flux densities are characterized by latitudinal gradients captured by both pCO$_2$-products and models (Figure 5). Mid- and high-latitude regions (poleward of 25° of latitude) are characterized by annual mean surface ocean pCO$_2$ lower than the atmosphere (pCO$_{2a}$ = 385 ppm for 1998–2018) and thus by oceanic CO_2 uptake, whereas tropical coastal oceans (equatorward of 25° of latitude) are generally associated with pCO$_2$ similar or slightly higher than the atmospheric level and weak or near-zero CO_2 outgassing (Figure 5 and Figure S4 in Supporting Information S1). When averaged latitudinally over the wide coastal ocean, models and products follow a similar pattern, with most negative flux densities (<-1 mol m^2 year^{-1}, i.e., strongest sinks) at mid-latitudes in both hemispheres (50°S–25°S and 25°N–50°N) and high latitudes in the northern hemisphere (50°N–80°N), and weak sources in the tropical band (typically between 0 and 0.5 mol m^2 year^{-1} in 25°S–25°N, Figure 6a).

Largest departures between pCO$_2$-products and models are found in the northern mid- and high latitudes, where the model median flux densities are often more negative (stronger sink) than the pCO$_2$-product median (down to -4 mol m^2 year^{-1} in models vs. -2 mol m^2 year^{-1} in pCO$_2$-products, Figure 6a). These systematically more negative flux densities in the models extend over large coastal areas of the northern hemisphere, including the shelves of western boundary currents (Gulf Stream and Kuroshio), the Norwegian Sea and the southern Greenland basin (blue colors in Figure 5c), and therefore largely explain the stronger globally integrated coastal sink found in the model median (Figure 2a). These northern hemisphere regions are relatively well sampled by the SOCAT pCO$_2$ database (Figure S1 in Supporting Information S1). In regions such as the coasts of Japan and eastern US, the comparison of SOCAT pCO$_2$ data to the pCO$_2$-product and model medians suggests that models are indeed underestimating ocean surface pCO$_2$ and that the model-product difference might be largely attributable to model biases (Figure S5 in Supporting Information S1).

Models and pCO$_2$-products also differ on Antarctic shelves, in particular at the tip of the Antarctic Peninsula (around 60°S which is also relatively well sampled compared to the rest of the coastal ocean) where models simulate a weak sink (about -1 mol m^2 year^{-1}) but pCO$_2$-products show a weak source (about $+1$ mol m^2 year^{-1}, Figures 5 and 6a) supported by the comparison to the raw SOCAT data indicating that the model median underestimate surface ocean pCO$_2$ in this region (Figure S6 in Supporting Information S1). In the Antarctic Peninsula, however, the model-product mismatch is confined to a relatively small surface area and the impact on the net global flux is smaller compared to the mismatch found in the northern extratropics. Finally, we note that the model median yields less negative or more positive flux densities (i.e., weaker sinks or stronger sources) in some coastal regions, such as the California Current, Peruvian margin, Sea of Okhotsk, or Hudson Bay (red colors in Figure 5c), which offsets part of the stronger sinks simulated in northern and southern extratropical latitudes in the latitudinal mean and global integral. Comparison to SOCAT pCO$_2$ in the well-sampled California Current suggests that the model median overestimates ocean near-shore pCO$_2$ in the northern part of the region, likely due to the poor representation of the upwelling system, but that the pCO$_2$-product median underestimates pCO$_2$ in the southern part of the region (Figure S6 in Supporting Information S1). This suggests that both pCO$_2$-product bias and model bias might contribute to the model-product difference in this region. In poorly sampled regions, these model-product differences could be attributable to model bias, pCO$_2$-product bias, or both.

3.2.3. Seasonal Variability in Coastal Ocean CO_2 Sources and Sinks

The global coastal ocean is a sink of CO_2 in all seasons (Figures 6c–6f). In the pCO$_2$-products, the seasonal amplitude of the air-sea CO_2 flux is similar in both hemispheres and shows a strong latitudinal contrast between (a) the tropics (25°S–25°N) where the flux is weak and the seasonal amplitude is small (absolute values <1 mol m^2 year^{-1}); (b) the mid-latitudes (50°S–25°S and 25°N–50°N) where the seasonal amplitude is relatively large (absolute values of 1–2.5 mol m^2 year^{-1}) and the sink is stronger in winter and spring; and (c) high-latitudes (poleward of 50°N and 50°S) where the seasonal amplitude is also large (similar to mid-latitudes) but the CO_2 sink is stronger in summer (except in the Arctic, north of 80°N, where the seasonal amplitude is small, Figures 6b–6f).

Global ocean biogeochemical models largely agree with the pCO$_2$-products on the latitudinal patterns of seasonality but differences emerge in the seasonal phasing and amplitude, in particular north of 25°N (Figures 6c–6f).
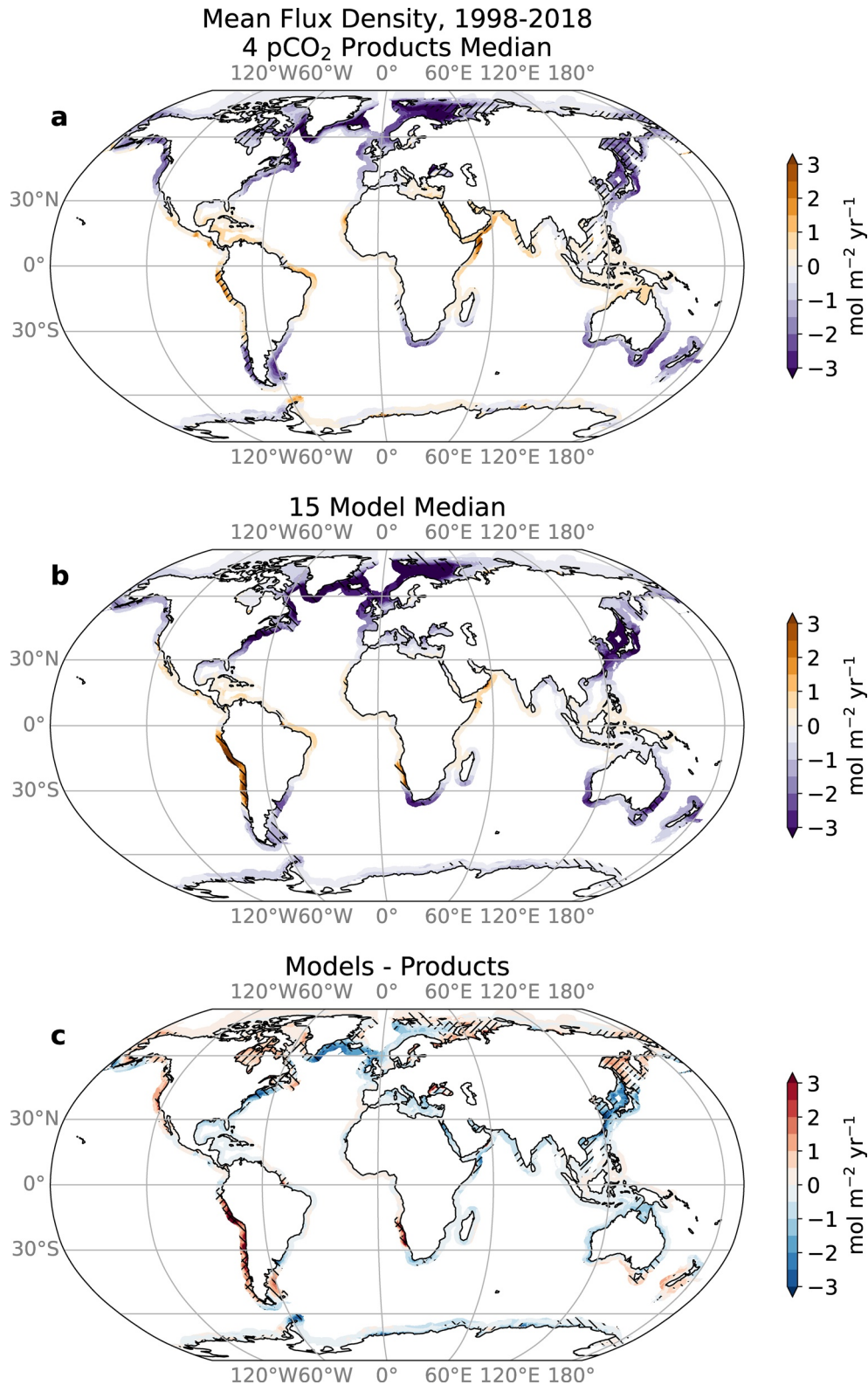
Figure 5. Annual-mean CO_2 flux density [mol C m^2 $year^{-1}$] in the wide coastal ocean for (a) the median across the 4 pCO_2-products, (b) the median across the 15 models, and (c) the difference between model and pCO_2-product medians. The model-median is calculated using the 11 global models and the 4 regional models, where available. Hatching indicates the coastal area with root mean square difference (RMSD) greater than 0.60 mol C m^2 $year^{-1}$ across pCO_2 products (panels a and c) or 0.95 mol C m^2 $year^{-1}$ across models (panels b and c) (in both cases the RMSD values correspond to the 20% of coastal area with highest RMSD).
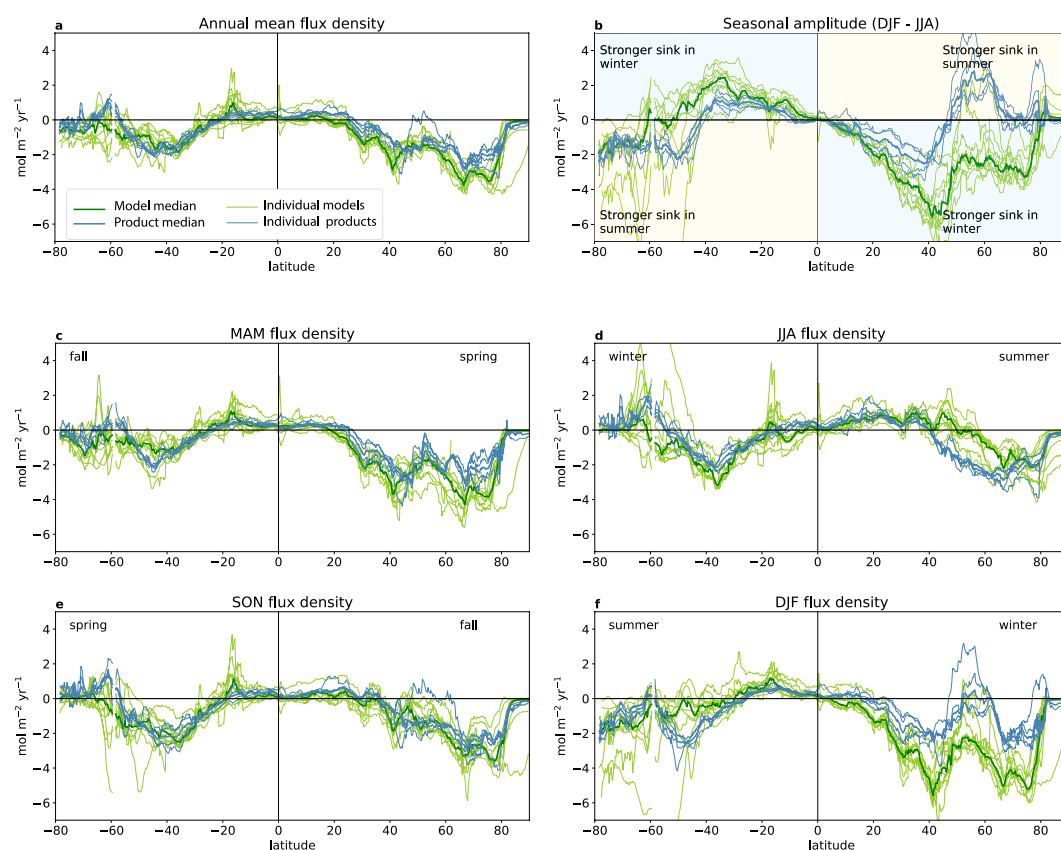
Figure 6. The latitudinal distribution of coastal ocean CO_2 flux and seasonal amplitude (using the wide coastal ocean). The latitudinal distribution of (a) annual mean flux density, (b) seasonal flux density amplitude, calculated as December–February (DJF) minus June–August (JJA), the blue (orange) quadrants indicate when the ocean uptake is stronger in winter (summer). (c–f) Seasonal mean flux density for March–May, JJA, September–November and DJF. Product and model medians are shown with thick lines and the individual 11 global models and 4 products with thin lines. Units are in mol C m^{-2} year^{-1} in all panels for consistency, converting from per month to per year also for the 3-month periods.

The seasonal amplitude of the CO_2 flux is 50%–100% larger in the models at mid-latitudes (despite having a similar phasing, i.e., stronger sink in winter and spring, Figure 6b). In addition, the CO_2 sink is systematically stronger in winter than in summer at all latitudes (except around Antarctica) and does not reproduce the latitudinal change in seasonal phasing obtained in the pCO$_2$-products (from stronger winter uptake in the tropics to stronger summer uptake at high-latitudes, Figure 6b).

The products show little seasonality when averaged globally across coastal ocean waters (net median flux of −0.35 PgC year^{-1} for December–February [DJF] vs. −0.32 PgC year^{-1} for June–August [JJA], Figure 7a). This is largely explained by compensations between mid-latitudes (stronger uptake in winter) and high-latitudes (strong uptake in summer) within each hemisphere (Figure 6), which results in a relatively weak seasonality in both the northern (−0.24 in DJF and −0.22 in JJA) and southern (−0.11 PgC year^{-1} in DJF and −0.10 PgC year^{-1} in JJA) hemi-spheres (Figures 7b and 7c). In the case of the 11-model median, however, this compensation between the mid- and high-latitudes is much weaker and the seasonal cycle is stronger, especially in the northern hemisphere (−0.73 in DJF and 0.00 PgC year^{-1} in JJA, Figures 7b and 7c). As a result, the global coastal ocean in the model median displays a marked seasonality controlled by the seasonality of the northern hemisphere, resulting in a net global coastal sink for DJF (−1.15 PgC year^{-1}) that is about four times the sink for JJA (−0.29 PgC year^{-1}, Figure 7). This model-product difference in CO_2 flux seasonality and specifically the extremely large boreal winter uptake explains the stronger annual mean global CO_2 sink found in the model median compared to the pCO$_2$-products (Figures 2a, 6a, and 7b).

Model-product differences in CO_2 flux seasonality are largely tied to differences in the surface ocean pCO$_2$. The stronger flux seasonality at mid-latitudes in models and the opposed flux seasonality at high latitudes (i.e., stronger uptake in winter in models vs. stronger uptake in summer in products) are both explained by the higher summer ocean pCO$_2$ (leading to weaker summer uptake) and the lower winter ocean pCO$_2$ (leading
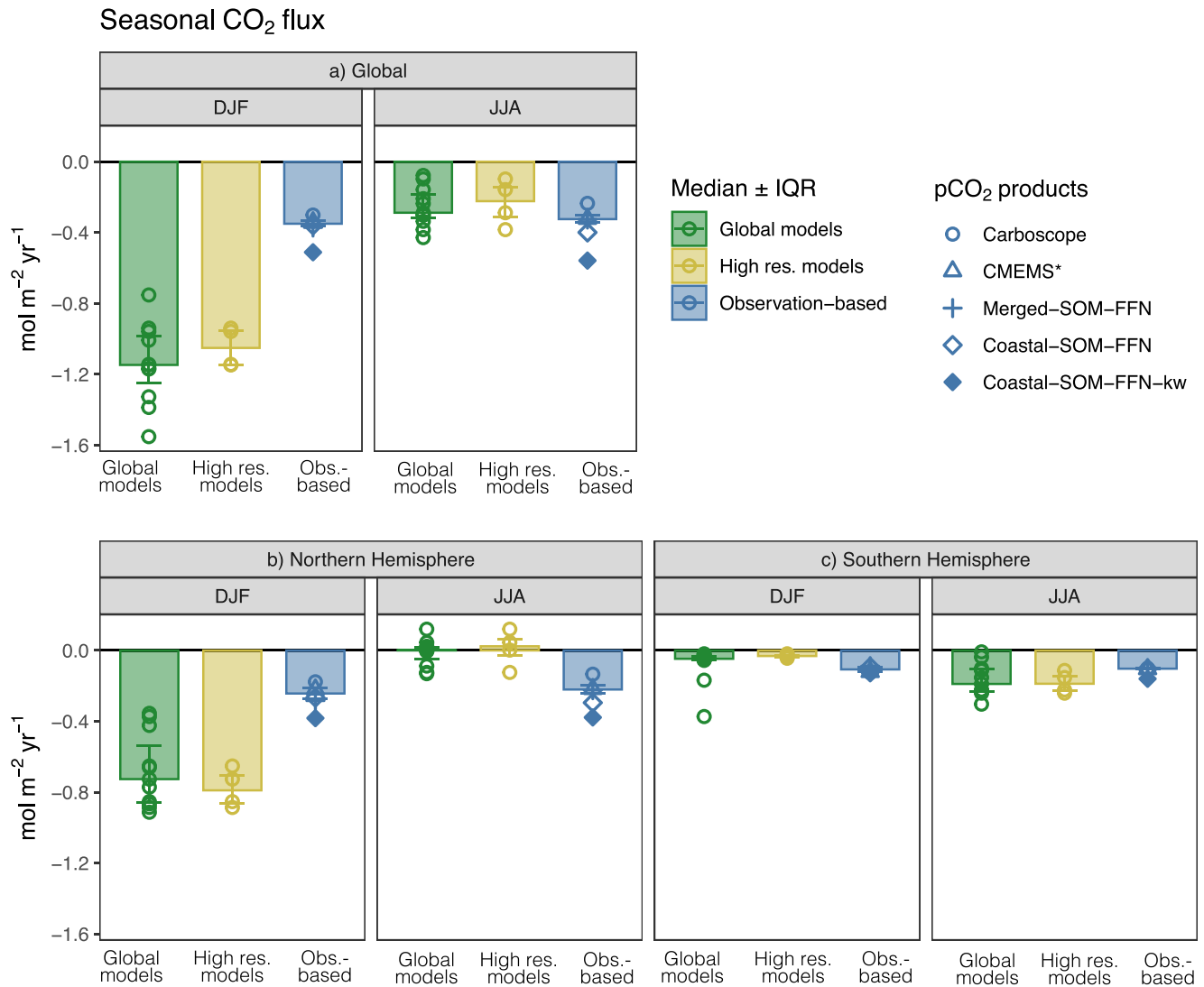
Figure 7. Net air-sea CO_2 flux in December–February and June–August for (a) the global coastal ocean and (b, c) the northern and southern hemispheres. Figure shows individual products and models (symbols) and their median and interquartile ranges. Models are shown for the full ensemble available (11 models) and a subset of higher resolution models (4 models, see Methods and Table 2 for details). Coastal-SOM-FFN-k_w, which is a second version of Coastal-SOM-FFN computed using different wind speeds and k_w formulations (filled diamond, see Methods), is not used in the pCO$_2$-product median. Units are in PgC year^{-1} in all panels for consistency, using a 12-month scale up value for the 3-month periods.

to stronger winter uptake) found in the model median compared to the pCO$_2$-product median (Figure S7 in Supporting Information S1). This systematic model/product difference in seasonality is also found in the open ocean but the amplitude of this mismatch is amplified in the coastal ocean (see Figures S9 and S10 in Supporting Information S1).

These differences in ocean pCO$_2$ seasonality can be amplified by the choice of wind speed and gas exchange coefficient formulation. The comparison of the two Coastal-SOM-FFN versions reveals that both the high-latitude summer uptake and the mid-latitude winter uptake are enhanced in Coastal-SOM-FFN-k_w compared to Coastal-SOM-FFN (Figure 7 and Figure S8 in Supporting Information S1). This enhancement occurs in both hemispheres, but the impact of the northern hemisphere on the global coastal annual mean uptake is larger due to the larger coastal surface area. Finally, we note that some models reproduce better the latitudinal pattern expected from the pCO$_2$-products, in particular the stronger summer uptake at high-latitude in the northern hemisphere (e.g., MOM6-Princeton and MPIOM-HAMOCC, see individual models in Figure S9 in Supporting Information S1 and thin green lines overlapping with thin blue lines in Figure 6).
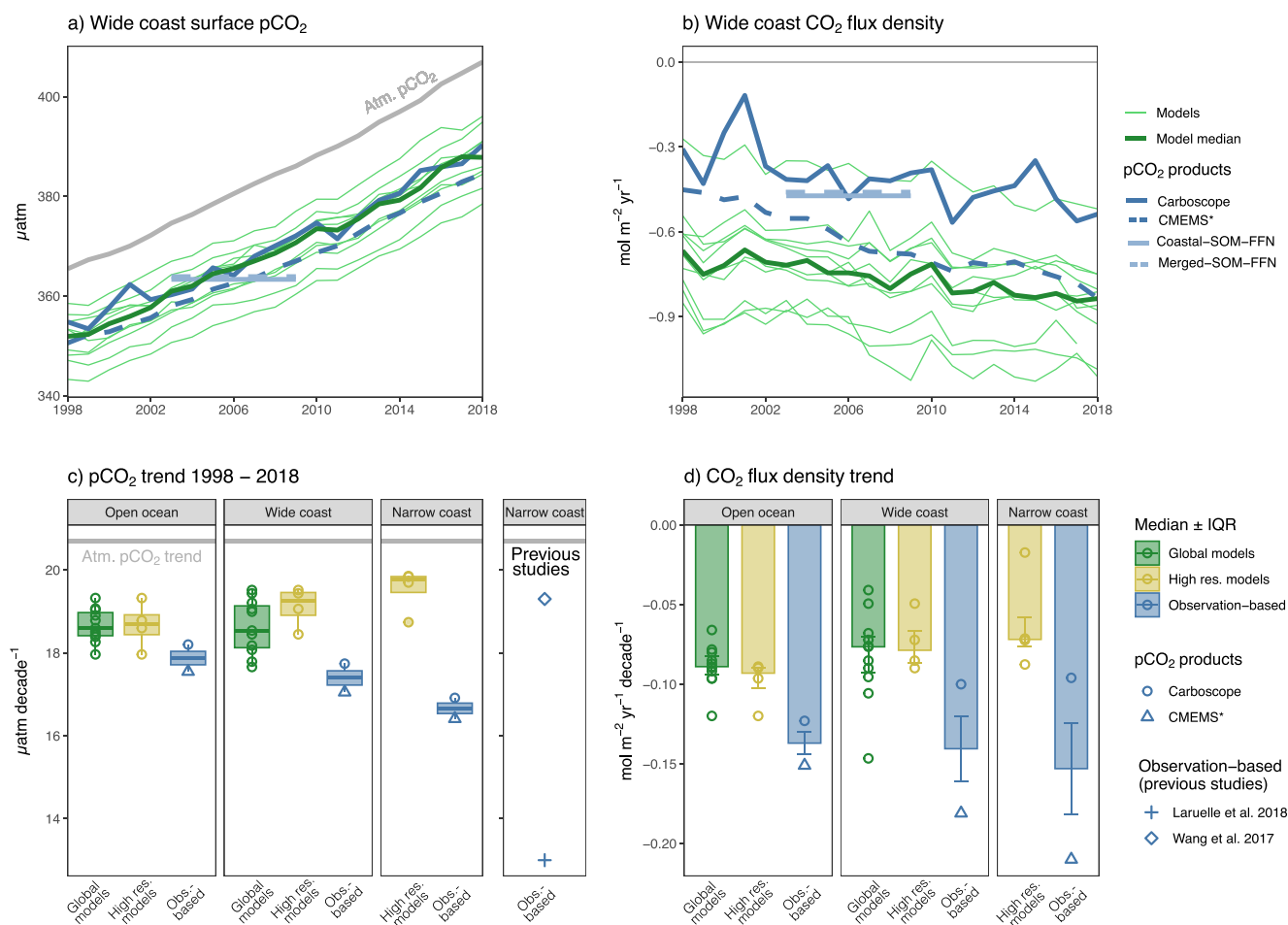
Figure 8. Temporal evolution of the global annual mean (a) surface ocean pCO$_2$ [μatm] and (b) net air-sea CO$_2$ flux density [mol C m^{-2} year^{-1}] in the four pCO$_2$-products (blue lines) and the 11 global ocean models (thin green lines) and model median (thick green lines) in the wide coastal ocean. Trends in (c) ocean surface pCO$_2$ [μatm decade^{-1}] and (d) flux density [mol C m^{-2} year^{-1}] for the open ocean, wide coastal and narrow coastal waters. Panels b and c show individual products and models (symbols), the model median and interquartile range for the full model ensemble (11 models) and a subset of higher resolution models (4 models, see Methods and Table 2 for details). Note that only two time-varying pCO$_2$-based products are available to calculate trends (Carboscope-1 and CMEMS*, other products are monthly 1998–2015 climatologies). Prior estimates are shown on the right of panel c (see Table S1 in Supporting Information S1).

3.2.4. Trends in Coastal Ocean CO$_2$ Flux and Surface pCO$_2$

For the 1998–2018 period, global coastal pCO$_2$ trends are slightly weaker than the atmospheric pCO$_2$ trend (+20.7 μatm/decade) in the two pCO$_2$-products that are time-varying (about +17–18 μatm/decade in the wide coastal ocean) and in the models (+17–20 μatm/decade in the wide coastal ocean; see Figures 8a and 8c). In the narrow coastal ocean, the pCO$_2$ trends from the pCO$_2$-products are lower than in the wide coastal ocean, and fall halfway between the two central values published in previous observation-based estimates (+16–17 μatm/decade vs. +19.3 μatm/decade in Wang et al., 2017 and +13 μatm/decade in Laruelle et al., 2018). In contrast, the pCO$_2$ trends found in the subset of four high resolution ocean biogeochemical models are higher in the narrow coastal ocean (+19.8 μatm/decade) than in the wide coastal ocean, and in good agreement with the highest of the previous observation-based estimate (Wang et al., 2017).

The trend difference between atmospheric and oceanic pCO$_2$ leads to an increase in the coastal carbon sink from 1998 to 2018 in pCO$_2$-products and models (flux density trends between −0.15 and −0.04 mol m^2 year^{-1} per decade in the wide coastal ocean, Figures 8b and 8d). Yet, because the rate of increase in coastal pCO$_2$ is lower in the pCO$_2$-products than in the models, their respective CO$_2$ uptake trend is larger (Figure 8c). This is consistent with the expectation that a slower increase in sea surface pCO$_2$, which does not closely follow the atmospheric pCO$_2$ trend, should result in a stronger increase in the flux density (e.g., Laruelle et al., 2018).

Our results show, however, that pCO_2 trends and flux trends are not directly proportional, suggesting that factors other than pCO_2 variability are at play. These include trends in sea-ice cover (e.g., sea-ice retreat influence on flux trends in the Arctic Ocean) and/or in surface winds (via their effect on the gas exchange transfer velocity). For instance, the Carboscope-1 pCO_2 trends are slightly weaker than the CMEMS* pCO_2 trends in the narrow and wide coastal oceans, and yet the increase in the coastal sink is lower in Carboscope-1 than in CMEMS* (Figures 8c and 8d). Another example of the decoupling between pCO_2 trends and flux trends is found in the coastal to open ocean difference. The global ocean biogeochemical model ensemble simulates smaller differences between atmospheric and oceanic pCO_2 trends in the coastal ocean than in the open ocean, resulting in a weaker increase in the carbon sink in the coastal ocean (following here the expected link between pCO_2 and flux trends, Figures 8c and 8d). In contrast to the models, both time-resolving pCO_2-products reveal higher differences between atmospheric and oceanic pCO_2 trends in the coastal ocean than in the open ocean (Figure 8c), which would suggest a stronger trend in the flux density in the coastal ocean (i.e., a stronger increase in the uptake). This expected increase in the uptake is, however, only found in CMEMS* and not in Carboscope-1 (Figure 8d).

Inconsistencies between pCO_2 trends and flux trends arise from the complex and uncertain interplay between the spatio-temporal changes in ocean pCO_2, wind speed and sea-ice coverage. Trends in ocean pCO_2 and therefore in ΔpCO_2 (difference between coastal ocean surface ocean pCO_2 and atmospheric pCO_2) strongly differ between the two time-varying pCO_2-products (Figure S11 in Supporting Information S1). CMEMS*, as well as the multi-model median, show more negative ΔpCO_2 trends (potentially stronger uptake or weaker sources with time) in mid-to-high latitudes, but less negative or even positive ΔpCO_2 trends in the tropics and in the Arctic (Figure S12 in Supporting Information S1). In contrast, the Carboscope-1 product shows strongly negative ΔpCO_2 trends in the Arctic, and much larger variability in trends at other latitudes. These differences in ΔpCO_2 trends explain, to the first order, the differences in flux density trends (negative ΔpCO_2 trends generally yield negative flux trends, i.e., stronger uptake or weaker sources with time, Figure 9 and Figure S12 in Supporting Information S1).

The ΔpCO_2 trends can be amplified or dampened by trends in wind speed and sea-ice coverage, which are also strongly spatially heterogeneous (see sea-ice trends in Figure S13 in Supporting Information S1). This effect is highlighted by the spatial differences and sometimes even a switch in sign between ΔpCO_2 trends and air-sea CO_2 flux trends in the model median in sea-ice regions (hatching in Figure 9). This is true, for instance, in the Arctic where the ocean models tend to simulate an increase in ocean CO_2 uptake despite a positive trend in ΔpCO_2 (i.e., ocean pCO_2 increases at a high rate than atmospheric pCO_2 which would reduce ocean uptake with constant sea-ice coverage and winds, Figure 9 and Figure S12 in Supporting Information S1). This decoupling between CO_2 flux and ΔpCO_2 in the Arctic is indeed associated with a decrease in sea ice coverage in most models (Figure S13 in Supporting Information S1) and an increase in wind speed in two of the wind products that are widely used in these models (JRA-55 and ERA-5, Figure S14 in Supporting Information S1 and Tables 2 and 3), both effects inducing an increase in the flux with time despite the reduction in ΔpCO_2. These results clearly indicate that the global coastal sinks are increasing. However, the magnitude of this increase, its spatial patterns and how it compares to the open ocean are still uncertain.

3.3. Coastal Ocean Nitrous Oxide and Methane Spatial Variability

The spatial distribution of the coastal N_2O fluxes computed with the observation-based (i.e., Yang-N2O) and the mean of the model-based approaches are shown in Figure 10. Coastal N_2O fluxes are generally positive, indicating that coastal areas are a source of atmospheric N_2O. Flux densities vary considerably, from 0 (=equilibrium with the atmosphere) to about 10 g N m^{-2} $year^{-1}$. The results from Yang-N2O reveal hotspots of N_2O emissions in eastern boundary upwelling systems, the upwelling areas of the northwestern Indian Ocean, the subpolar North Pacific, the Baltic Sea, the Black Sea and the shallow marginal seas of Southeast and East Asia. These are generally characterized by high surface productivity, low subsurface oxygen, and shallow oxyclines. High N_2O emissions from these regions thus likely reflect subsurface water-column production by a combination of nitrification and denitrification pathways, both of which are enhanced in the presence of low O_2 and high remineralization rates, and subsequent transport to the surface by upwelling and mixing processes. Similar hotspot regions are detected in the model-ensemble median, although with somewhat reduced magnitude relative to the observational products, and with the notable exception of marginal seas in Asia and Europe, suggesting
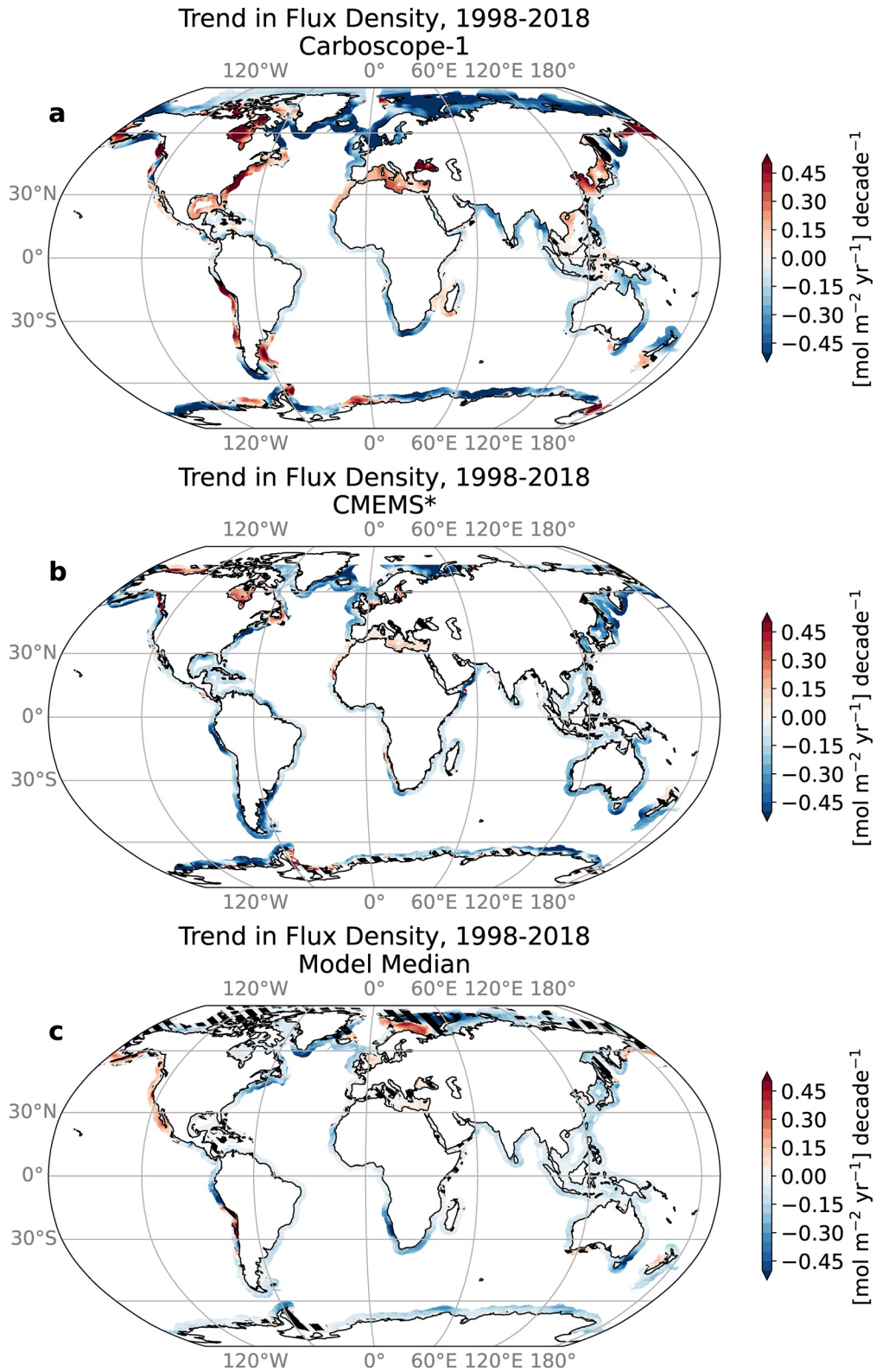
Figure 9.

that global models might not fully capture the nitrogen cycle in these regions, or the mechanisms transporting N_2O-laden waters to the surface.

The model-ensemble also identifies mid-latitude western boundary systems, including the US East Coast, the North Pacific east of Japan, the southeast coast of Australia, and the southeastern tip of Africa, as additional areas of intense N_2O emissions that are not captured by the Yang-N2O product. Notably, these regions are not generally characterized by high surface productivity and low subsurface O_2 as coastal upwelling systems, although vigorous mixing along western boundary currents may favor local N_2O outgassing in the models. Most of these regions are also not densely sampled by observations in the MEMENTO database, in particular along the US, South Africa, and Japan eastern coasts, and thus the Yang-N2O observational extrapolation may be poorly constrained there. The magnitude of the flux in these hotspots often differs among the data products and model-ensemble (Figure 10c). The N_2O flux distributions shown in Figure 10 likely reflect the fact that enhanced coastal N_2O concentrations—and thus enhanced N_2O emissions fluxes—are associated with enhanced land-sea inputs of nitrogen (as nitrate or ammonium) or with upwelling of N_2O-enriched subsurface water masses in upwelling systems.

The spatial distribution of the coastal CH_4 fluxes computed with the observation-based Weber-CH4 product are shown in Figure 11. Coastal CH_4 fluxes are generally positive and range from 0 to 0.4 g CH_4 m^{-2} $year^{-1}$ indicating that coastal areas are a source of atmospheric CH_4. Patterns in CH_4 emissions in Weber-CH4 are largely correlated with water depth, with the most intense emissions cooccuring at depth shallower than 50 m (Figure 11). Indeed, coastal emissions of CH_4 are largely fueled by benthic-sourced biogenic methane, which is produced via methanogenesis in anoxic sediments and diffusively released into the overlying water column (Arndt et al., 2013; Bourgeois et al., 2016; Reeburgh, 2007). The benthic CH_4 source is enhanced in coastal waters where the rapid organic matter flux to the seafloor drives sediment anoxia and rapid sediment accumulation inhibits the growth of methane oxidizing microbes (e.g., Egger et al., 2016). Furthermore, aerobic respiration acts as an efficient sink of CH_4 in the water column (Mao et al., 2022), meaning that transfer from the seafloor to the surface must be extremely rapid if CH_4 is to be emitted to the atmosphere. Ebullition (bubbling) from CH_4-enriched sediments can provide an important alternative pathway for CH_4 to surface (Rehder et al., 1998), but CH_4 is rapidly stripped from rising bubbles (McGinnis et al., 2006) and a small fraction reaches the surface only in shallow water depths. This further strengthens the coastal-offshore gradient in CH_4 emissions and explains why total emissions differ very little between the narrow and wide coast regions in Weber-CH4 (Figure 2c).

We find that coastal CH_4 emissions are further enhanced in hotspots under the significant influence of freshwater discharge (Rosentreter et al., 2021), which, due to their low sulfate concentration, promotes the degradation of organic matter through the methanogenesis pathway. In addition to the biogenic CH_4 production pathway, CH_4 emissions can also be driven by geologically sourced methane originating from shallow seafloor seeps fed by hydrocarbon reservoirs or high-latitude hydrates (Puglini et al., 2020; Ruppel & Kessler, 2017). Overall, the distribution of coastal CH_4 emissions (Figure 11) can largely be understood in terms of water depth, organic matter production and delivery to sediments, and freshwater inputs.

4. Discussion

4.1. Coastal Ocean CO_2 Fluxes

4.1.1. Net CO_2 Uptake and Challenges Tied to Spatial Variability

This study presents a synthesis of the global coastal ocean air-sea CO_2 fluxes combining observational pCO_2-based products and an ensemble of ocean biogeochemical models. The global ocean biogeochemical models yield a net median CO_2 uptake in the wide coastal ocean that is about 0.28 PgC stronger than the one inferred from pCO_2-products for the 1998–2018 period, equivalent to a ~60% stronger sink (−0.44 PgC $year^{-1}$ for products vs. −0.72 PgC $year^{-1}$ for models in the wide coastal ocean). This mismatch of model- and product-based work in the net coastal CO_2 sink arises from a combination of factors, including strong differences in the coastal CO_2 flux

Figure 9. 1998–2018 trend in CO_2 flux [mol C m^{-2} $year^{-1}$] for (a) Carboscope-1; (b) CMEMS* (area north of 75°N removed) (c) multi-model median (global and regional models). Hatching indicates regions where the flux trend has a different sign than the ΔpCO_2 trend (shown in Figure S12 in Supporting Information S1), highlighting the influence of wind and/or sea-ice trends. Negative values indicate that the ocean uptake increases or the ocean outgassing decreases with time (both leading to more carbon accumulation in the ocean). Trends are shown for the only two time-varying pCO_2-based products available (Carboscope-1 and CMEMS* in blue, other pCO_2-based products are monthly climatologies).
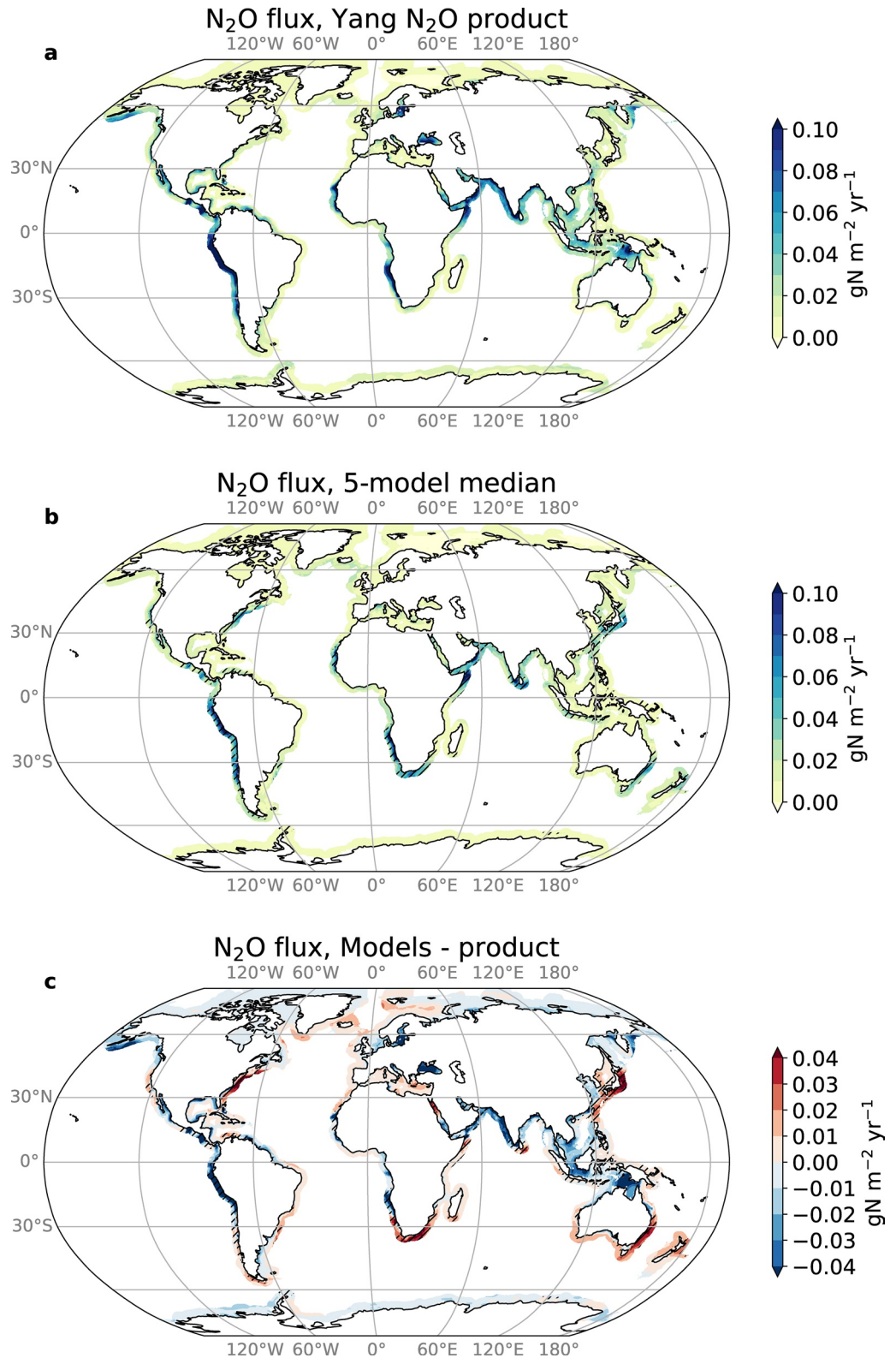
Figure 10. Maps of coastal N_2O flux (in g N m^{-2} $year^{-1}$) from (a) Yang-N2O product, (b) the mean of the 5 global ocean models that simulate N_2O (CNRM-LR, CNRM-HR, ECCO-Darwin, ECCO2-Darwin, and NEMO-PlankTOM5), and (c) the difference between models and the Yang-N2O product. Hatching in panels (b, c) shows where root mean square difference (RMSD) among models exceeds 0.016 g N m^{-2} $year^{-1}$ (RMSD threshold corresponds to the 20% of coastal area with highest RMSD).
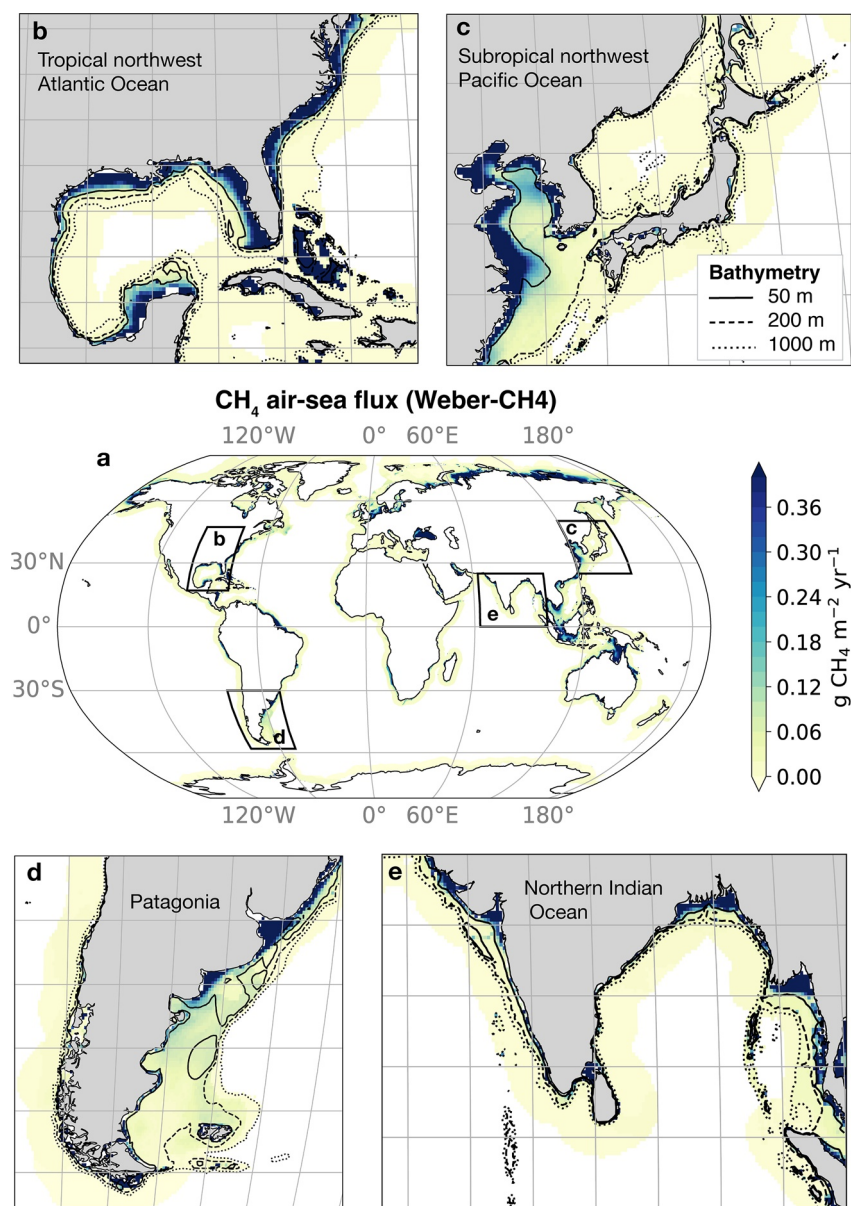
Figure 11. (a) Global maps of coastal CH_4 flux from the Weber-CH4 product (includes diffusive and ebullitive flux, in g CH_4 m^{-2} year^{-1}); (b–e) insets show the CH_4 flux in four coastal regions along with 50, 200 and 1,000 m bathymetry contours. CH_4 emissions are most intense in shallow coastal environments.

seasonality (themselves attributed to differences in ocean pCO$_2$ seasonality and potentially wind speed and gas exchange transfer coefficient formulation) resulting in a stronger wintertime CO_2 uptake in northern subpolar and polar coastal systems in models (see Section 4.1.2).

We find that the subset of global ocean biogeochemical models with the highest spatial resolution yields a slightly weaker net CO_2 uptake (-0.65 PgC year^{-1}) in better agreement with the pCO$_2$-products than the full model ensemble. The small number of models in that subset (4) makes any statistical argument about resolution difficult. Yet, this result suggests that a better representation of fine scale coastal dynamics improves the representation of the CO_2 flux, likely by improving the representation of the physical and biogeochemical processes controlling CO_2 seasonality in the northern hemisphere (Laurent et al., 2021; Rutherford et al., 2021; Rutherford & Fennel, 2022). The horizontal resolution of the global ocean biogeochemical models used in this synthesis (about 1/4° or coarser) is, however, still too coarse to fully capture coastal ocean dynamics (coastal oceans require resolutions of 1/16° or higher, Hallberg, 2013).

This synthesis confirms the hypothesis of prior work that when averaged globally, CO_2 flux densities are more negative (stronger sinks) in the coastal ocean than in the open ocean waters (Dai et al., 2022; Laruelle et al., 2010, 2014; Roobaert et al., 2019). As put forward by Roobaert et al. (2019), we find that the differences between coastal and open ocean flux densities are largely explained by the disproportionate contribution of high latitude systems (generally strong sinks) to the coastal ocean surface area. Global ocean biogeochemical models and pCO_2-products agree relatively well on this coast-to-open ocean contrast in CO_2 flux densities, but recent syntheses of discrete observations (Cao et al., 2020; Dai et al., 2022) find stronger heterogeneity than the global pCO_2-products and global ocean models presented here, suggesting that gap-filling approaches might smooth some of the coastal ocean spatial variability and supporting the fact that higher horizontal resolution is needed to resolve coastal oceans in models (Hallberg, 2013).

4.1.2. Differences in Seasonality Influence the Net Coastal Ocean CO_2 Uptake

The seasonality in the four pCO_2-products used here falls into three latitudinal regimes. Tropical coastal waters (25°S–25°N) are characterized by small seasonal amplitudes and a stronger sink or weaker source in winter, both attributed to the weak seasonal thermal changes that slightly reduce surface ocean pCO_2 in winter (Laruelle et al., 2014; Roobaert et al., 2019). Mid-latitude coastal waters (50°S–25°S and 25°N–50°N) are characterized by larger seasonal amplitudes and a stronger CO_2 sink in winter and spring, likely due to the combined effect of thermal changes which lowers ocean pCO_2 in winter, biological drawdown of dissolved inorganic carbon (DIC) which further lowers pCO_2 during the spring bloom, and the influence of stronger winds in winter (Laruelle et al., 2014; Roobaert et al., 2022). High latitude coastal waters (poleward of 50°N and 50°S) are characterized by seasonal variations similar in magnitude to mid-latitudes, but where the maximum CO_2 uptake occurs in summer in response to intense biological drawdown. The biologically-driven uptake in high-latitude systems peaks a few months later than in mid-latitude systems because of the poleward propagation of the bloom (Ouyang et al., 2020, 2022; Roobaert et al., 2019, 2022; Siegel et al., 2002).

This marked seasonality in CO_2 fluxes contrasts with the RECCAP synthesis, which found very little seasonality in global coastal CO_2 flux densities, although the results were deemed inconclusive because of the sparse data and averaging process required to analyze the data available at the time (Chen et al., 2013). The results found here are, however, consistent with more recent work. In particular, the transition from thermally driven systems in the tropics (stronger winter sinks) to biologically driven systems at high latitudes (stronger summer sinks), and the increase in seasonal amplitude from tropical to high-latitude systems found in the pCO_2-products, are consistent with the global seasonal patterns in the coastal ocean described by Roobaert et al. (2019), the global open ocean seasonality patterns assessed in the framework of RECCAP2 (Rodgers et al., submitted to the RECCAP2 special issue) and supported by field and remote sensing studies at regional scale (Ouyang et al., 2022; Signorini et al., 2013; Tu et al., 2021).

Our synthesis reveals, however, strong differences in seasonality between pCO_2-products and global ocean biogeochemical models. The model median simulates a weak CO_2 flux seasonality in tropical coastal oceans similar to the pCO_2-products, but yields a CO_2 uptake that is stronger in winter at mid- and high-latitudes. This is likely due to a weaker contribution of biologically induced seasonality compared to thermal changes in the models, which would explain the lower surface ocean pCO_2 simulated in winter (due to an underestimated upward transport of remineralized DIC) and the higher pCO_2 simulated in spring/summer (due to a weaker biological drawdown). Part of these systematic differences compensate for the global mean coastal flux (winter vs. summer, northern vs. southern hemisphere), but because the model-product difference is larger in winter in the northern hemisphere, the net CO_2 uptake in the wide coastal ocean is about 60% larger in the model median.

The RECCAP2 chapter on open ocean seasonality (Rodgers et al., submitted to the RECCAP2 special issue) finds a similar systematic bias in model winter-to-summer pCO_2, which they attribute to a generally too small surface DIC seasonal cycle in models compared to observation-based reconstructions. This bias is particularly evident in the subpolar North Atlantic and North Pacific Oceans, where it manifests itself not only as a difference in amplitude but also in phasing. In these regions, the simulated too low DIC seasonality results in a thermal control of the pCO_2 seasonality in the global ocean biogeochemical models and thus in a phase shift of the seasonal pCO_2 cycle compared to the observation-based estimate dominated by non-thermal forcing. This suggests that the systematically stronger winter sink and weaker summer sink found in northern coastal waters in the models are at least partly attributable to general biases in the biogeochemical (e.g., bloom dynamics) or physical (e.g., vertical mixing) components of the ocean models, rather than a characteristic of the models that is specific to the

coastal ocean. See details in the RECCAP2 studies of (Rodgers et al., submitted to the RECCAP2 special issue). Nevertheless, we find that the amplitude of this systematic model/product difference in seasonality is amplified in the coastal ocean (see Figures S9 and S10 in Supporting Information S1).

Differences in ocean pCO_2 seasonality between models and pCO_2 products can be amplified by differences in gas exchange coefficient k_w, either through the influence of winds or the gas exchange coefficient formulation (which are different across the different ocean biogeochemical models and pCO_2-products, Tables 1–3), and maybe to a lesser extent spatio-temporal differences in sea-ice cover (e.g., lower ice cover in some products/models could yield stronger fluxes). In models, the surface pCO_2 and k_w are tightly coupled in the sense that a larger k_w drives down the air-sea pCO_2 disequilibrium and therefore the air-sea CO_2 flux. In contrast, the calculation of the flux in pCO_2 products (except for Carboscope-1 which links fluxes and pCO_2 changes in a mixed-layer carbon budget equation) is done offline without any compensatory effect between k_w and air-sea pCO_2 disequilibrium. Therefore, the observation-based flux assessments are even more sensitive to the choice of the wind and k_w parameterization. For instance, we find that the net global coastal CO_2 uptake in the Coastal-SOM-FFN product is increased by nearly 50% in the wide and the narrow coastal oceans when changing the wind product (from ERA-interim to JRAv1.3) and gas exchange parametrization (from Ho et al., 2011 to Wanninkhof, 1992, see Table 1). These results are in line with published literature that assessed the impact of k_w parametrizations on global air-sea CO_2 fluxes (Boutin et al., 2009; Reichl & Deike, 2020; Roobaert et al., 2018) but highlight that its influence is also crucial in the coastal ocean because of the disproportionate contribution of mid- to high-latitude/high-wind systems in the total coastal area. The sensitivity of CO_2 flux estimates to the k_w parameterizations and their disparate implementation in the different assessments (including among ocean biogeochemical models, Tables 1–3) calls for more consistent approaches in future research. Furthermore, global wind-based gas exchange parameterization might not capture the complexity of the coastal ocean processes, such as the influence of bubbles entrained by wave breaking (Deike & Melville, 2018; Woolf et al., 2019), the presence of high surfactant concentrations (Pereira et al., 2018), or fine scale water-side convection (Gutiérrez-Loza et al., 2022).

4.1.3. Land-Sea Carbon and Nutrient Fluxes

An additional factor that could explain part of the difference in the net CO_2 uptake between pCO_2-products and models is the presence of systematic bias in global ocean biogeochemical models, in particular the contribution of carbon land-sea riverine inputs or the models' horizontal resolution and ability to resolve coastal dynamics. At pre-industrial times (and assuming steady-state consistent with stable ice-core atmosphere CO_2 values; Elsig et al., 2009), the supply of carbon from land must have been balanced by burial in sediments and an outgassing of CO_2 from the ocean to the atmosphere. This land-driven outgassing flux, recently estimated to be 0.65 ± 0.3 PgC year^{-1} (mean $\pm$ 2-sigma) for the global open ocean (Regnier et al., 2022, note that this outgassing of 0.65 PgC year^{-1} is quantified for the open ocean outside of the narrow coastal ocean and thus include part of the wide coastal ocean), is still active today and therefore partially offsets the ingassing CO_2 flux that is directly driven by anthropogenic CO_2 emissions to the atmosphere (e.g., Friedlingstein et al., 2022; Regnier et al., 2022; Resplandy et al., 2018). Observation-based pCO_2-products estimate the net contemporary flux of CO_2, and therefore implicitly include the fluxes of natural and anthropogenic carbon, as well as the outgassing fluxes of carbon from land origin (e.g., Hauck et al., 2020). Most models, however, do not or only partially include these land-sea carbon inputs (see Tables 2 and 3) and are therefore likely to overestimate the net CO_2 ocean uptake, in particular in coastal waters adjacent to the land (Lacroix et al., 2020).

In globally integrated estimates, such as analyzed in the Global Carbon Budget (e.g., Friedlingstein et al., 2022) or the IPCC (Arias et al., 2021), the net air-sea CO_2 flux can in principle be adjusted for the outgassing of carbon from land to isolate the oceanic net sink, or it can be used to shed light on differences between modeled and observation-based flux estimates (e.g., Friedlingstein et al., 2022; Hauck et al., 2020). The RECCAP2 open ocean chapters estimated the spatial distribution of this land-driven CO_2 outgassing by upscaling the spatial distribution from an open-ocean model (Lacroix et al., 2020) to match an independent bottom up constraint on its global magnitude (0.65 ± 0.3 PgC/year; Regnier et al., 2022). This estimate suggests that 0.12 PgC year^{-1} out of the 0.65 PgC year^{-1} of land-driven CO_2 outgassing occurs in the wide coastal ocean, which could explain part of the model-product discrepancy. It is important to recognize, however, that the spatial distribution of this land-driven outgassing and contribution to the coastal ocean air-sea flux are very poorly constrained. In particular, we note that the model used to estimate the land-driven outgassing pattern (Lacroix et al., 2020) lacks some of the processes that control the magnitude (hence the upscaling to match the global number of 0.65 PgC year^{-1} from Regnier et al. (2022) but also the spatial distribution of this outgassing (e.g., CO_2 uptake by coastal vegetation).

Another factor to consider is the land-sea input of nutrients, which could promote biological CO_2 uptake in coastal waters downstream of the river mouth (e.g., Gao et al., 2023; Louchard et al., 2021; Terhaar et al., 2021). However, we find no clear relationship between the strength of the simulated net coastal CO_2 uptake and the presence or absence or land-sea inputs in the global ocean biogeochemical models used here (i.e., models with weaker coastal CO_2 uptake more in line with pCO_2-products are not systematically the ones with land-sea inputs), suggesting that land-driven inputs are likely not the main factor in this discrepancy. This result is in agreement with prior work showing a relatively modest impact of riverine nutrient inputs on coastal productivity compared to the physical supply by cross-shelf and along-shelf exchanges on the shelf (e.g., Cotrim Da Cunha et al., 2007; Wollast, 1998). In addition, the models considered here either include both carbon and nutrient land-sea inputs or neither (Tables 2 and 3), leading to a potential offset between land-driven CO_2 outgassing associated with carbon runoffs and biological CO_2 uptake associated with nutrient runoffs (although we do not expect the patterns of the CO_2 outgassing and biological CO_2 uptake to match). This might explain why models with land-sea carbon inputs did not systematically yield weaker CO_2 uptake in the coastal ocean compared to the one without land-sea inputs.

4.1.4. Uncertain Trends in Coastal Ocean CO_2 Flux and Decoupling From pCO_2

This synthesis indicates that the coastal ocean CO_2 sink has increased between 1998 and 2018, in line with the expectation from previous work that showed surface pCO_2 in the narrow coastal ocean increasing at a smaller rate than in the atmosphere (Laruelle et al., 2018; Wang et al., 2017). The rate at which the coastal sink has increased is, however, poorly constrained by the models and products presented here (flux density trend varies by a factor 2 between the two time-varying pCO_2-products and by a factor 3 between the 11 models). In addition, it is still unclear if this increase in the global coastal CO_2 sink is comparable, slower, or faster than in the open ocean due to the inconsistent responses found in models and the two time-varying pCO_2-products but also in prior modeling and observation-based work (Bourgeois et al., 2016; Lacroix et al., 2021; Laruelle et al., 2018; Wang et al., 2017). The CMEMS* pCO_2-product suggests that the CO_2 uptake increases faster in the coastal ocean than in the open ocean, which is in line with the prior observation-based results of Laruelle et al. (2018). In contrast, the ensemble of 11 global ocean models and the Carboscope-1 pCO_2-product suggest that the coastal ocean sink is increasing at a slightly smaller rate than the open ocean, a result in line with another prior work based on pCO_2 observations (Wang et al., 2017) and global ocean biogeochemical models (Bourgeois et al., 2016; Lacroix et al., 2021).

Bourgeois et al. (2016) explained the weaker increase in the coastal carbon sink compared to the open ocean by a bottleneck in offshore transport, which leads to anthropogenic carbon accumulation and limits the ability of coastal waters to take up anthropogenic carbon. Although we did not quantify surface residence time or off-shelf transport in this study, our finding that the modeled CO_2 sink increases at a lower rate in the coastal region than in the open ocean lends support for this interpretation. Other processes at play could explain this behavior. For instance, relatively shallow waters in coastal oceans might limit the exchanges with deep (free of anthropogenic CO_2) waters, such that the coastal ocean surface layer saturates more quickly with additional CO_2 added to the atmosphere. In models, this slower rate is associated with regions of increased outgassing or reduced uptake, but the specific regions at play vary across models (e.g., North Pacific, Mediterranean Sea and Parts of the Arctic in the model median in this study vs. tropical ocean and parts of the Arctic in Lacroix et al., 2021), highlighting further the uncertainties that remain in constraining coastal trends.

Discrepancies between the different estimates of the CO_2 flux trends at least partly arise from the sparse temporal pCO_2 observational coverage. For instance, the prior studies of Laruelle et al. (2018) and Wang et al. (2017) only covered a small portion of the coastal surface area and might not be representative of the global ocean. This is supported by regional studies that identified coastal ocean pCO_2 trend weaker than the atmospheric pCO_2 trend (i.e., potentially yielding intensified CO_2 uptake or decreased outgassing) such as the northern Gulf Stream margin, the South China Sea, the Sea of Japan, the North Sea and the Antarctic Peninsula (Bauer et al., 2013; Dai et al., 2022; Laruelle et al., 2018; Wang et al., 2017), but also regions where coastal ocean pCO_2 increases at a similar rate (i.e., near-zero changes in the flux) or even higher rates (i.e., reduced CO_2 uptake or intensified outgassing) than atmospheric pCO_2, such as in the Baltic Sea (Schneider & Müller, 2018), the California Current or along the eastern US coast (Dai et al., 2022; Laruelle et al., 2018; Reimer et al., 2017; Salisbury & Jönsson, 2018; Xu et al., 2020).

Another source of discrepancy is the decoupling found between global coastal pCO_2 trends and flux trends, suggesting that the CO_2 flux trends are sensitive to trends in winds and sea-ice (via the gas exchange coefficient), and how they combine with the pCO_2 trends. This sensitivity to sea-ice and winds is likely more pronounced in

the observation-based estimates, which rely on an "offline" calculation of the flux (no mechanistic link between pCO_2 disequilibrium, wind and sea-ice, except for CarboScope-1), or even more simply assume that slower trends in coastal ocean pCO_2 translate into faster growing coastal CO_2 flux (e.g., Laruelle et al., 2018), an assumption that is not fulfilled in the 2 pCO_2-products used in this study (although it does work in the multi-model median).

4.1.5. Confidence in pCO_2-Products and Ocean Biogeochemical Models

The systematic differences found between the ensemble median of global ocean models and pCO_2-products (including the larger net annual mean CO_2 uptake found in global ocean models, the different timing of mid- and high-latitude seasonality and the large range found in flux density trends) should be interpreted with caution. First, some models capture better than others the patterns reconstructed by the pCO_2-products. In particular, some models are able to reproduce the stronger summer sink found at high-latitudes, or simulate a net annual mean CO_2 flux that better matches the product-based estimates. In addition, differences between products and models do not necessarily equate to model bias. Observation-based products rely on gap-filling techniques (mixed layer model or machine learning), and regions of largest product-model mismatch often correspond to regions where the observational sampling is sparse (68% of the wide coastal ocean surface area was never sampled, and of the sampled area, 33% has data for only 1 month in a single year, Figure S1 in Supporting Information S1) and where the spread across the observation-based products and across the global models is the highest (hatching on Figures 5a and 5b). In contrast, coastal regions that are relatively well sampled by observations and well constrained by the products generally correspond to regions of agreement between the observation-based and model-based estimates (Roobaert et al., 2022). Thus, while we have overall more confidence in the observation-based estimates of the ocean carbon sink, the uncertainties associated with these reconstructed estimates remain high. This precludes a clear conclusion about whether the observation- or model-based estimates are closer to the truth.

4.2. Coastal Ocean N_2O and CH_4

The coastal ocean is a substantial source of atmospheric N_2O (Yang et al., 2020) and a minor source of atmospheric CH_4 (Saunois et al., 2020; Weber et al., 2019). The N_2O flux estimates presented here for the narrow coastal ocean (0.14–0.75 Tg N year^{-1}) is lower than a previous estimate of the mean global N_2O fluxes from coastal waters (including upwelling and marginal seas) in the range of 1.9–3.0 Tg N year^{-1} (Bange et al., 1996). The mean CH_4 flux estimates for the narrow coastal ocean (2.46–3.19 Tg CH_4 year^{-1} for the diffusive flux and up to 6.79 Tg CH_4 year^{-1} when accounting for the ebullitive flux in the narrow coastal ocean) are also in good agreement with a recently published mean CH_4 flux from shelves (0–200 m water depth) of 5.7 Tg CH_4 year^{-1} (Rosentreter et al., 2021). Nevertheless, quantitative estimates of N_2O and CH_4 emissions remain highly uncertain, in particular due to the presence of poorly sampled or unresolved spatio-temporal variability.

We find that observation-based estimates of the N_2O emissions and the diffusive flux of CH_4 vary by about 20%–30% in the narrow coastal ocean and by about a factor 2 to 3.5 in the wide coastal ocean. The increase in the spread amongst these observational products (which use the same data sets and are therefore not independent) reflects the low number of oceanic N_2O and CH_4 measurements to date, in particular in many coastal regions, as compared to CO_2. Specifically, the observation density decreases by about a factor 3 from narrow to wide (number of observations per million km^2 three times lower in the wide coastal ocean in more than 30 of the 45 regions used for the interpolation, see Table S1 in Supporting Information S1). Furthermore, significant differences between the observation-based estimates (MARCATS-N2O, MARCATS-CH4 on the one hand, and Yang-N2O and Weber-CH4 on the other hand) can result from (a) applying different approaches for estimating the air-sea gas exchange in combination with using different wind speed products (e.g., Garbe et al., 2014) and (b) applying different inter- and extrapolation techniques which can introduce significant uncertainties when applied to sparse data. The increase in discrepancy from narrow to wide coastal waters suggests that MARCATS-N2O and MARCATS-CH4 may extrapolate local observations over spatial domains where they are not representative anymore. In contrast, the neural networks of Yang-N2O and Weber-CH4, albeit also relying on the same MEMENTO data set, may better capture spatial patterns, such as the overall decrease in CH_4 emissions as the shelf water depth increases.

Current observational products only provide a climatological view of N_2O and an annual mean view of CH_4 emissions, and the global models used here are limited by their relatively coarse horizontal resolution. Both observation-based products and models have therefore limited or missing information on (a) seasonal and

inter-annual variability, (b) fine-scale (i.e., few 10s of km or less) land-ocean gradients, (c) the effects of mesoscale and submesoscale features such as eddies (Grundle et al., 2017), and (d) extreme events such as storms and marine heat waves (Borges et al., 2019; Gindorf et al., 2022). Our study reveals, for instance, that while coastal N_2O flux emissions from observational products and models generally agree in terms of main patterns and magnitude, emission hotspots in productive low-O_2 upwelling systems appear to be underestimated by models. In contrast, there are regions where models point to coastal N_2O flux hotspots along mid-latitude western boundaries that are not evident in observational reconstructions. In addition, the observation-based CH_4 product or the N_2O models presented here do not capture features evidenced by field data in prior work, such as the persistent CH_4 under-saturation observed in the Ross Sea (Ye et al., 2023) and Weddell Sea (Heeschen et al., 2004) or the N_2O under-saturation observed in the Arctic Ocean (Wu et al., 2017; Zhang et al., 2015). The reasons for these mismatches remain unclear but likely reflect the presence of unresolved (e.g., complex microbial production/consumption, sedimentary processes, production in estuarine and coastal vegetation systems transported to the coastal ocean) or spatially under-resolved processes (e.g., high production and remineralization in shallow shelves, and shallow coastal oxygen minimum zones where N_2O emissions take place) in ocean biogeochemical models. In addition, the lack of observations in these regions (see Table S1 in Supporting Information S1) could limit the ability of reconstructions to reflect mean coastal conditions or capture undersaturation and emission hotspots. The recently proposed Global N_2O Ocean Observation Network (N_2O-ON) (Bange, 2022; Bange et al., 2019) might help to better constrain and understand temporal and spatial variability as well as reduce uncertainties in current global N_2O oceanic emission estimates.

Aspects of air-sea gas exchange that remain poorly understood are the effects of surface micro-layers on these gases (Kock et al., 2012). In parallel, commonly adopted model parameterizations greatly simplify complex source and sink processes that are the focus of ongoing research. For example, there remain significant uncertainty in the relative importance of the various (micro)biological and photochemical processes driving the production and consumption of N_2O and CH_4 in coastal waters and sediments, and their potential responses to changing oceanic conditions (Bange, 2022). The relationship between CH_4 concentration and floor depth shown by Weber et al. (2019) suggests that sediments are the major source of CH_4 to the water column over continental shelves, but the contribution of other biological and photochemical CH_4 sources remains poorly understood.

Methane can be produced aerobically in situ in surface waters, providing the most direct route to the atmosphere. Pathways that have been identified in the marine environment include (a) methanogenesis by phytoplankton during primary production (e.g., Bižić et al., 2020), which is potentially driven by reactive oxygen species (Ernst et al., 2022); (b) egestion by zooplankton (Schmale et al., 2018); and (c) decomposition of dissolved organic matter compounds including methylphosphonate (MPn, Karl et al., 2008; Repeta et al., 2016; von Arx et al., 2023) and dimethylsulfoniopropionate (DMSP, Damm et al., 2010). These processes have mostly been studied in the open ocean, where they explain the ubiquitous weak supersaturation of CH_4 in remote surface waters, referred to as the "Marine Methane Paradox" (Reeburgh, 2007). Recent evidence suggests that the MPn pathway is also active in some coastal waters (Mao et al., 2022), but its importance relative to benthic-sourced CH_4 in maintaining the strong supersaturation of coastal waters seems to be low (Kanwischer et al., 2023). In the North Sea, seasonal fluctuations in coastal CH_4 that align with temperature (a driver of benthic production and degassing) rather than chlorophyll or DMSP suggest that sedimentary sources of CH_4 overwhelm the biological production in the water column (Borges et al., 2018). Additional sources of N_2O and CH_4 remain poorly characterized and are not represented by models, including submarine groundwater discharge (Arévalo-Martínez et al., 2023) and production associated with marine microplastic (Royer et al., 2018; Su et al., 2022) and submerged aquatic vegetation (Hilt et al., 2022; Rosentreter et al., 2021, 2023; Roth et al., 2023).

Ongoing environmental changes such as ocean warming, decreasing pH, loss of dissolved oxygen, and eutrophication might significantly alter the production and consumption of both N_2O and CH_4 as well as their distribution patterns in coastal waters and, consequently, their release to the atmosphere (e.g., Rees et al., 2022; Zhou et al., 2023). However, our knowledge of recent trends on which future emission scenarios of N_2O and CH_4 from the coastal ocean rely is still far from complete. In particular, hydrate dissolution due to ocean warming may enhance this flux at the seafloor, but only at the feather-edge of the hydrate stability zone, which occurs in ~400 m deep water in mid-latitudes—which could be too deep for the methane to make it to the surface and escape to the atmosphere (Joung et al., 2022). Shallow hydrocarbon-fed seep fields allow for more efficient methane release to the atmosphere (Hovland et al., 1993), but their impact appears to be highly localized (Joung et al., 2020), and the global-scale contribution of geological CH_4 to marine emissions remains highly uncertain

(Etiope et al., 2019). Understanding CH_4 oxidation dynamics in coastal environments is therefore an important focus area for future research. Although N_2O-ON was originally designed for N_2O only, adding measurements of CH_4 will be facilitated by deploying instruments on the basis of the same technique used for N_2O measurements (i.e., cavity-enhanced absorption spectroscopy), providing new opportunities to establish long-term time-series for these two greenhouse gases.

4.3. Coastal Ocean Greenhouse Gas Atmospheric Influence

This synthesis provides an estimate of the coastal contribution to the atmospheric radiative balance using an ensemble of observation-based products and global ocean biogeochemical models (in CO_2-equivalent). In both products and models, we find that a significant proportion of the coastal CO_2 uptake (~30%–60%) is offset by the radiative contribution of N_2O and CH_4 emissions, despite large uncertainties in the magnitude of the mean CO_2 uptake (large uptake in models) and relatively limited numbers of observation-based products and models available for N_2O and CH_4 fluxes. This offset is significantly larger than in the global ocean, for which a value of about 10% can be calculated based on the CO_2 (Le Quéré et al., 2018), N_2O (Tian et al., 2020), and CH_4 (Saunois et al., 2020) global budgets by the GCP. A smaller offset value of the order of 10%–20% has also been reported for estuaries and coastal vegetated ecosystems (Rosentreter et al., 2023), highlighting that the radiative balance on the shelf results from a significant contribution of the 3 greenhouse gases. Such an offset does not occur in inland waters either (rivers, lakes and reservoirs), as freshwater aquatic systems are a net source of CO_2, CH_4 and N_2O (Battin et al., 2023; Lauerwald et al., 2023), with CO_2 and CH_4 contributing roughly 75% and 25% to radiative balance, respectively, while N_2O is only a marginal contributor.

Integrating the three compartments of the land-to-ocean aquatic continuum (LOAC) from streams to the coastal oceans (i.e., inland waters, estuaries and coastal vegetation, and coastal ocean waters (Regnier et al., 2013; Regnier et al., 2022)), we find that the LOAC has a net-positive contribution to the radiative balance. Indeed, the 8.3 (range of 5.8–12.7) $PgCO_2$-e year^{-1} emitted by inland waters (Lauerwald et al., 2023) are only partly compensated by the net uptakes of 0.4 (range 0.2–0.7) $PgCO_2$-e year^{-1} from estuaries and coastal vegetation (Rosentreter et al., 2023) and 1.3 (range 0.7–1.8) $PgCO_2$-e year^{-1} from wide coastal waters. For the 100 year time horizon, the LOAC as a whole thus contributes about 6.6 $PgCO_2$-e year^{-1} globally to the radiative balance. These studies focus on the LOAC contemporary fluxes of greenhouse gases and their contribution to the radiative balance. An assessment of the historical changes in these fluxes compared to the pre-industrial baseline has been attempted in particular for CO_2 (e.g., Bourgeois et al., 2016; Lacroix et al., 2021; Mackenzie et al., 1998). Process-based model assessments and dedicated observation-based coastal products with a global coverage that resolve recent trends are, however, still missing informing on the LOAC contribution to the anthropogenic radiative forcing.

5. Conclusion

The main findings of the RECCAP2 global coastal ocean synthesis are:

- *Net global CO_2 uptake*—wide coastal ocean CO_2 uptake for the 1998–2018 period is estimated to −0.44 PgC year^{-1} from pCO_2-products (median of 4 products) and −0.72 PgC year^{-1} from global ocean biogeochemical models (median of 11 models). This 60% mismatch is attributed to the stronger wintertime CO_2 uptake in northern mid- and high-latitude systems in models due to a weak biologically induced seasonality compared to thermal changes in models. Biologically induced biases can be amplified by the choice of the wind product and gas exchange coefficient parameterization.

- *Trends in CO_2 uptake*—coastal ocean CO_2 uptake has increased during the 1998–2018 period but this increase is poorly constrained, with trends varying by a factor two across pCO_2-products and by a factor three across models (trends between −0.15 and −0.04 mol m^{-2} year^{-1} per decade) due to differences in ocean pCO_2, wind and sea-ice coverage trends.

- *N_2O and CH_4 emissions*—wide coastal ocean N_2O emissions are estimated to +1.63 Tg N year^{-1} in the Yang et al. (2020) observation-based product, and to +1.27 Tg N year^{-1} from global ocean biogeochemical models (median of 5 models). Emissions of CH_4 are estimated to +7.85 [2.50–9.20] $TgCH_4$ year^{-1} from the Weber et al. (2019) observation-based product. N_2O and CH_4 flux estimates are fewer and more uncertain than CO_2 fluxes.

- *Net coastal radiative balance*—despite uncertainties, N_2O and CH_4 emissions strongly offset the CO_2 uptake in the net radiative balance of the coastal ocean (offset of 30%–60%), emphasizing the need to consider N_2O and CH_4 when examining the influence of coastal ocean on climate.

Based on the main challenges identified in this synthesis, we suggest a focus on the following points:

- Expand the number of observation-based products and models specifically designed for coastal oceans (higher spatial resolution, account for land imprint, etc.).
- Develop pCO_2-based products that resolve interannual and decadal changes (only two out of four pCO_2-products provided time-varying information, while others were climatologies).
- Constrain changes in wind and sea-ice, which have strong implications for flux trend estimation.
- Better constrain the biological pump in the mid- and high-latitude coastal oceans in ocean biogeochemical models.
- Refine coastal N_2O and CH_4 emission estimates from observations (very few estimates available) and models (few N_2O estimates, no CH_4 estimates) to gain an understanding of their dynamics and close the gap with CO_2 estimates.

Conflict of Interest

The authors declare no conflicts of interest relevant to this study.

Data Availability Statement

The data used in this chapter are available in Resplandy et al. (2023) https://zenodo.org/record/8326096 doi: 10.5281/ZENODO.8326096 and Müller (2023) https://zenodo.org/record/7990823 doi: 10.5281/ZENODO.7990823.

References

Anderson, L. G., Jutterström, S., Hjalmarsson, S., Wåhlström, I., & Semiletov, I. P. (2009). Out-gassing of CO_2 from Siberian Shelf seas by terrestrial organic matter decomposition. *Geophysical Research Letters*, *36*(20), L20601. https://doi.org/10.1029/2009GL040046

Arévalo-Martínez, D. L., Haroon, A., Bange, H. W., Erkul, E., Jegen, M., Moosdorf, N., et al. (2023). Ideas and perspectives: Land–ocean connectivity through groundwater. *Biogeosciences*, *20*(3), 647–662. https://doi.org/10.5194/bg-20-647-2023

Arévalo-Martínez, D. L., Kock, A., Löscher, C. R., Schmitz, R. A., & Bange, H. W. (2015). Massive nitrous oxide emissions from the tropical South Pacific Ocean. *Nature Geoscience*, *8*(7), 530–533. https://doi.org/10.1038/ngeo2469

Arias, P. A., Bellouin, N., Coppola, E., Jones, R. G., Krinner, G., Marotzke, J., et al. (2021). Technical summary. In V. Masson-Delmotte, et al. (Eds.), *Climate change 2021: The physical science basis. Contribution of Working Group I to the sixth assessment report of the Intergovernmental Panel on Climate Change*. Cambridge University Press. (Type: Book Section). https://doi.org/10.1017/9781009157896.002

Arndt, S., Jørgensen, B., LaRowe, D., Middelburg, J., Pancost, R., & Regnier, P. (2013). Quantifying the degradation of organic matter in marine sediments: A review and synthesis. *Earth-Science Reviews*, *123*, 53–86. https://doi.org/10.1016/j.earscirev.2013.02.008

Arrigo, K. R., van Dijken, G., & Long, M. (2008). Coastal Southern Ocean: A strong anthropogenic CO_2 sink. *Geophysical Research Letters*, *35*(21), L21602. https://doi.org/10.1029/2008GL035624

Bakker, D. C. E., Alin, S. R., Becker, M., Bittig, H. C., Castaño-Primo, R., Feely, R. A., et al. (2022). *Surface Ocean CO_2 Atlas Database Version 2022 (SOCATv2022) (NCEI Accession 0253659)*. NOAA National Centers for Environmental Information. https://doi.org/10.25921/1H9F-NB73

Bakker, D. C. E., Pfeil, B., Landa, C. S., Metzl, N., O'Brien, K. M., Olsen, A., et al. (2016). A multi-decade record of high-quality fCO_2 data in version 3 of the Surface Ocean CO_2 Atlas (SOCAT). *Earth System Science Data*, *8*(2), 383–413. https://doi.org/10.5194/essd-8-383-2016

Bakker, D. C. E., Pfeil, B., Smith, K., Hankin, S., Olsen, A., Alin, S. R., et al. (2014). An update to the Surface Ocean CO_2 Atlas (SOCAT version 2). *Earth System Science Data*, *6*(1), 69–90. https://doi.org/10.5194/essd-6-69-2014

Bange, H. W. (2022). Non-CO_2 greenhouse gases (N_2O, CH_4, CO) and the ocean. *One Earth*, *5*(12), 1316–1318. https://doi.org/10.1016/j.oneear.2022.11.011

Bange, H. W., Arévalo-Martínez, D. L., de la Paz, M., Farías, L., Kaiser, J., Kock, A., et al. (2019). A harmonized nitrous oxide (N_2O) ocean observation network for the 21st century. *Frontiers in Marine Science*, *6*, 157. https://doi.org/10.3389/fmars.2019.00157

Bange, H. W., Rapsomanikis, S., & Andreae, M. O. (1996). Nitrous oxide in coastal waters. *Global Biogeochemical Cycles*, *10*(1), 197–207. https://doi.org/10.1029/95GB03834

Battin, T. J., Lauerwald, R., Bernhardt, E. S., Bertuzzo, E., Gener, L. G., Hall, R. O., et al. (2023). River ecosystem metabolism and carbon biogeochemistry in a changing world. *Nature*, *613*(7944), 449–459. https://doi.org/10.1038/s41586-022-05500-8

Bauer, J. E., Cai, W.-J., Raymond, P. A., Bianchi, T. S., Hopkinson, C. S., & Regnier, P. A. G. (2013). The changing carbon cycle of the coastal ocean. *Nature*, *504*(7478), 61–70. https://doi.org/10.1038/nature12857

Berthet, S., Jouanno, J., Séférian, R., Gehlen, M., & Llovel, W. (2023). How does the phytoplankton–light feedback affect the marine N_2O inventory? *Earth System Dynamics*, *14*(2), 399–412. https://doi.org/10.5194/esd-14-399-2023

Berthet, S., Séférian, R., Bricaud, C., Chevallier, M., Voldoire, A., & Ethé, C. (2019). Evaluation of an online grid-coarsening algorithm in a global eddy-admitting ocean biogeochemical model. *Journal of Advances in Modeling Earth Systems*, *11*(6), 1759–1783. https://doi.org/10.1029/2019MS001644

Bižić, M., Klintzsch, T., Ionescu, D., Hindiyeh, M. Y., Günthel, M., Muro-Pastor, A. M., et al. (2020). Aquatic and terrestrial cyanobacteria produce methane. *Science Advances*, *6*(3), eaax5343. https://doi.org/10.1126/sciadv.aax5343

Bopp, L., Lévy, M., Resplandy, L., & Sallée, J. B. (2015). Pathways of anthropogenic carbon subduction in the global ocean. *Geophysical Research Letters*, *42*(15), 2015GL065073. https://doi.org/10.1002/2015GL065073

Borges, A. V., Delille, B., & Frankignoulle, M. (2005). Budgeting sinks and sources of CO_2 in the coastal ocean: Diversity of ecosystems counts. *Geophysical Research Letters*, *32*, L14601. https://doi.org/10.1029/2005GL023053

Borges, A. V., Royer, C., Martin, J. L., Champenois, W., & Gypens, N. (2019). Response of marine methane dissolved concentrations and emissions in the Southern North Sea to the European 2018 heatwave. *Continental Shelf Research*, *190*, 104004. https://doi.org/10.1016/j.csr.2019.104004

Borges, A. V., Speeckaert, G., Champenois, W., Scranton, M. I., & Gypens, N. (2018). Productivity and temperature as drivers of seasonal and spatial variations of dissolved methane in the southern bight of the North Sea. *Ecosystems*, *21*(4), 583–599. https://doi.org/10.1007/s10021-017-0171-7

Bourgeois, T., Orr, J. C., Resplandy, L., Terhaar, J., Ethé, C., Gehlen, M., & Bopp, L. (2016). Coastal-ocean uptake of anthropogenic carbon. *Biogeosciences*, *13*(14), 4167–4185. https://doi.org/10.5194/bg-13-4167-2016

Boutin, J., Quilfen, Y., Merlivat, L., & Piolle, J. F. (2009). Global average of air-sea CO_2 transfer velocity from QuikSCAT scatterometer wind speeds. *Journal of Geophysical Research*, *114*(C4), C04007. https://doi.org/10.1029/2007JC004168

Buitenhuis, E. T., Suntharalingam, P., & Le Quéré, C. (2018). Constraints on global oceanic emissions of N_2O from observations and models. *Biogeosciences*, *15*(7), 2161–2175. https://doi.org/10.5194/bg-15-2161-2018

Cahill, B., Wilkin, J., Fennel, K., Vandemark, D., & Friedrichs, M. A. M. (2016). Interannual and seasonal variabilities in air-sea CO_2 fluxes along the U.S. eastern continental shelf and their sensitivity to increasing air temperatures and variable winds: U.S. East Coast Shelf air-sea CO_2 fluxes. *Journal of Geophysical Research: Biogeosciences*, *121*(2), 295–311. https://doi.org/10.1002/2015JG002939

Cai, W.-J. (2011). Estuarine and coastal ocean carbon paradox: CO_2 sinks or sites of terrestrial carbon incineration? *Annual Review of Marine Science*, *3*(1), 123–145. https://doi.org/10.1146/annurev-marine-120709-142723

Cai, W.-J., Dai, M., & Wang, Y. (2006). Air-sea exchange of carbon dioxide in ocean margins: A province-based synthesis. *Geophysical Research Letters*, *33*(12), L12603. https://doi.org/10.1029/2006GL026219

Cao, Z., Yang, W., Zhao, Y., Guo, X., Yin, Z., Du, et al. (2020). Diagnosis of CO_2 dynamics and fluxes in global coastal oceans. *National Science Review*, *7*(4), 786–797. https://doi.org/10.1093/nsr/nwz105

Carroll, D., Menemenlis, D., Adkins, J. F., Bowman, K. W., Brix, H., Dutkiewicz, S., et al. (2020). The ECCO-Darwin data-assimilative global ocean biogeochemistry model: Estimates of seasonal to multidecadal surface ocean pCO_2 and air-sea CO_2 flux. *Journal of Advances in Modeling Earth Systems*, *12*(10). https://doi.org/10.1029/2019MS001888

Chau, T. T. T., Gehlen, M., & Chevallier, F. (2022). A seamless ensemble-based reconstruction of surface ocean pCO_2 and air–sea CO_2 fluxes over the global coastal and open oceans. *Biogeosciences*, *19*(4), 1087–1109. https://doi.org/10.5194/bg-19-1087-2022

Chen, C.-T. A., & Borges, A. V. (2009). Reconciling opposing views on carbon cycling in the coastal ocean: Continental shelves as sinks and near-shore ecosystems as sources of atmospheric CO_2. *Deep Sea Research Part II: Topical Studies in Oceanography*, *56*(8–10), 578–590. https://doi.org/10.1016/j.dsr2.2009.01.001

Chen, C.-T. A., Huang, T.-H., Chen, Y.-C., Bai, Y., He, X., & Kang, Y. (2013). Air–sea exchanges of CO_2 in the world's coastal seas. *Biogeosciences*, *10*(10), 6509–6544. https://doi.org/10.5194/bg-10-6509-2013

Cossarini, G., Querin, S., & Solidoro, C. (2015). The continental shelf carbon pump in the northern Adriatic Sea (Mediterranean Sea): Influence of wintertime variability. *Ecological Modelling*, *314*, 118–134. https://doi.org/10.1016/j.ecolmodel.2015.07.024

Cotrim Da Cunha, L., Buitenhuis, E. T., Le Quéré, C., Giraud, X., & Ludwig, W. (2007). Potential impact of changes in river nutrient supply on global ocean biogeochemistry: Impact of river nutrients on the ocean. *Global Biogeochemical Cycles*, *21*(4), n/a. https://doi.org/10.1029/2006GB002718

Dai, M., Cao, Z., Guo, X., Zhai, W., Liu, Z., Yin, Z., et al. (2013). Why are some marginal seas sources of atmospheric CO_2? *Geophysical Research Letters*, *40*(10), 2154–2158. https://doi.org/10.1002/grl.50390

Dai, M., Su, J., Zhao, Y., Hofmann, E. E., Cao, Z., Cai, W.-J., et al. (2022). Carbon fluxes in the coastal ocean: Synthesis, boundary processes, and future trends. *Annual Review of Earth and Planetary Sciences*, *50*(1), 593–626. https://doi.org/10.1146/annurev-earth-032320-090746

Damien, P., Bianchi, D., McWilliams, J. C., Kessouri, F., Deutsch, C., Chen, R., & Renault, L. (2023). Enhanced biogeochemical cycling along the U.S. West Coast Shelf. *Global Biogeochemical Cycles*, *37*(1). https://doi.org/10.1029/2022GB007572

Damm, E., Helmke, E., Thoms, S., Schauer, U., Nöthig, E., Bakker, K., & Kiene, R. P. (2010). Methane production in aerobic oligotrophic surface water in the central Arctic Ocean. *Biogeosciences*, *7*(3), 1099–1108. https://doi.org/10.5194/bg-7-1099-2010

Deike, L., & Melville, W. K. (2018). Gas transfer by breaking waves. *Geophysical Research Letters*, *45*(19), 10482–10492. https://doi.org/10.1029/2018GL078758

Desmet, F., Gruber, N., Köhn, E. E., Münnich, M., & Vogt, M. (2022). Tracking the space-time evolution of ocean acidification extremes in the California Current System and Northeast Pacific. *Journal of Geophysical Research: Oceans*, *127*(5), e2021JC018159. https://doi.org/10.1029/2021JC018159

DeVries, T., Yamamoto, K., Wanninkhof, R., Gruber, N., Hauck, J., Müller, J. D., et al. (2023). Magnitude, trends, and variability of the global ocean carbon sink from 1985 to 2018. *Global Biogeochemical Cycles*, *37*(10), e2023GB007780. https://doi.org/10.1029/2023GB007780

Doney, S. C., Lima, I., Feely, R. A., Glover, D. M., Lindsay, K., Mahowald, N., et al. (2009). Mechanisms governing interannual variability in upper-ocean inorganic carbon system and air–sea CO_2 fluxes: Physical climate and atmospheric dust. *Deep Sea Research Part II: Topical Studies in Oceanography*, *56*(8–10), 640–655. https://doi.org/10.1016/j.dsr2.2008.12.006

Egger, M., Lenstra, W., Jong, D., Meysman, F. J. R., Sapart, C. J., van der Veen, C., et al. (2016). Rapid sediment accumulation results in high methane effluxes from coastal sediments. *PLoS One*, *11*(8), e0161609. https://doi.org/10.1371/journal.pone.0161609

Elsig, J., Schmitt, J., Leuenberger, D., Schneider, R., Eyer, M., Leuenberger, M., et al. (2009). Stable isotope constraints on Holocene carbon cycle changes from an Antarctic ice core. *Nature*, *461*(7263), 507–510. https://doi.org/10.1038/nature08393

Ernst, L., Steinfeld, B., Barayeu, U., Klintzsch, T., Kurth, M., Grimm, D., et al. (2022). Methane formation driven by reactive oxygen species across all living organisms. *Nature*, *603*(7901), 482–487. https://doi.org/10.1038/s41586-022-04511-9

Etiope, G., Ciotoli, G., Schwietzke, S., & Schoell, M. (2019). Gridded maps of geological methane emissions and their isotopic signature. *Earth System Science Data*, *11*(1), 1–22. https://doi.org/10.5194/essd-11-1-2019

Fennel, K., Alin, S., Barbero, L., Evans, W., Bourgeois, T., Cooley, S., et al. (2019). Carbon cycling in the North American coastal ocean: A synthesis. *Biogeosciences*, *16*(6), 1281–1304. https://doi.org/10.5194/bg-16-1281-2019

Fennel, K., & Testa, J. M. (2019). Biogeochemical controls on coastal hypoxia. *Annual Review of Marine Science*, *11*(1), 105–130. https://doi.org/10.1146/annurev-marine-010318-095138

Fennel, K., & Wilkin, J. (2009). Quantifying biological carbon export for the northwest North Atlantic continental shelves. *Geophysical Research Letters*, *36*(18), L18605. https://doi.org/10.1029/2009GL039818

Fiechter, J., Curchitser, E. N., Edwards, C. A., Chai, F., Goebel, N. L., & Chavez, F. P. (2014). Air-sea CO_2 fluxes in the California Current: Impacts of model resolution and coastal topography. *Global Biogeochemical Cycles*, *28*(4), 371–385. https://doi.org/10.1002/2013GB004683

Friedlingstein, P., Jones, M. W., O'Sullivan, M., Andrew, R. M., Bakker, D. C. E., Hauck, J., et al. (2022). Global carbon budget 2021. *Earth System Science Data*, *14*(4), 1917–2005. https://doi.org/10.5194/essd-14-1917-2022

Ganesan, A. L., Manizza, M., Morgan, E. J., Harth, C. M., Kozlova, E., Lueker, T., et al. (2020). Marine nitrous oxide emissions from three eastern boundary upwelling systems inferred from atmospheric observations. *Geophysical Research Letters*, *47*(14), e2020GL087822. https://doi.org/10.1029/2020GL087822

Gao, S., Schwinger, J., Tjiputra, J., Bethke, I., Hartmann, J., Mayorga, E., & Heinze, C. (2023). Riverine impact on future projections of marine primary production and carbon uptake. *Biogeosciences*, *20*(1), 93–119. https://doi.org/10.5194/bg-20-93-2023

Garbe, C. S., Rutgersson, A., Boutin, J., de Leeuw, G., Delille, B., Fairall, C. W., et al. (2014). Transfer across the air-sea interface. In P. S. Liss & M. T. Johnson (Eds.), *Ocean-atmosphere interactions of gases and particles* (pp. 55–112). Springer. https://doi.org/10.1007/978-3-642-25643-1_2

Gindorf, S., Bange, H. W., Booge, D., & Kock, A. (2022). Seasonal study of the small-scale variability in dissolved methane in the western Kiel Bight (Baltic Sea) during the European heatwave in 2018. *Biogeosciences*, *19*(20), 4993–5006. https://doi.org/10.5194/bg-19-4993-2022

Gomez, F. A., Wanninkhof, R., Barbero, L., Lee, S.-K., & Hernandez, F. J., Jr. (2020). Seasonal patterns of surface inorganic carbon system variables in the Gulf of Mexico inferred from a regional high-resolution ocean biogeochemical model. *Biogeosciences*, *17*(6), 1685–1700. https://doi.org/10.5194/bg-17-1685-2020

Grundle, D. S., Löscher, C. R., Krahmann, G., Altabet, M. A., Bange, H. W., Karstensen, J., et al. (2017). Low oxygen eddies in the eastern tropical North Atlantic: Implications for N_2O cycling. *Scientific Reports*, *7*(1), 4806. https://doi.org/10.1038/s41598-017-04745-y

Gülzow, W., Rehder, G., Schneider v Deimling, J. V., Tóth, Z., Deimling, J., Seifert, T., & Tóth, Z. (2013). One year of continuous measurements constraining methane emissions from the Baltic Sea to the atmosphere using a ship of opportunity. *Biogeosciences*, *10*(1), 81–99. https://doi.org/10.5194/bg-10-81-2013

Gustafsson, E., Hagens, M., Sun, X., Reed, D. C., Humborg, C., Slomp, C. P., & Gustafsson, B. G. (2019). Sedimentary alkalinity generation and long-term alkalinity development in the Baltic Sea. *Biogeosciences*, *16*(2), 437–456. https://doi.org/10.5194/bg-16-437-2019

Gutiérrez-Loza, L., Nilsson, E., Wallin, M. B., Sahlée, E., & Rutgersson, A. (2022). On physical mechanisms enhancing air–sea CO_2 exchange. *Biogeosciences*, *19*(24), 5645–5665. https://doi.org/10.5194/bg-19-5645-2022

Hallberg, R. (2013). Using a resolution function to regulate parameterizations of oceanic mesoscale eddy effects. *Ocean Modelling*, *72*, 92–103. https://doi.org/10.1016/j.ocemod.2013.08.007

Hauck, J., Zeising, M., Le Quéré, C., Gruber, N., Bakker, D. C. E., Bopp, L., et al. (2020). Consistency and challenges in the ocean carbon sink estimate for the global carbon budget. *Frontiers in Marine Science*, *7*, 571720. https://doi.org/10.3389/fmars.2020.571720

Hauri, C., Pagès, R., McDonnell, A. M. P., Stuecker, M. F., Danielson, S. L., Hedstrom, K., et al. (2021). Modulation of ocean acidification by decadal climate variability in the Gulf of Alaska. *Communications Earth & Environment*, *2*(1), 191. https://doi.org/10.1038/s43247-021-00254-z

Heeschen, K. U., Keir, R. S., Rehder, G., Klatt, O., & Suess, E. (2004). Methane dynamics in the Weddell Sea determined via stable isotope ratios and CFC-11. *Global Biogeochemical Cycles*, *18*(2), n/a. https://doi.org/10.1029/2003GB002151

Hilt, S., Grossart, H., McGinnis, D. F., & Keppler, F. (2022). Potential role of submerged macrophytes for oxic methane production in aquatic ecosystems. *Limnology and Oceanography*, *67*(S2), S76–S88. https://doi.org/10.1002/lno.12095

Ho, D. T., Law, C. S., Smith, M. J., Schlosser, P., Harvey, M., & Hill, P. (2006). Measurements of air-sea gas exchange at high wind speeds in the Southern Ocean: Implications for global parameterizations. *Geophysical Research Letters*, *33*(16). https://doi.org/10.1029/2006GL026817

Ho, D. T., Wanninkhof, R., Schlosser, P., Ullman, D. S., Hebert, D., & Sullivan, K. F. (2011). Toward a universal relationship between wind speed and gas exchange: Gas transfer velocities measured with ^{3}He/SF$_6$ during the Southern Ocean Gas Exchange Experiment. *Journal of Geophysical Research*, *116*, C00F04. https://doi.org/10.1029/2010JC006854

Hovland, M., Judd, A., & Burke, R. (1993). The global flux of methane from shallow submarine sediments. *Chemosphere*, *26*(1–4), 559–578. https://doi.org/10.1016/0045-6535(93)90442-8

Ilyina, T., Six, K. D., Segschneider, J., Maier-Reimer, E., Li, H., & Núñez-Riboni, I. (2013). Global ocean biogeochemistry model HAMOCC: Model architecture and performance as component of the MPI-Earth system model in different CMIP5 experimental realizations. *Journal of Advances in Modeling Earth Systems*, *5*(2), 287–315. https://doi.org/10.1029/2012MS000178

Joung, D., Leonte, M., Valentine, D. L., Sparrow, K. J., Weber, T., & Kessler, J. D. (2020). Radiocarbon in marine methane reveals patchy impact of seeps on surface waters. *Geophysical Research Letters*, *47*(20), e2020GL089516. https://doi.org/10.1029/2020GL089516

Joung, D., Ruppel, C., Southon, J., Weber, T. S., & Kessler, J. D. (2022). Negligible atmospheric release of methane from decomposing hydrates in mid-latitude oceans. *Nature Geoscience*, *15*(11), 885–891. https://doi.org/10.1038/s41561-022-01044-8

Kanwischer, M., Klintzsch, T., & Schmale, O. (2023). Stable isotope approach to assess the production and consumption of methylphosphonate and its contribution to oxic methane formation in surface waters. *Environmental Science & Technology*, *57*(42), 15904–15913. https://doi.org/10.1021/acs.est.3c04098

Karl, D. M., Beversdorf, L., Björkman, K. M., Church, M. J., Martinez, A., & Delong, E. F. (2008). Aerobic production of methane in the sea. *Nature Geoscience*, *1*(7), 473–478. https://doi.org/10.1038/ngeo234

Kock, A., & Bange, H. (2015). Counting the ocean's greenhouse gas emissions. *Eos*, *96*. https://doi.org/10.1029/2015EO023665

Kock, A., Schafstall, J., Dengler, M., Brandt, P., & Bange, H. W. (2012). Sea-to-air and diapycnal nitrous oxide fluxes in the eastern tropical North Atlantic Ocean. *Biogeosciences*, *9*(3), 957–964. https://doi.org/10.5194/bg-9-957-2012

Lachkar, Z., & Gruber, N. (2013). Response of biological production and air–sea CO_2 fluxes to upwelling intensification in the California and Canary Current Systems. *Journal of Marine Systems*, *109–110*, 149–160. https://doi.org/10.1016/j.jmarsys.2012.04.003

Lachkar, Z., Mehari, M., Al Azhar, M., Lévy, M., & Smith, S. (2021). Fast local warming is the main driver of recent deoxygenation in the northern Arabian Sea. *Biogeosciences*, *18*(20), 5831–5849. https://doi.org/10.5194/bg-18-5831-2021

Lacroix, F., Ilyina, T., & Hartmann, J. (2020). Oceanic CO_2 outgassing and biological production hotspots induced by pre-industrial river loads of nutrients and carbon in a global modeling approach. *Biogeosciences*, *17*(1), 55–88. https://doi.org/10.5194/bg-17-55-2020

Lacroix, F., Ilyina, T., Laruelle, G. G., & Regnier, P. (2021). Reconstructing the preindustrial coastal carbon cycle through a global ocean circulation model: Was the global continental shelf already both autotrophic and a CO_2 sink? *Global Biogeochemical Cycles*, *35*(2), e2020GB006603. https://doi.org/10.1029/2020GB006603

Landschützer, P., Gruber, N., Bakker, D. C. E., & Schuster, U. (2014). Recent variability of the global ocean carbon sink. *Global Biogeochemical Cycles*, *28*(9), 927–949. https://doi.org/10.1002/2014GB004853

Landschützer, P., Laruelle, G. G., Roobaert, A., & Regnier, P. (2020). A uniform pCO$_2$ climatology combining open and coastal oceans. *Earth System Science Data*, *12*(4), 2537–2553. https://doi.org/10.5194/essd-12-2537-2020

Laruelle, G. G., Cai, W.-J., Hu, X., Gruber, N., Mackenzie, F. T., & Regnier, P. (2018). Continental shelves as a variable but increasing global sink for atmospheric carbon dioxide. *Nature Communications*, *9*(1), 454. https://doi.org/10.1038/s41467-017-02738-z

Laruelle, G. G., Dürr, H. H., Lauerwald, R., Hartmann, J., Slomp, C. P., Goossens, N., & Regnier, P. A. G. (2013). Global multi-scale segmentation of continental and coastal waters from the watersheds to the continental margins. *Hydrology and Earth System Sciences*, *17*(5), 2029–2051. https://doi.org/10.5194/hess-17-2029-2013

Laruelle, G. G., Dürr, H. H., Slomp, C. P., & Borges, A. V. (2010). Evaluation of sinks and sources of CO_2 in the global coastal ocean using a spatially-explicit typology of estuaries and continental shelves. *Geophysical Research Letters*, *37*(15), e2010GL043691. https://doi.org/10.1029/2010GL043691

Laruelle, G. G., Landschützer, P., Gruber, N., Tison, J.-L., Delille, B., & Regnier, P. (2017). Global high-resolution monthly pCO_2 climatology for the coastal ocean derived from neural network interpolation. *Biogeosciences*, *14*(19), 4545–4561. https://doi.org/10.5194/bg-14-4545-2017

Laruelle, G. G., Lauerwald, R., Pfeil, B., & Regnier, P. (2014). Regionalized global budget of the CO_2 exchange at the air-water interface in continental shelf seas. *Global Biogeochemical Cycles*, *28*(11), 1199–1214. https://doi.org/10.1002/2014GB004832

Laruelle, G. G., Lauerwald, R., Rotschi, J., Raymond, P. A., Hartmann, J., & Regnier, P. (2015). Seasonal response of air–water CO_2 exchange along the land–ocean aquatic continuum of the northeast North American coast. *Biogeosciences*, *12*(5), 1447–1458. https://doi.org/10.5194/bg-12-1447-2015

Lauerwald, R., Allen, G. H., Deemer, B. R., Liu, S., Maavara, T., Raymond, P., et al. (2023). Inland water greenhouse gas budgets for RECCAP2: 1. State-of-the-art of global scale assessments. *Global Biogeochemical Cycles*, *37*(5), e2022GB007657. https://doi.org/10.1029/2022GB007657

Laurent, A., Fennel, K., Cai, W., Huang, W., Barbero, L., & Wanninkhof, R. (2017). Eutrophication-induced acidification of coastal waters in the northern Gulf of Mexico: Insights into origin and processes from a coupled physical-biogeochemical model. *Geophysical Research Letters*, *44*(2), 946–956. https://doi.org/10.1002/2016GL071881

Laurent, A., Fennel, K., & Kuhn, A. (2021). An observation-based evaluation and ranking of historical Earth system model simulations in the northwest North Atlantic Ocean. *Biogeosciences*, *18*(5), 1803–1822. https://doi.org/10.5194/bg-18-1803-2021

Legge, O., Johnson, M., Hicks, N., Jickells, T., Diesing, M., Aldridge, J., et al. (2020). Carbon on the Northwest European Shelf: Contemporary budget and future influences. *Frontiers in Marine Science*, *7*, 143. https://doi.org/10.3389/fmars.2020.00143

Le Quéré, C. L., Andrew, R. M., Friedlingstein, P., Sitch, S., Pongratz, J., Manning, A. C., et al. (2018). Global carbon budget 2017. *Earth System Science Data*, *10*(1), 405–448. https://doi.org/10.5194/essd-10-405-2018

Liang, J.-H., Deutsch, C., McWilliams, J. C., Baschek, B., Sullivan, P. P., & Chiba, D. (2013). Parameterizing bubble-mediated air-sea gas exchange and its effect on ocean ventilation. *Global Biogeochemical Cycles*, *27*(3), 894–905. https://doi.org/10.1002/gbc.20080

Liao, E., Resplandy, L., Liu, J., & Bowman, K. W. (2020). Amplification of the ocean carbon sink during El Niños: Role of Poleward Ekman transport and influence on atmospheric CO_2. *Global Biogeochemical Cycles*, *34*(9), e2020GB006574. https://doi.org/10.1029/2020GB006574

Liu, Q., Guo, X., Yin, Z., Zhou, K., Roberts, E. G., & Dai, M. (2018). Carbon fluxes in the China Seas: An overview and perspective. *Science China Earth Sciences*, *61*(11), 1564–1582. https://doi.org/10.1007/s11430-017-9267-4

Louchard, D., Gruber, N., & Münnich, M. (2021). The impact of the Amazon on the biological pump and the air-sea CO_2 balance of the western tropical Atlantic. *Global Biogeochemical Cycles*, *35*(6), e2020GB006818. https://doi.org/10.1029/2020GB006818

Mackenzie, F. T., Andersson, A. J., Lerman, A., & Ver, L. M. (2005). Boundary exchanges in the global coastal margin: Implications for the organic and inorganic carbon cycles. In A. R. Robinson & K. H. Brink (Eds.), *The sea* (Vol. 13, pp. 193–225). Harvard Univ. Press.

Mackenzie, F. T., Lerman, A., & Ver, L. (1998). Role of the continental margin in the global carbon balance during the past three centuries. *Geology*, *26*(5), 423. https://doi.org/10.1130/0091-7613(1998)026⟨0423:ROTCMI⟩2.3.CO;2

Manizza, M., Menemenlis, D., Zhang, H., & Miller, C. E. (2019). Modeling the recent changes in the Arctic Ocean CO_2 sink (2006–2013). *Global Biogeochemical Cycles*, *33*(3), 420–438. https://doi.org/10.1029/2018GB006070

Mao, S.-H., Zhang, H.-H., Zhuang, G.-C., Li, X.-J., Liu, Q., Zhou, Z., et al. (2022). Aerobic oxidation of methane significantly reduces global diffusive methane emissions from shallow marine waters. *Nature Communications*, *13*(1), 7309. https://doi.org/10.1038/s41467-022-35082-y

Mathis, M., Logemann, K., Maerz, J., Lacroix, F., Hagemann, S., Chegini, F., et al. (2022). Seamless integration of the coastal ocean in global marine carbon cycle modeling. *Journal of Advances in Modeling Earth Systems*, *n/a*(n/a), e2021MS002789. https://doi.org/10.1029/2021MS002789

Mayer, B., Rixen, T., & Pohlmann, T. (2018). The spatial and temporal variability of air-sea CO_2 fluxes and the effect of net coral reef calcification in the Indonesian Seas: A numerical sensitivity study. *Frontiers in Marine Science*, *5*, 116. https://doi.org/10.3389/fmars.2018.00116

McGinnis, D. F., Greinert, J., Artemov, Y., Beaubien, S. E., & Wüest, A. (2006). Fate of rising methane bubbles in stratified waters: How much methane reaches the atmosphere? *Journal of Geophysical Research*, *111*(C9), C09007. https://doi.org/10.1029/2005JC003183

Müller, J. D. (2023). RECCAP2-ocean data collection [Dataset]. Zenodo. https://doi.org/10.5281/ZENODO.7990823

Neubauer, S. C. (2021). Global warming potential is not an ecosystem property. *Ecosystems*, *24*(8), 2079–2089. https://doi.org/10.1007/s10021-021-00631-x

Neumann, T., Radtke, H., Cahill, B., Schmidt, M., & Rehder, G. (2022). Non-Redfieldian carbon model for the Baltic Sea (ERGOM version 1.2) – Implementation and budget estimates. *Geoscientific Model Development*, *15*(22), 8473–8540. https://doi.org/10.5194/gmd-15-8473-2022

Nightingale, P. D., Malin, G., Law, C. S., Watson, A. J., Liss, P. S., Liddicoat, M. I., et al. (2000). In situ evaluation of air-sea gas exchange parameterizations using novel conservative and volatile tracers. *Global Biogeochemical Cycles*, *14*(1), 373–387. https://doi.org/10.1029/1999GB900091

Ouyang, Z., Li, Y., Qi, D., Zhong, W., Murata, A., Nishino, S., et al. (2022). The changing CO_2 sink in the western Arctic Ocean from 1994 to 2019. *Global Biogeochemical Cycles*, *36*(1), e2021GB007032. https://doi.org/10.1029/2021GB007032

Ouyang, Z., Qi, D., Chen, L., Takahashi, T., Zhong, W., DeGrandpre, M. D., et al. (2020). Sea-ice loss amplifies summertime decadal CO_2 increase in the western Arctic Ocean. *Nature Climate Change*, *10*(7), 678–684. https://doi.org/10.1038/s41558-020-0784-2

Pereira, R., Ashton, I., Sabbaghzadeh, B., Shutler, J. D., & Upstill-Goddard, R. C. (2018). Reduced air–sea CO_2 exchange in the Atlantic Ocean due to biological surfactants. *Nature Geoscience*, *11*(7), 492–496. https://doi.org/10.1038/s41561-018-0136-2

Pipko, I. I., Pugach, S. P., Luchin, V. A., Francis, O. P., Savelieva, N. I., Charkin, A. N., et al. (2021). Surface CO_2 system dynamics in the Gulf of Anadyr during the open water season. *Continental Shelf Research*, *217*, 104371. https://doi.org/10.1016/j.csr.2021.104371

Pipko, I. I., Pugach, S. P., Semiletov, I. P., Anderson, L. G., Shakhova, N. E., Gustafsson, r., et al. (2017). The spatial and interannual dynamics of the surface water carbonate system and air–sea CO_2 fluxes in the outer shelf and slope of the Eurasian Arctic Ocean. *Ocean Science*, *13*(6), 997–1016. https://doi.org/10.5194/os-13-997-2017

Previdi, M., Fennel, K., Wilkin, J., & Haidvogel, D. (2009). Interannual variability in atmospheric CO_2 uptake on the northeast U.S. continental shelf. *Journal of Geophysical Research*, *114*(G4), G04003. https://doi.org/10.1029/2008JG000881

Puglini, M., Brovkin, V., Regnier, P., & Arndt, S. (2020). Assessing the potential for non-turbulent methane escape from the East Siberian Arctic Shelf. *Biogeosciences*, *17*(12), 3247–3275. https://doi.org/10.5194/bg-17-3247-2020

Reeburgh, W. S. (2007). Oceanic methane biogeochemistry. *Chemical Reviews*, *107*(2), 486–513. https://doi.org/10.1021/cr050362v

Rees, A. P., Bange, H. W., Arévalo-Martínez, D. L., Artioli, Y., Ashby, D. M., Brown, I., et al. (2022). Nitrous oxide and methane in a changing Arctic Ocean. *Ambio*, *51*(2), 398–410. https://doi.org/10.1007/s13280-021-01633-8

Regnier, P., Friedlingstein, P., Ciais, P., Mackenzie, F. T., Gruber, N., Janssens, I. A., et al. (2013). Anthropogenic perturbation of the carbon fluxes from land to ocean. *Nature Geoscience*, *6*(8), 597–607. https://doi.org/10.1038/ngeo1830

Regnier, P., Resplandy, L., Najjar, R. G., & Ciais, P. (2022). The land-to-ocean loops of the global carbon cycle. *Nature*, *603*(7901), 401–410. https://doi.org/10.1038/s41586-021-04339-9

Rehder, G., Keir, R. S., Suess, E., & Pohlmann, T. (1998). The multiple sources and patterns of methane in North Sea Waters. *Aquatic Geochemistry*, *4*(3), 403–427. https://doi.org/10.1023/A:1009644600833

Reichl, B. G., & Deike, L. (2020). Contribution of sea-state dependent bubbles to air-sea carbon dioxide fluxes. *Geophysical Research Letters*, *47*(9). https://doi.org/10.1029/2020GL087267

Reimer, J. J., Wang, H., Vargas, R., & Cai, W. (2017). Multidecadal fCO$_2$ increase along the United States southeast coastal margin. *Journal of Geophysical Research: Oceans*, *122*(12), 10061–10072. https://doi.org/10.1002/2017JC013170

Repeta, D. J., Ferrón, S., Sosa, O. A., Johnson, C. G., Repeta, L. D., Acker, M., et al. (2016). Marine methane paradox explained by bacterial degradation of dissolved organic matter. *Nature Geoscience*, *9*(12), 884–887. https://doi.org/10.1038/ngeo2837

Resplandy, L., Hogikyan, A., Bange, H. W., Bianchi, D., Weber, T., Cai, W.-J., et al. (2023). Datasets: RECCAP2 A synthesis of global coastal ocean greenhouse gas fluxes [Dataset]. Zenodo. https://doi.org/10.5281/ZENODO.8326096

Resplandy, L., Keeling, R. F., Rödenbeck, C., Stephens, B. B., Khatiwala, S., Rodgers, K. B., et al. (2018). Revision of global carbon fluxes based on a reassessment of oceanic and riverine carbon transport. *Nature Geoscience*, *11*(7), 504–509. https://doi.org/10.1038/s41561-018-0151-3

Reynolds, R. W., Smith, T. M., Liu, C., Chelton, D. B., Casey, K. S., & Schlax, M. G. (2007). Daily high-resolution-blended analyses for sea surface temperature. *Journal of Climate*, *20*(22), 5473–5496. https://doi.org/10.1175/2007JCLI1824.1

Rödenbeck, C., DeVries, T., Hauck, J., Le Quéré, C., & Keeling, R. F. (2022). Data-based estimates of interannual sea–air CO$_2$ flux variations 1957–2020 and their relation to environmental drivers. *Biogeosciences*, *19*(10), 2627–2652. https://doi.org/10.5194/bg-19-2627-2022

Roobaert, A., Laruelle, G. G., Landschützer, P., Gruber, N., Chou, L., & Regnier, P. (2019). The spatiotemporal dynamics of the sources and sinks of CO$_2$ in the global coastal ocean. *Global Biogeochemical Cycles*, *33*(12), 1693–1714. https://doi.org/10.1029/2019GB006239

Roobaert, A., Laruelle, G. G., Landschützer, P., & Regnier, P. (2018). Uncertainty in the global oceanic CO$_2$ uptake induced by wind forcing: Quantification and spatial analysis. *Biogeosciences*, *15*(6), 1701–1720. https://doi.org/10.5194/bg-15-1701-2018

Roobaert, A., Resplandy, L., Laruelle, G. G., Liao, E., & Regnier, P. (2022). A framework to evaluate and elucidate the driving mechanisms of coastal sea surface pCO$_2$ seasonality using an ocean general circulation model (MOM6-COBALT). *Ocean Science*, *18*(1), 67–88. https://doi.org/10.5194/os-18-67-2022

Rosentreter, J. A., Borges, A. V., Deemer, B. R., Holgerson, M. A., Liu, S., Song, C., et al. (2021). Half of global methane emissions come from highly variable aquatic ecosystem sources. *Nature Geoscience*, *14*(4), 225–230. https://doi.org/10.1038/s41561-021-00715-2

Rosentreter, J. A., Laruelle, G. G., Bange, H. W., Bianchi, T. S., Busecke, J. J. M., Cai, W.-J., et al. (2023). Coastal vegetation and estuaries are collectively a greenhouse gas sink. *Nature Climate Change*, *13*(6), 579–587. https://doi.org/10.1038/s41558-023-01682-9

Roth, F., Broman, E., Sun, X., Bonaglia, S., Nascimento, F., Prytherch, J., et al. (2023). Methane emissions offset atmospheric carbon dioxide uptake in coastal macroalgae, mixed vegetation and sediment ecosystems. *Nature Communications*, *14*(1), 42. https://doi.org/10.1038/s41467-022-35673-9

Royer, S.-J., Ferrón, S., Wilson, S. T., & Karl, D. M. (2018). Production of methane and ethylene from plastic in the environment. *PLoS One*, *13*(8), e0200574. https://doi.org/10.1371/journal.pone.0200574

Ruppel, C. D., & Kessler, J. D. (2017). The interaction of climate change and methane hydrates. *Reviews of Geophysics*, *55*(1), 126–168. https://doi.org/10.1002/2016RG000534

Rutherford, K., & Fennel, K. (2018). Diagnosing transit times on the northwestern North Atlantic continental shelf. *Ocean Science*, *14*(5), 1207–1221. https://doi.org/10.5194/os-14-1207-2018

Rutherford, K., & Fennel, K. (2022). Elucidating coastal ocean carbon transport processes: A novel approach applied to the northwest North Atlantic Shelf. *Geophysical Research Letters*, *49*(6), e2021GL97614. https://doi.org/10.1029/2021GL097614

Rutherford, K., Fennel, K., Atamanchuk, D., Wallace, D., & Thomas, H. (2021). A modelling study of temporal and spatial pCO$_2$ variability on the biologically active and temperature-dominated Scotian Shelf. *Biogeosciences*, *18*(23), 6271–6286. https://doi.org/10.5194/bg-18-6271-2021

Salisbury, J. E., & Jönsson, B. F. (2018). Rapid warming and salinity changes in the Gulf of Maine alter surface ocean carbonate parameters and hide ocean acidification. *Biogeochemistry*, *141*(3), 401–418. https://doi.org/10.1007/s10533-018-0505-3

Saunois, M., Stavert, A. R., Poulter, B., Bousquet, P., Canadell, J. G., Jackson, R. B., et al. (2020). The global methane budget 2000–2017. *Earth System Science Data*, *12*(3), 1561–1623. https://doi.org/10.5194/essd-12-1561-2020

Schmale, O., Wäge, J., Mohrholz, V., Wasmund, N., Gräwe, U., Rehder, G., et al. (2018). The contribution of zooplankton to methane supersaturation in the oxygenated upper waters of the central Baltic Sea: Methane supersaturation in the Baltic Sea. *Limnology and Oceanography*, *63*(1), 412–430. https://doi.org/10.1002/lno.10640

Schneider, B., & Müller, J. D. (2018). *Biogeochemical transformations in the Baltic Sea*. Springer International Publishing. https://doi.org/10.1007/978-3-319-61699-5

Séférian, R., Nabat, P., Michou, M., Saint-Martin, D., Voldoire, A., Colin, J., et al. (2019). Evaluation of CNRM Earth System Model, CNRM-ESM2-1: Role of earth system processes in present-day and future climate. *Journal of Advances in Modeling Earth Systems*, *11*(12), 4182–4227. https://doi.org/10.1029/2019MS001791

Siegel, D. A., Doney, S. C., & Yoder, J. A. (2002). The North Atlantic spring phytoplankton bloom and Sverdrup's critical depth hypothesis. *Science*, *296*(5568), 730–733. https://doi.org/10.1126/science.1069174

Signorini, S. R., Mannino, A., Najjar Jr, R. G., Friedrichs, M. A. M., Cai, W.-J., Salisbury, J., et al. (2013). Surface ocean pCO$_2$ seasonality and sea-air CO$_2$ flux estimates for the North American east coast. *Journal of Geophysical Research: Oceans*, *118*(10), 5439–5460. https://doi.org/10.1002/jgrc.20369

Stell, A. C., Bertolacci, M., Zammit-Mangion, A., Rigby, M., Fraser, P. J., Harth, C. M., et al. (2022). Modelling the growth of atmospheric nitrous oxide using a global hierarchical inversion. *Atmospheric Chemistry and Physics*, *22*(19), 12945–12960. https://doi.org/10.5194/acp-22-12945-2022

Su, X., Yang, L., Yang, K., Tang, Y., Wen, T., Wang, Y., et al. (2022). Estuarine plastisphere as an overlooked source of N$_2$O production. *Nature Communications*, *13*(1), 3884. https://doi.org/10.1038/s41467-022-31584-x

Terhaar, J., Lauerwald, R., Regnier, P., Gruber, N., & Bopp, L. (2021). Around one third of current Arctic Ocean primary production sustained by rivers and coastal erosion. *Nature Communications*, *12*(1), 169. https://doi.org/10.1038/s41467-020-20470-z

Thomas, H., Bozec, Y., Elkalay, K., & de Baar, H. J. W. (2004). Enhanced open ocean storage of CO$_2$ from shelf sea pumping. *Science (New York, N.Y.)*, *304*(5673), 1005–1008. https://doi.org/10.1126/science.1095491

Tian, H., Xu, R., Canadell, J. G., Thompson, R. L., Winiwarter, W., Suntharalingam, P., et al. (2020). A comprehensive quantification of global nitrous oxide sources and sinks. *Nature*, *586*(7828), 248–256. https://doi.org/10.1038/s41586-020-2780-0

Tjiputra, J. F., Schwinger, J., Bentsen, M., Morée, A. L., Gao, S., Bethke, I., et al. (2020). Ocean biogeochemistry in the Norwegian Earth System Model version 2 (NorESM2). *Geoscientific Model Development*, *13*(5), 2393–2431. https://doi.org/10.5194/gmd-13-2393-2020

Tu, Z., Le, C., Bai, Y., Jiang, Z., Wu, Y., Ouyang, Z., et al. (2021). Increase in CO$_2$ uptake capacity in the Arctic Chukchi Sea during summer revealed by satellite-based estimation. *Geophysical Research Letters*, *48*(15). https://doi.org/10.1029/2021GL093844

Turi, G., Lachkar, Z., & Gruber, N. (2014). Spatiotemporal variability and drivers of pCO_2 and air–sea CO_2 fluxes in the California Current System: An eddy-resolving modeling study. *Biogeosciences*, *11*(3), 671–690. https://doi.org/10.5194/bg-11-671-2014

von Arx, J. N., Kidane, A. T., Philippi, M., Mohr, W., Lavik, G., Schorn, S., et al. (2023). Methylphosphonate-driven methane formation and its link to primary production in the oligotrophic North Atlantic. *Nature Communications*, *14*(1), 6529. https://doi.org/10.1038/s41467-023-42304-4

Wan, X. S., Lin, H., Ward, B. B., Kao, S.-J., & Dai, M. (2022). Significant seasonal N_2O dynamics revealed by multi-year observations in the northern South China Sea. *Global Biogeochemical Cycles*, *36*(10), e2022GB007333. https://doi.org/10.1029/2022GB007333

Wang, H., Hu, X., Cai, W.-J., & Sterba-Boatwright, B. (2017). Decadal fCO_2 trends in global ocean margins and adjacent boundary current-influenced areas. *Geophysical Research Letters*, *44*(17), 8962–8970. https://doi.org/10.1002/2017GL074724

Wanninkhof, R. (1992). Relationship between wind speed and gas exchange over the ocean. *Journal of Geophysical Research*, *97*(C5), 7373–7382. https://doi.org/10.1029/92JC00188

Wanninkhof, R. (2014). Relationship between wind speed and gas exchange over the ocean revisited. *Limnology and Oceanography: Methods*, *12*(6), 351–362. https://doi.org/10.4319/lom.2014.12.351

Ward, N. D., Megonigal, J. P., Bond-Lamberty, B., Bailey, V. L., Butman, D., Canuel, E. A., et al. (2020). Representing the function and sensitivity of coastal interfaces in Earth system models. *Nature Communications*, *11*(1), 2458. https://doi.org/10.1038/s41467-020-16236-2

Weber, T., Wiseman, N. A., & Kock, A. (2019). Global ocean methane emissions dominated by shallow coastal waters. *Nature Communications*, *10*(1), 4584. https://doi.org/10.1038/s41467-019-12541-7

Wollast, R. (1998). Evaluation and comparison of the global carbon cycle in the coastal zone and in the open ocean. In *The sea* (Vol. 10, pp. 213–252). Retrieved from https://cir.nii.ac.jp/crid/1572543025013898496

Woolf, D., Shutler, J., Goddijn-Murphy, L., Watson, A., Chapron, B., Nightingale, P., et al. (2019). Key uncertainties in the recent air-sea flux of CO_2. *Global Biogeochemical Cycles*, *33*(12), 1548–1563. https://doi.org/10.1029/2018GB006041

Wright, R. M., Le Quéré, C., Buitenhuis, E., Pitois, S., & Gibbons, M. J. (2021). Role of jellyfish in the plankton ecosystem revealed using a global ocean biogeochemical model. *Biogeosciences*, *18*(4), 1291–1320. https://doi.org/10.5194/bg-18-1291-2021

Wu, M., Chen, L., Zhan, L., Zhang, J., Li, Y., & Liu, J. (2017). Spatial variability and factors influencing the air-sea N_2O flux in the Bering Sea, Chukchi Sea and Chukchi Abyssal Plain. *Atmosphere*, *8*(4), 65. https://doi.org/10.3390/atmos8040065

Xu, Y., Cai, W., Wanninkhof, R., Salisbury, J., Reimer, J., & Chen, B. (2020). Long-term changes of carbonate chemistry variables along the North American East Coast. *Journal of Geophysical Research: Oceans*, *125*(7), e2019JC015982. https://doi.org/10.1029/2019JC015982

Xue, Z., He, R., Fennel, K., Cai, W.-J., Lohrenz, S., Huang, W.-J., et al. (2016). Modeling pCO_2 variability in the Gulf of Mexico. *Biogeosciences*, *13*(15), 4359–4377. https://doi.org/10.5194/bg-13-4359-2016

Yang, S., Chang, B. X., Warner, M. J., Weber, T. S., Bourbonnais, A. M., Santoro, A. E., et al. (2020). Global reconstruction reduces the uncertainty of oceanic nitrous oxide emissions and reveals a vigorous seasonal cycle. *Proceedings of the National Academy of Sciences*, *117*(22), 11954–11960. https://doi.org/10.1073/pnas.1921914117

Ye, W., Arévalo-Martínez, D. L., Li, Y., Wen, J., He, H., Zhang, J., et al. (2023). Significant methane undersaturation during austral summer in the Ross Sea (Southern Ocean). *Limnology and Oceanography Letters*, *8*(2), 305–312. https://doi.org/10.1002/lol2.10315

Yukimoto, S., Kawai, H., Koshiro, T., Oshima, N., Yoshida, K., Urakawa, S., et al. (2019). The meteorological research institute earth system Model Version 2.0, MRI-ESM2.0: Description and basic evaluation of the physical component. *Journal of the Meteorological Society of Japan. Series II*, *97*(5), 931–965. https://doi.org/10.2151/jmsj.2019-051

Zhang, J., Zhan, L., Chen, L., Li, Y., & Chen, J. (2015). Coexistence of nitrous oxide undersaturation and oversaturation in the surface and subsurface of the western Arctic Ocean. *Journal of Geophysical Research: Oceans*, *120*(12), 8392–8401. https://doi.org/10.1002/2015JC011245

Zhou, J., Zheng, Y., Hou, L., An, Z., Chen, F., Liu, B., et al. (2023). Effects of acidification on nitrification and associated nitrous oxide emission in estuarine and coastal waters. *Nature Communications*, *14*(1), 1380. https://doi.org/10.1038/s41467-023-37104-9

References From the Supporting Information

Adcroft, A., Anderson, W., Balaji, V., Blanton, C., Bushuk, M., Dufour, C. O., et al. (2019). The GFDL global ocean and sea ice model OM4.0: Model description and simulation features. *Journal of Advances in Modeling Earth Systems*, *11*(10), 3167–3211. https://doi.org/10.1029/2019MS001726

Araujo, M., Noriega, C., & Lefevre, N. (2014). Nutrients and carbon fluxes in the estuaries of major rivers flowing into the tropical Atlantic. *Frontiers in Marine Science*, *1*, 10. https://doi.org/10.3389/fmars.2014.00010

Armstrong, R. A., Lee, C., Hedges, J. I., Honjo, S., & Wakeham, S. G. (2001). A new, mechanistic model for organic carbon fluxes in the ocean based on the quantitative association of POC with ballast minerals. *Deep Sea Research Part II: Topical Studies in Oceanography*, *49*(1–3), 219–236. https://doi.org/10.1016/S0967-0645(01)00101-1

Aumont, O., Ethé, C., Tagliabue, A., Bopp, L., & Gehlen, M. (2015). PISCES-v2: An ocean biogeochemical model for carbon and ecosystem studies. *Geoscientific Model Development*, *8*(8), 2465–2513. https://doi.org/10.5194/gmd-8-2465-2015

Barnier, B., Madec, G., Penduff, T., Molines, J., Treguier, A.-M., Le Sommer, J., et al. (2006). Impact of partial steps and momentum advection schemes in a global ocean circulation model at eddy-permitting resolution. *Ocean Dynamics*, *56*(5–6), 543–567. https://doi.org/10.1007/s10236-006-0082-1

Bernard, B., Madec, G., Penduff, T., Molines, J.-M., Treguier, A.-M., Le Sommer, J., et al. (2006). Impact of partial steps and momentum advection schemes in a global ocean circulation model at eddy-permitting resolution. *Ocean Dynamics*, *56*(5), 543–567. https://doi.org/10.1007/s10236-006-0082-1

Brennan, C. E., Bianucci, L., & Fennel, K. (2016). Sensitivity of Northwest North Atlantic shelf circulation to surface and boundary forcing: A regional model assessment. *Atmosphere-Ocean*, *54*(3), 230–247. https://doi.org/10.1080/07055900.2016.1147416

Buitenhuis, E. T., Le Quéré, C., Bednaršek, N., & Schiebel, R. (2019). Large contribution of Pteropods to shallow $CaCO_3$ export. *Global Biogeochemical Cycles*, *33*(3), 458–468. https://doi.org/10.1029/2018GB006110

de Verneil, A., Lachkar, Z., Smith, S., & Lévy, M. (2022). Evaluating the Arabian Sea as a regional source of atmospheric CO_2: Seasonal variability and drivers. *Biogeosciences*, *19*(3), 907–929. https://doi.org/10.5194/bg-19-907-2022

Dee, D. P., Uppala, S. M., Simmons, A. J., Berrisford, P., Poli, P., Kobayashi, S., et al. (2011). The ERAInterim reanalysis: Configuration and performance of the data assimilation system. *Quarterly Journal of the Royal Meteorological Society*, *137*(656), 553–597. https://doi.org/10.1002/qj.828

Dickson, A. G., Sabine, C. L., Christian, J. R., Bargeron, C. P., & North Pacific Marine Science Organization (Eds.). (2007). *Guide to best practices for ocean CO_2 measurements (No. 3)*. North Pacific Marine Science Organization.

Dunne, J. P., Horowitz, L. W., Adcroft, A. J., Ginoux, P., Held, I. M., John, J. G., et al. (2020). The GFDL Earth System Model Version 4.1 (GFDL-ESM 4.1): Overall coupled model description and simulation characteristics. *Journal of Advances in Modeling Earth Systems*, *12*(11), e2019MS002015. https://doi.org/10.1029/2019MS002015

Dunne, J. P., Sarmiento, J. L., & Gnanadesikan, A. (2007). A synthesis of global particle export from the surface ocean and cycling through the ocean interior and on the seafloor. *Global Biogeochemical Cycles*, *21*(4), GB4006. https://doi.org/10.1029/2006GB002907

Fennel, K., Wilkin, J., Levin, J., Moisan, J., O'Reilly, J., & Haidvogel, D. (2006). Nitrogen cycling in the Middle Atlantic Bight: Results from a three-dimensional model and implications for the North Atlantic nitrogen budget: Nitrogen cycling in the middle Atlantic. *Global Biogeochemical Cycles*, *20*(3), e2005GB002456. https://doi.org/10.1029/2005GB002456

Franco, A. C., Gruber, N., Frölicher, T. L., & Kropuenske Artman, L. (2018). Contrasting impact of future CO_2 emission scenarios on the extent of $CaCO_3$ mineral undersaturation in the Humboldt Current System. *Journal of Geophysical Research: Oceans*, *123*(3), 2018–2036. https://doi.org/10.1002/2018JC013857

Friedlingstein, P., O'Sullivan, M., Jones, M. W., Andrew, R. M., Hauck, J., Olsen, A., et al., (2020). Global carbon budget 2020. *Earth System Science Data*, *12*(4), 3269–3340. https://doi.org/10.5194/essd-12-3269-2020

Frischknecht, M. (2018). New perspectives on the three-dimensional cycling of carbon and nutrients in the California Current System and its response to ENSO (Doctoral dissertation, ETH Zurich) (Artwork Size: 254 p. Medium: application/pdf Pages: 254 p.). https://doi.org/10.3929/ETHZ-B-000283522

Garcia, H. E., Locarnini, R. A., Boyer, T. P., Baranova, O. K., Zweng, M. M., Reagan, J. R., & Johnson, D. R. (2014). World Ocean Atlas 2013, Volume 3: Dissolved oxygen, apparent oxygen utilization, and oxygen saturation (Tech. Rep.). In S. Levitus (Ed.), *NOAA Atlas NESDIS 75* (p. 27). A. Mishonov Technical Ed.

Good, S., Fiedler, E., Mao, C., Martin, M. J., Maycock, A., Reid, R., et al. (2020). The current configuration of the OSTIA system for operational production of foundation sea surface temperature and ice concentration analyses. *Remote Sensing*, *12*(4), 720. https://doi.org/10.3390/rs12040720

Good, S. A., Martin, M. J., & Rayner, N. A. (2013). EN4: Quality controlled ocean temperature and salinity profiles and monthly objective analyses with uncertainty estimates: The EN4 data set. *Journal of Geophysical Research: Oceans*, *118*(12), 6704–6716. https://doi.org/10.1002/2013JC009067

Gruber, N., Clement, D., Carter, B. R., Feely, R. A., Heuven, S. V., Hoppema, M., et al. (2019). The oceanic sink for anthropogenic CO_2 from 1994 to 2007. *Science*, *363*(6432), 1193–1199. https://doi.org/10.1126/science.aau5153

Gruber, N., Frenzel, H., Doney, S. C., Marchesiello, P., McWilliams, J. C., Moisan, J. R., et al. (2006). Eddy-resolving simulation of plankton ecosystem dynamics in the California Current System. *Deep Sea Research Part I: Oceanographic Research Papers*, *53*(9), 1483–1516. https://doi.org/10.1016/j.dsr.2006.06.005

Gruber, N., Hauri, C., Lachkar, Z., Loher, D., Frölicher, T. L., & Plattner, G.-K. (2012). Rapid progression of ocean acidification in the California Current System. *Science*, *337*(6091), 220–223. https://doi.org/10.1126/science.1216773

Haidvogel, D., Arango, H., Budgell, W., Cornuelle, B., Curchitser, E., Di Lorenzo, E., et al. (2008). Ocean forecasting in terrain-following coordinates: Formulation and skill assessment of the Regional Ocean Modeling System. *Journal of Computational Physics*, *227*(7), 3595–3624. https://doi.org/10.1016/j.jcp.2007.06.016

Hartmann, J., Jansen, N., Dürr, H. H., Kempe, S., & Köhler, P. (2009). Global CO_2-consumption by chemical weathering: What is the contribution of highly active weathering regions? *Global and Planetary Change*, *69*(4), 185–194. https://doi.org/10.1016/j.gloplacha.2009.07.007

Hauck, J., Völker, C., Wang, T., Hoppema, M., Losch, M., & Wolf-Gladrow, D. A. (2013). Seasonally different carbon flux changes in the Southern Ocean in response to the southern annular mode. *Global Biogeochemical Cycles*, *27*(4), 1236–1245. https://doi.org/10.1002/2013GB004600

Hersbach, H., Bell, B., Berrisford, P., Hirahara, S., Horányi, A., Muñoz-Sabater, J., et al. (2020). The ERA5 global reanalysis. *Quarterly Journal of the Royal Meteorological Society*, *146*(730), 1999–2049. https://doi.org/10.1002/qj.3803

Hornafius, J. S., Quigley, D., & Luyendyk, B. P. (1999). The world's most spectacular marine hydrocarbon seeps (Coal Oil Point, Santa Barbara Channel, California): Quantification of emissions. *Journal of Geophysical Research*, *104*(C9), 20703–20711. https://doi.org/10.1029/1999JC900148

Joos, F., & Spahni, R. (2008). Rates of change in natural and anthropogenic radiative forcing over the past 20,000 years. *Proceedings of the National Academy of Sciences*, *105*(5), 1425–1430. https://doi.org/10.1073/pnas.0707386105

Jungclaus, J. H., Fischer, N., Haak, H., Lohmann, K., Marotzke, J., Matei, D., et al. (2013). Characteristics of the ocean simulations in the Max Planck Institute Ocean Model (MPIOM) the ocean component of the MPI-Earth system model. *Journal of Advances in Modeling Earth Systems*, *5*(2), 422–446. https://doi.org/10.1002/jame.20023

Kanamitsu, M., Ebisuzaki, W., Woollen, J., Yang, S.-K., Hnilo, J. J., Fiorino, M., & Potter, G. L. (2002). NCEP-DOE AMIP-II Reanalysis (R-2). *Bulletin of the American Meteorological Society*, *83*(11), 1631–1644. https://doi.org/10.1175/BAMS-83-11-1631

Keeling, C. D., Piper, S. C., Bacastow, R. B., Wahlen, M., Whorf, T. P., Heimann, M., & Meijer, H. A. (2005). Atmospheric CO_2 and $13CO_2$ exchange with the terrestrial biosphere and oceans from 1978 to 2000: Observations and carbon cycle implications. In I. T. Baldwin, et al. (Eds.), *A history of atmospheric CO_2 and its effects on plants, animals, and ecosystems* (pp. 83–113). Springer New York. https://doi.org/10.1007/0-387-27048-5_5

Key, R. M., Kozyr, A., Sabine, C. L., Lee, K., Wanninkhof, R., Bullister, J. L., et al. (2004). A global ocean carbon climatology: Results from Global Data Analysis Project (GLODAP): Global ocean carbon climatology. *Global Biogeochemical Cycles*, *18*(4), n/a. https://doi.org/10.1029/2004GB002247

Khatiwala, S., Tanhua, T., Mikaloff Fletcher, S., Gerber, M., Doney, S. C., Graven, H. D., et al. (2013). Global ocean storage of anthropogenic carbon. *Biogeosciences*, *10*(4), 2169–2191. https://doi.org/10.5194/bg-10-2169-2013

Krishna, M., Prasad, M., Rao, D., Viswanadham, R., Sarma, V., & Reddy, N. (2016). Export of dissolved inorganic nutrients to the northern Indian Ocean from the Indian monsoonal rivers during discharge period. *Geochimica et Cosmochimica Acta*, *172*, 430–443. https://doi.org/10.1016/j.gca.2015.10.013

Lachkar, Z., Smith, S., Lévy, M., & Pauluis, O. (2016). Eddies reduce denitrification and compress habitats in the Arabian Sea. *Geophysical Research Letters*, *43*(17), 9148–9156. https://doi.org/10.1002/2016GL069876

Landschützer, P., Gruber, N., Bakker, D. C. E., Schuster, U., Nakaoka, S., Payne, M. R., et al. (2013). A neural network-based estimate of the seasonal to inter-annual variability of the Atlantic Ocean carbon sink. *Biogeosciences*, *10*(11), 7793–7815. https://doi.org/10.5194/bg-10-7793-2013

Large, W. G., & Yeager, S. G. (2009). The global climatology of an interannually varying air-sea flux data set. *Climate Dynamics*, *33*(2–3), 341–364. https://doi.org/10.1007/s00382-008-0441-3

Large, W. G., McWilliams, J. C., & Doney, S. C. (1994). Oceanic vertical mixing: A review and a model with a nonlocal boundary layer parameterization. *Reviews of Geophysics*, *32*(4), 363–403. https://doi.org/10.1029/94RG01872

Lauvset, S. K., Key, R. M., Olsen, A., Heuven, S. V., Velo, A., Lin, X., et al. (2016). A new global interior ocean mapped climatology: The $1° \times 1°$ GLODAP version 2. *Earth System Science Data*, *8*(2), 325–340. https://doi.org/10.5194/essd-8-325-2016

Liss, P. S., & Merlivat, L. (1986). Air-sea gas exchange rates: Introduction and synthesis. In P. Buat-Ménard (Ed.), *The role of air-sea exchange in geochemical cycling* (pp. 113–127). Springer Netherlands. https://doi.org/10.1007/978-94-009-4738-25

Locarnini, R. A., Mishonov, A. V., Antonov, J. I., Boyer, T. P., Garcia, H. E., Baranova, O. K., et al. (2014). World Ocean Atlas 2013, Volume 1: Temperature (Tech. Rep.). In S. Levitus (Ed.), *NOAA Atlas NESDIS 73* (p. 40). A. Mishonov Technical Ed.

Ludwig, W., Amiotte Suchet, P., & Probst, J.-L. (1996). River discharges of carbon to the world's oceans: Determining local inputs of alkalinity and of dissolved and particulate organic carbon. *Sciences de la Terre et des Planètes (Comptes Rendus de l'Académie des Sciences)*, *323*, 1007–1014. Retrieved from https://oatao.univ-toulouse.fr/3498/

Madec, G., Bourdallé-Badie, R., Bouttier, P.-A., Bricaud, C., Bruciaferri, D., Calvert, D., et al. (2017). NEMO ocean engine. https://doi.org/10.5281/ZENODO.1472492

Mahowald, N. M., Engelstaedter, S., Luo, C., Sealy, A., Artaxo, P., Benitez-Nelson, C., et al. (2009). Atmospheric iron deposition: Global distribution, variability, and human perturbations. *Annual Review of Marine Science*, *1*(1), 245–278. https://doi.org/10.1146/annurev.marine.010908.163727

Manizza, M., Keeling, R. F., & Nevison, C. D. (2012). On the processes controlling the seasonal cycles of the air-sea fluxes of O_2 and N_2O: A modelling study. *Tellus B: Chemical and Physical Meteorology*, *64*(1), 18429. https://doi.org/10.3402/tellusb.v64i0.18429

Martinez-Rey, J., Bopp, L., Gehlen, M., Tagliabue, A., & Gruber, N. (2015). Projections of oceanic N_2O emissions in the 21st century using the IPSL Earth system model. *Biogeosciences*, *12*(13), 4133–4148. https://doi.org/10.5194/bg-12-4133-2015

Mayorga, E., Seitzinger, S. P., Harrison, J. A., Dumont, E., Beusen, A. H., Bouwman, A., et al. (2010). Global Nutrient Export from Water-Sheds 2 (NEWS 2): Model development and implementation. *Environmental Modelling & Software*, *25*(7), 837–853. https://doi.org/10.1016/j.envsoft.2010.01.007

Middelburg, J. J., Soetaert, K., Herman, P. M. J., & Heip, C. H. R. (1996). Denitrification in marine sediments: A model study. *Global Biogeochemical Cycles*, *10*(4), 661–673. https://doi.org/10.1029/96GB02562

Moore, J. K., Lindsay, K., Doney, S. C., Long, M. C., & Misumi, K. (2013). Marine ecosystem dynamics and biogeochemical cycling in the Community Earth System Model [CESM1(BGC)]: Comparison of the 1990s with the 2090s under the RCP4.5 and RCP8.5 scenarios. *Journal of Climate*, *26*(23), 9291–9312. https://doi.org/10.1175/JCLI-D-12-00566.1

Naegler, T. (2009). Reconciliation of excess 14C-constrained global CO_2 piston velocity estimates. *Tellus B: Chemical and Physical Meteorology*, *61*(2), 372–384. https://doi.org/10.1111/j.1600-0889.2008.00408.x

Nakano, H., Tsujino, H., Hirabara, M., Yasuda, T., Motoi, T., Ishii, M., & Yamanaka, G. (2011). Uptake mechanism of anthropogenic CO_2 in the Kuroshio Extension region in an ocean general circulation model. *Journal of Oceanography*, *67*(6), 765–783. https://doi.org/10.1007/s10872-011-0075-7

Nevison, C., Butler, J. H., & Elkins, J. W. (2003). Global distribution of N_2O and the N_2O-AOU yield in the subsurface ocean. *Global Biogeochemical Cycles*, *17*(4), n/a. https://doi.org/10.1029/2003GB002068

Olsen, A., Key, R. M., van Heuven, S., Lauvset, S. K., Velo, A., Lin, X., et al. (2016). The Global Ocean Data Analysis Project version 2 (GLODAPv2) - An internally consistent data product for the world ocean. *Earth System Science Data*, *8*(2), 297–323. https://doi.org/10.5194/essd-8-297-2016

Olsen, A., Lange, N., Key, R. M., Tanhua, T., Álvarez, M., Becker, S., et al. (2019). GLODAPv2.2019 - An update of GLODAPv2. *Earth System Science Data*, *11*(3), 1437–1461. https://doi.org/10.5194/essd-11-1437-2019

Orr, J. C., Epitalon, J.-M., & Gattuso, J.-P. (2015). Comparison of ten packages that compute ocean carbonate chemistry. *Biogeosciences*, *12*(5), 1483–1510. https://doi.org/10.5194/bg-12-1483-2015

Orr, J. C., Fabry, V. J., Aumont, O., Bopp, L., Doney, S. C., Feely, R. A., et al. (2005). Anthropogenic ocean acidification over the twenty-first century and its impact on calcifying organisms. *Nature*, *437*(7059), 681–686. https://doi.org/10.1038/nature04095

Orr, J. C., Najjar, R. G., Aumont, O., Bopp, L., Bullister, J. L., Danabasoglu, G., et al. (2017). Biogeochemical protocols and diagnostics for the CMIP6 Ocean Model Intercomparison Project (OMIP). *Geoscientific Model Development*, *10*(6), 2169–2199. https://doi.org/10.5194/gmd-10-2169-2017

Paulsen, H., Ilyina, T., Six, K. D., & Stemmler, I. (2017). Incorporating a prognostic representation of marine nitrogen fixers into the global ocean biogeochemical model HAMOCC: Prognostic nitrogen fixers in HAMOCC. *Journal of Advances in Modeling Earth Systems*, *9*(1), 438–464. https://doi.org/10.1002/2016MS000737

Rödenbeck, C., Keeling, R. F., Bakker, D. C. E., Metzl, N., Olsen, A., Sabine, C., & Heimann, M. (2013). Global surface-ocean pCO_2 and sea-air CO_2 flux variability from an observation-driven ocean mixed-layer scheme. *Ocean Science*, *9*(2), 193–216. https://doi.org/10.5194/os-9-193-2013

Ramesh, R., Purvaja, G. R., & Subramanian, V. (1995). Carbon and phosphorus transport by the major Indian Rivers. *Journal of Biogeography*, *22*(2/3), 409–415. https://doi.org/10.2307/2845937

Rousset, C., Vancoppenolle, M., Madec, G., Fichefet, T., Flavoni, S., Barthélemy, A., et al. (2015). The Louvain-La- Neuve sea ice model LIM3.6: Global and regional capabilities. *Geoscientific Model Development*, *8*(10), 2991–3005. https://doi.org/10.5194/gmd-8-2991-2015

Schourup-Kristensen, V., Sidorenko, D., Wolf- Gladrow, D. A., & Völker, C. (2014). A skill assessment of the biogeochemical model REcoM2 coupled to the Finite Element Sea Ice-Ocean Model (FESOM 1.3). *Geoscientific Model Development*, *7*(6), 2769–2802. https://doi.org/10.5194/gmd-7-2769-2014

Sein, D. V., Koldunov, N. V., Danilov, S., Sidorenko, D., Wekerle, C., Cabos, W., et al. (2018). The relative influence of atmospheric and oceanic model resolution on the circulation of the North Atlantic Ocean in a coupled climate model. *Journal of Advances in Modeling Earth Systems*, *10*(8), 2026–2041. https://doi.org/10.1029/2018MS001327

Seitzinger, S. P., Harrison, J. A., Dumont, E., Beusen, A. H. W., & Bouwman, A. F. (2005). Sources and delivery of carbon, nitrogen, and phosphorus to the coastal zone: An overview of Global Nutrient Export from Watersheds (NEWS) models and their application: Global export of C, N, and P to coastal systems. *Global Biogeochemical Cycles*, *19*(4), n/a. https://doi.org/10.1029/2005GB002606

Seland, O., Bentsen, M., Olivié, D., Toniazzo, T., Gjermundsen, A., Graff, L. S., et al. (2020). Overview of the Norwegian Earth System Model (NorESM2) and key climate response of CMIP6 DECK, historical, and scenario simulations. *Geoscientific Model Development*, *13*(12), 6165–6200. https://doi.org/10.5194/gmd-13-6165-2020

Shchepetkin, A. F., & McWilliams, J. C. (2005). The regional oceanic modeling system (ROMS): A split-explicit, free-surface, topography-following-coordinate oceanic model. *Ocean Modelling*, *9*(4), 347–404. https://doi.org/10.1016/j.ocemod.2004.08.002

Six, K. D., & Maier-Reimer, E. (1996). Effects of plankton dynamics on seasonal carbon fluxes in an ocean general circulation model. *Global Biogeochemical Cycles*, *10*(4), 559–583. https://doi.org/10.1029/96GB02561

Stock, C. A., Dunne, J. P., Fan, S., Ginoux, P., John, J., Krasting, J. P., et al. (2020). Ocean biogeochemistry in GFDL's Earth System Model 4.1 and its response to increasing atmospheric CO_2. *Journal of Advances in Modeling Earth Systems*, *12*(10), e2019MS002043. https://doi.org/10.1029/2019MS002043

Stock, C. A., Dunne, J. P., & John, J. G. (2014). Global-scale carbon and energy flows through the marine planktonic food web: An analysis with a coupled physical-biological model. *Progress in Oceanography*, *120*, 1–28. https://doi.org/10.1016/j.pocean.2013.07.001

Titchner, H. A., & Rayner, N. A. (2014). The Met Office Hadley Centre sea ice and sea surface temperature data set, version 2: 1. Sea ice concentrations: HadISST.2.1.0.0 sea ice concentrations. *Journal of Geophysical Research: Atmospheres*, *119*(6), 2864–2889. https://doi.org/10.1002/2013JD020316

Tsujino, H., Nakano, H., Sakamoto, K., Urakawa, S., Hirabara, M., Ishizaki, H., & Yamanaka, G. (2017). Reference manual for the Meteorological Research Institute Community Ocean Model version 4(MRI.COMv4). Technical Reports of the Meteorological Research Institute No. 80. https://doi.org/10.11483/mritechrepo.80

Tsujino, H., Urakawa, S., Nakano, H., Small, R. J., Kim, W. M., Yeager, S. G., et al. (2018). JRA-55 based surface dataset for driving ocean-sea-ice models (JRA55-do). *Ocean Modelling*, *130*, 79–139. https://doi.org/10.1016/j.ocemod.2018.07.002

Umlauf, L., & Burchard, H. (2003). A generic length-scale equation for geophysical turbulence models. *Journal of Marine Research*, *61*(2), 235–265. https://doi.org/10.1357/002224003322005087

Urakawa, L. S., Tsujino, H., Nakano, H., Sakamoto, K., Yamanaka, G., & Toyoda, T. (2020). The sensitivity of a depth-coordinate model to diapycnal mixing induced by practical implementations of the isopycnal tracer diffusion scheme. *Ocean Modelling*, *154*, 101693. https://doi.org/10.1016/j.ocemod.2020.101693

Urrego-Blanco, J., & Sheng, J. (2012). Interannual variability of the circulation over the Eastern Canadian Shelf. *Atmosphere-Ocean*, *50*(3), 277–300. https://doi.org/10.1080/07055900.2012.680430

Wang, C., Zhang, L., Lee, S.-K., Wu, L., & Mechoso, C. R. (2014). A global perspective on CMIP5 climate model biases. *Nature Climate Change*, *4*(3), 201–205. https://doi.org/10.1038/nclimate2118

Warner, J. C., Sherwood, C. R., Arango, H. G., & Signell, R. P. (2005). Performance of four turbulence closure models implemented using a generic length scale method. *Ocean Modelling*, *8*(1–2), 81–113. https://doi.org/10.1016/j.ocemod.2003.12.003

Wu, H., & Zhu, J. (2010). Advection scheme with 3rd high-order spatial interpolation at the middle temporal level and its application to saltwater intrusion in the Changjiang Estuary. *Ocean Modelling*, *33*(1–2), 33–51. https://doi.org/10.1016/j.ocemod.2009.12.001

Zweng, M. M., Reagan, J. R., Antonov, J. I., Lo-carnini, R. A., Mishonov, A. V., Boyer, T. P., et al. (2014). World Ocean Atlas 2013, Volume 2: Salinity (Tech. Rep.). In S. Levitus (Ed.), *NOAA Atlas NESDIS 74* (p. 39). A. Mishonov Technical Ed.